SAFETY IN PROCESS SCALE-UP OF MXENE AND GRAPHITE OXIDE PRODUCTION

A Dissertation

by

PRITISHMA LAKHE

Submitted to the Office of Graduate and Professional Studies of
Texas A&M University
in partial fulfillment of the requirements for the degree of

DOCTOR OF PHILOSOPHY

Chair of Committee,	Micah J. Green
Committee Members,	Michael B. Hall
	Chad V. Mashuga
	Benjamin A. Wilhite
Head of Department,	Arul Jayaraman

May 2020

Major Subject: Chemical Engineering

ABSTRACT

This research investigates and addresses potential process safety issues with scaling up two-dimensional nanomaterial synthesis. The area of nanomaterial, particularly MXenes and graphite oxide (GO), was chosen because of the growing research interest in commercializing these materials.

MXenes are metal carbides with promising applications in energy storage and gas sensors. Here we investigate hazards associated with MXene production, including MAX phase synthesis from raw materials, etching of MAX phase to MXene clay, exfoliation to MXene nanosheets, and post-processing of MXenes with $Ti_3C_2T_x$ as a model species. The major hazards in MXene synthesis are the potential for dust ignition, runaway reactions, and toxic chemical exposure. This study is intended to facilitate safer MXene synthesis across various levels of scale-up, from large laboratory batches to commercial production.

GO is a precursor to making bulk quantities of graphene-like materials consistently and economically. Prior studies show that GO has the potential to undergo explosive decomposition. In this study, a reactive system screening tool was used to track the temperature and pressure of the explosive decomposition of GO. The data showed that the explosive decomposition temperature of GO strongly depends on sample size and surface area. Finally, the Frank-Kamenetskii model was used to predict the critical mass necessary for GO to undergo explosive decomposition, the model predicted the mass within a factor of experimental data. The results of this study are beneficial in assessing the hazards of bulk GO during storage and handling.

Finally, a reaction calorimeter is used to report the heat of oxidation reaction in the modified Hummers' method to synthesize GO. The heat of reaction increased when graphite is soaked in sulfuric acid for an extended time, which gave more basal functionalization compared to an oxidation process without an extended soaking of graphite in acid. The study showed the heat of solution and reaction is high enough to reach the reported unstable temperature of Mn_2O_7, but the

amount of Mn_2O_7 generated in a typical modified Hummers' method is dilute enough to avoid a violent reaction at 55 °C.

In addition to investigating the safety considerations, in this dissertation, an electro-chemical exfoliation (ECE) method is studied to synthesize graphene-like product from alternative carbon sources such as petroleum-derived cokes.

ACKNOWLEDGMENTS

First and foremost, I want to thank my advisors Dr. Micah J. Green and Dr. Sam M. Mannan (taken too soon) for their wisdom, guidance, and encouragement. You have both been an incredible supporter of graduate students and advocated for their best interest professionally and personally; I couldn't have asked for a better graduate school experience. The opportunities and exposures I got during my time at Texas A & M University have been unparallel; and you have encouraged me to pursue these, and giving me a great sense of confidence to approach my professional career ahead. I also want to thank my committee members, Dr. Hall, Dr. Mashuga, and Dr. Wilhite for their time, patience, and inputs over the years. I am very thankful to the Mary Kay O'Connor Process Safety Center for the funding.

I want to thank Dr. Smit Shah, Dr. Wanmei Sun, Dr. Noor Quddus, Dr. Maria Papadaki, and Xiaofei Zhao for helping me navigate the research hurdles and Devon Kulhanek for helping me with the experiments from the very beginning. I also want to thank Kailash Arole and Matthew Mason for their help on EEG. Cassio, Pilar, Patrick, Anish - thank you for your friendship. I also want to thank my fellow graduate students and the faculty at the Department of Chemical Engineering for their support. I have learnt something from each one of you and will treasure it. I want to thank Ashley, Terah, and Sheera for making sure I was on track with the program, meeting the deadlines/ paperwork, and making accommodations whenever I needed one.

I want to acknowledge the present and past members of Dr. Green and the MKOPSC research groups, the Technical Advisory and the Steering Committee members of the MKOPSC.

Last but not the least, I want to thank my mother, my father, my brother, and my husband for their patience, support, and encouragements over the years. The last five years in graduate school has been anything but smooth. Their constant support is one thing that kept me going. Thank you.

CONTRIBUTORS AND FUNDING SOURCES

Contributors

This work was supported by a dissertation committee consisting of Dr. Micah J. Green (advisor) and Dr. Chad V. Mashuga, Dr. Benjamin A. Wilhite of the Department of Chemical Engineering and Dr. Michael B. Hall of the Department of Chemistry.

The analyses depicted in Chapter two were conducted in part by Evan M. Prehn of the Department of Material Science and Engineering and were published in 2019. The BET data analyzed for Chapter three was provided by Jingze Sun and Dr. Hae-Kwon Jeong. Parts of experiments in chapter four were conducted with help from Devon Kulhanek. Characterizations of electro-chemical graphene in chapter five was conducted in part by Xiaofei Zhao, Muhammad Anas, and Kailash Arole. All other work conducted for the dissertation was completed by the student independently.

Funding Sources

Graduate study was supported by the Mary Kay O'Connor Process Safety Centre and the Artie McFerrin Department of Chemical Engineering with their graduate student assistantship. This work was funded in part by the US National Science Foundation under CAREER award number CMMI-1253085 and CMMI- 1760859.

NOMENCLATURE

A	Pre-exponential factor
AFM	Atomic force microscope
ANOVA	One way analysis variance
ARSST	Advanced reactive system screening tool
b	Heating rate
C	Geometry factor
Ck	Coke
CSB	Chemical safety board
CVD	Chemical vapor deposition
C_p	Heat capacity
d	Linear distance
D_{AB}	Diffusivity of A in B
d_p	diameter
Dow F&EI	Dow fire and explosion index
EA	Elemental analysis
ECE	Electro-chemical exfoliation
EG-C	Exfoliated graphene from coke
EG-GC	Exfoliated graphene from graphitized coke
EEG	Electro-chemical exfoliated graphene
EPA	Environmental protection agency
E_a	Activation energy
GO	Graphite oxide

GO-C	Graphite oxide from coke
GO-GC	Graphite oxide from graphitized coke
GIC	Graphite intercalated compound
GO - FD	Graphite oxide freeze dried
GQD	Graphene quantum dots
h	Heat transfer coefficient
HDPE	High density polyethylene
HIP	Hot isostatic pressure
ISD	Inherently safer design
k_c	mass transfer coefficient
m	Mass
M_R	Mass of the reactor
MIE	Minimum ignition energy
n	Reaction order
NC	Needle coke
ns	rotational speed
OSHA	Occupational safety and health administration
PECS	Pulsed electric current sintering
Pet. coke	Petroleum derived coke
PPE	Personal protective equipment
PTFE	Polytetrafluoroethylene or teflon
PVD	Physical vapor deposition
r	rate of reaction
R	Gas constant
RC1*e*	Reaction Calorimeter

Re	Reynolds number
rGO	reduced Graphite Oxide
RGO -NC	reduced Graphite Oxide from needle coke
RPM	Rotation per min
S or SA	Surface area
Sc	Schmidt number
s.g.	specific gravity
SDS	Safety data sheet
SEM	Scanning electron microscopy
Sh	Sherwood number
SHS	Self-propagating high-temperature synthesis
STEL	Short-term exposure limit
SPS	Spark plasma sintering
TGA	Thermogravimetric analysis
TWA	Time-weighted average
T_f	Temperature of vessel
T_{kis}	Temperature at which reaction rate is maximum
T_o	Temperature of surrounding
T_{onset}	Temperature at which onset is detected
q	Total heat release
v	Velocity
XPS	X-ray photoelectron spectroscopy
XRD	X-ray diffraction
Δ H	Heat of reaction
Δ P	Pressure difference

Δ T	Temperature increase
ΔT_{ad}	Adiabatic temperature increase
δ	Frank-Kamenetskii parameter
ε	RT_f/E_a
λ	Thermal conductiivity
μ	viscosity
ν	kinematic viscosity
ρ	Density
Θ_T	$(E_a * q)/(RT_f^2 C_p)$
dP/dt	Change in pressure with time

TABLE OF CONTENTS

Page

LIST OF FIGURES

FIGURE Page

LIST OF TABLES

TABLE Page

1. INTRODUCTION [1]

1.1 Outline of the Dissertation

This dissertation is divided into six sections and the first section gives an overview of the topics discussed in the dissertation along with a brief summary of each section. Section 2 discusses in detail the hazards associated with MXene production [1]. Section 3 pertains to thermal stability of bulk graphite oxide and the results of the work can be used in determining safer storage and handling conditions [2], and section 4 focuses on using a reaction calorimeter to determine the heat of oxidation reaction in Hummers' method and safety of the oxidation reaction. Section 5 discusses the use of alternate carbon materials as a parent material to synthesis graphene-like product. Finally, section 6 concludes the dissertation with a discussion of future work on graphene production.

1.2 Process Safety in Nanomaterials

A nanomaterial is a material with at least one dimension on the order of 100 nm or less, and also is controllable at that scale to get a desired behavior [3]. Because of surface and quantum effects, nanomaterials display unique properties compared to their bulk counterparts which have different physical and chemical properties. For example, graphite is grey/black, soft, and malleable material but a single atomic layer of graphite is transparent, strong, and flexible [4, 5].

The current advancement in technology has made it possible to isolate, manipulate, and use nanomaterials for the development of various applications. As the applications of novel nanomaterials are gaining popularity and interest, novel nanomaterials are being subjected to scale-up to meet the demand. Scale-up presents unique challenges of its own, but in this research, the process safety component of the scale-up will be investigated.

At a smaller laboratory scale, limited quantities of chemicals are used and often complete

[1] Part of this chapter is reprinted with permission from "Process Safety Analysis for Ti3C2Tx MXene Synthesis and Processing" by Lakhe, P., *et al.* (2019). Industrial & Engineering Chemistry Research, 58(4), 1570-1579, Copyright 2019 American Chemical Society and "Calorimetry of explosive thermal decomposition of graphite oxide" by Lakhe, P., *et al.* (2019). Journal of hazardous materials, 366, 275-281, Copyright 2018 Elsevier

information regarding the reaction and side reactions is not known. For example, T2 Laboratories in Florida were producing methylcyclopentadienyl manganese tricarbonyl, but they were not aware of the runaway reaction hazards with the process, and therefore the cooling system and the reactor relief system were not adequate to contain in a thermal runaway scenario. This led to an explosion of the reactor and four fatalities [6]. Similarly, scaling up processes, especially batch processes, have mass and heat transfer limitation which can lead to unintended process safety incidents [7].

As described by Mannan *et al.*, process safety engineering is understanding the complex interactions of chemical process technology, mechanical and process design, process controls, and process safety management systems and implementing engineering procedures to make processes safer [8]. One of the core steps in process safety engineering is identifying hazards [9]. For a relatively new chemistry, understanding reaction kinetics is an important step in recognizing and addressing hazards of the process. For example, it is critical to know the exotherm of the reaction, potential runaway reactions, gas generation rate, unstable by-product formation, interaction with impurities, *etc.* Only when these are known, can engineering solutions be implemented to make the process safer.

There are several studies in the literature concerning the biological and environmental safety of nanomaterial. However, relatively few studies have explored the process safety concerns of nanomaterials synthesis and handling. Although there have been no reported safety incidents related to nanomaterials synthesis, in this research, we are proactively looking into potential process safety issues that may arise in scaling up novel nanomaterials.

For a relatively new nanomaterial (MXene) synthesized on a laboratory scale, we used the process hazards identification technique to analyze each step of the reaction and proposed solutions or cautions as applicable. For the other nanomaterials (graphite oxide) whose synthesis process is relatively established and is being explored for scale-up, we conducted several thermal and calorimetry experiments to address potential process safety concerns.

1.3 MXenes

MXenes are two-dimensional nanomaterials composed of metal carbides and nitrides with the chemical formula of $M_{n+1}X_nT_x$. In this formula, M is an early transitional metal in the periodic table such as titanium and manganese, X is carbon or nitrogen, and T_x is a combination of several functional groups such as -F, -OH, -Cl, *etc.* MXenes are usually etched from MAX ($M_{n+1}AX_n$) phase where A is the post-transition metal or groups 13-15 in periodic table such as aluminum. MXenes are synthesized by etching out the A layers of $M_{n+1}AX_n$ phase in a harsh environment. As seen in the chemical formula of $M_{n+1}X_nT_x$, a number of MXenes can be derived based on the parent MAX phase. This work is focused on the $Ti_3C_2T_x$ form of MXenes.

$Ti_3C_2T_x$ is the most studied, characterized, and well-understood MXene [10, 11]. $Ti_3C_2T_x$ has shown immense potential in energy storage application, for sensor production, and other applications. Therefore, in this research $Ti_3C_2T_x$ is used as a model MXene to evaluate the process hazards and the results from this work can likely be generalized to other MXenes as well.

Synthesis of MXene is non-trivial and it includes multiple hazardous steps. In particular, the synthesis process includes handling flammable metal dust, exothermic reaction, and toxic chemicals. As the interest in developing novel nanomaterials is increasing, the hazards associated with its synthesis needs to be addressed early enough in the process to ensure safety of the researchers involved. In addition, with this work, we hope to raise awareness of safety concepts and considerations early on in the research to develop inherently safer processes.

1.4 Graphite Oxide

Graphite is a crystalline form of carbon where the atoms are arranged in a hexagonal lattice or honeycomb structure. Graphite occurs naturally and individual layers of graphite are called graphene as shown in schematic **Figure 1.1a**. Graphene is a two-dimensional nanomaterial that has sp^2 hybridization (*i.e.,* a combination of s, p_x, and p_y orbitals) and a tightly packed carbon atom structure which gives graphene unique thermal, electrical, mechanical, and optical properties [4, 12, 13, 14]. The structure of a single layer of graphene is shown in **Figure 1.1b**.

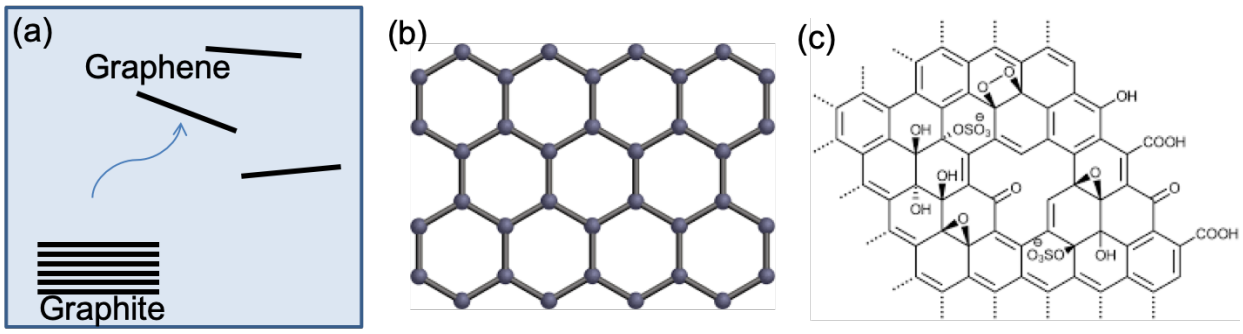

Figure 1.1: Schematic of (a) graphite to single layer graphene, (b) graphene, and (c) graphene oxide. [Figures (b) and (c) are obtained from Google Images search labeled for reuse with no restriction.]

Graphene was first isolated in 2004 by the Scotch tape method, where the graphite crystal was split using an adhesive tape repeatedly and transferring the residue to an oxidized silicon wafer [15]. Since graphene's isolation using the Scotch tape method, several alternative synthesis methods have been explored and developed. Two common techniques are bottom-up and top-down methods. The bottom-up method involves growing graphene layers on an electrically insulating substrate by sublimation or chemical vapor deposition. The bottom-up method synthesizes pristine graphene with excellent thermal and electrical properties, but this method is expensive and not scalable.

The top-down method involves using bulk graphite as source material to synthesize graphene. This method involves either solvent exfoliation or oxidation-exfoliation-reduction [16, 17, 18]. The top-down method is scalable and low-cost, especially the oxidation-exfoliation-reduction method.

In the oxidation-exfoliation-reduction method, a graphitic source is oxidized using a strong oxidizer in an acidic medium. The oxidized graphite, commonly known as graphite oxide (GO) is then exfoliated by ultrasonic agitation or rapid heating to get graphene oxide. The structure of a single layer of graphite oxide is shown in **Figure 1.1c**. In literature, both graphite oxide and graphene oxide have been given the label 'GO'. However, in this study GO refers to graphite oxide, and the exfoliated graphite oxide is called graphene oxide. The GO and graphene oxide are hydrophilic

meaning they can be dispersed in water and are electrically insulating. Therefore, in order to regain the electrical properties to that of graphene-like materials, graphene oxide is reduced, and some common reduction methods are chemical, thermal, and ultraviolet-assisted methods [19, 20].

Even though there are three methods to get GO (*i.e.,* Brodie [21], Staudenmaier [22], and Hummers methods [23]), Hummers method has gained the most popularity because of its comparatively milder and less hazardous oxidation conditions [20]. In the modified Hummers' method, excess sulfuric acid of concentrations 95 to 97 wt. % is used as a solvent and a 1:3 ratio of graphite and potassium permanganate ($KMnO_4$) is added to the solution. The oxidation reaction is done between 30 - 35 °C for 2 hours. The oxidation reaction is quenched using water and H_2O_2 is added to precipitate manganese from the solution. The solution is then washed over an extended period to get a neutral GO solution. Finally, the GO is centrifuged and dried to get powder GO. The GO can also be sonicated before centrifuging to get graphene oxide [24]. This top-down chemical synthesizes approach using modified Hummers' method is becoming a baseline for the production of graphene-like materials because this method gives higher yield products compared to other methods and is economically feasible.

Reduction of GO is an important step in obtaining graphene-like material from graphite. The reduction of GO removes most of the oxygen-containing functional groups added to graphite during oxidation. rGO has the electrical and thermal property close to graphene because the reduction process restores the pi-electron conjugation within the aromatic rings of graphite. However, the oxidation-exfoliation-reduction method introduces defects in the graphene structure and the mechanical and chemical properties are inferior compared to pristine graphene [25].

There are five different reduction methods employed as noted in a recent review of GO reduction [25]: (1) Chemical reduction uses organic and inorganic chemicals such as $NaBH_4$, hydrazine, ascorbic acid, hydroquinone, strong alkaline solutions, and urea among others. (2) Thermal reduction exposes GO to rapid heating to release the oxygen in the GO. The rapid heating at high temperature exfoliates and reduces at the same time because the heating causes the oxygen groups to leave as CO and CO_2 gases from the spaces between the GO sheets. Other reduction methods include (3)

microwave and photo reduction, (4) photo-catalytic reaction, and (5) solvothermal/hydrothermal reduction.

1.5 Process Safety Issues in GO Production

During the literature review, two areas of GO production and handling where process safety issues could escalate were noted. The first area of process safety concern is the storage and handling of solid GO or graphene oxide. GO is commonly stored and shipped in solid powder form. As noted in the earlier section, the thermal reduction of GO is one of the methods of reducing GO. However, some small-scale experiments showed that GO has the potential of undergoing thermal reduction violently and explosively [26]. The resulting material from the thermal explosion of GO is rGO but in the process of uncontrolled thermal reduction, the GO releases incondensable gas rapidly. There has been no known research done on quantifying the pressure generation rates or what causes some GO samples to explode while heating. Knowledge of the explosive decomposition of GO is critical if GO is to be scaled up, stored, and handled in bulk quantities.

The second area of process safety concern is with GO oxidation reaction. Multiple prior studies have pointed out the importance of adding the oxidizer, potassium permanganate ($KMnO_4$) slowly to maintain the reaction temperature below 55 °C. The literature point to a study from 1987 where the addition of potassium permanganate to sulfuric acid resulted in formation of explosive material [27]. However, there has been no study investigating the operating conditions of GO to ensure safe scale-up of oxidation of graphite.

1.6 Summary of Sections

Section 2 [1]

MXenes are two-dimensional metal carbides with promising applications in energy storage and gas sensors. Guidelines for safe, scalable MXene synthesis are important due to ongoing efforts to scale-up production of these novel nanomaterials. Hazard identification before scale-up will allow for inherently safer designs prior to actual implementation. Here, we investigate hazards associated with MXene production: MAX phase synthesis from raw materials, etching of MAX

phase to MXene clay, exfoliation to MXene nanosheets, and post-processing of MXenes with $Ti_3C_2T_x$ as a model species. The major hazards in MXene synthesis are potential for dust ignition, runaway reactions, and toxic chemical exposure. Because the synthesis of MXenes is a multi-step process, this study evaluated safety guidelines for each step, including preventive and mitigating measures, best practices, and emergency procedures and responses. This includes handling of combustible powders, exothermic reactions, and harsh chemical etchants. This study is intended to facilitate safer MXene synthesis across various levels of scale-up, from large laboratory batches to commercial production.

Section 3 [2]

Graphite oxide (GO) has shown immense potential in energy storage and composite filler applications, and large-scale production of GO is of increasing commercial and academic interest. However, prior studies show that GO has the potential to undergo explosive decomposition. In this study, an advanced Reactive System Screening Tool was used to track the temperature and pressure of the explosive decomposition of GO. The data showed that the explosive decomposition temperature of GO strongly depends on sample size. The temperature and pressure generation are on the order of 1000s of °C per minute and 1000s of psig per minute respectively for less than a gram of material. Therefore, the rapid decomposition of bulk GO can lead to catastrophic consequences. The paper further compared the thermal stability of GO from different sources and found that the GO surface area has significant effects on GO stability. Finally, the Frank-Kamenetskii model was used to predict the critical mass necessary for GO to undergo explosive decomposition, the model predicted the mass within a factor of experimental data. The results of this study are beneficial in assessing and predicting the hazards of bulk GO during storage and handling.

Section 4

While several published studies considered how to optimize the oxidation-exfoliation-reduction process of modified Hummers' method to make graphite oxide (GO) and reduced graphene oxide (rGO), relatively few studies have explored the effect of operating conditions on the final GO produced and the process safety concerns with the process. In this study, a reaction calorimeter is used

to determine the heat of solution and oxidation reaction in the modified Hummers' method as a function of reactor processing parameters. The heat of reaction increases when graphite is soaked in sulfuric acid for an extended time compared to an oxidation process without extended soaking of graphite in acid. GO synthesized with acid-soaked parent material has more surface functional groups and the heat of the oxidation reaction decreases with increasing stirring rate. However, the GO synthesized with non-acid soaked parent material has edge functional groups and the heat of reaction do not vary with stirring speed. The study shows the heat of solution and reaction is high enough to reach the reported unstable temperature of Mn_2O_7, but the amount of Mn_2O_7 generated in a typical modified Hummers' method is dilute enough to avoid a violent reaction at 55°C.

Section 5

There is a value in using alternate carbon sources such as petroleum and coal-based coke to make graphene-like materials. Petroleum coke is the by-product of coker units in petroleum refining and currently has limited application. However, converting these cokes to high value graphene-like product is of economic interest. There are few studies exploring the use of alternative carbon sources to make graphene-like product. In this chapter, we are interested in characterizing parent carbon sources and the products from these sources to determine what carbon sources can be converted to graphene-like product.

Section 6

Finally, chapter six presents the conclusions of the dissertation, discusses limitations of these studies, and suggests areas for future research in graphene and MXene production.

2. PROCESS SAFETY ANALYSIS FOR $TI_3C_2T_X$ MXENE SYNTHESIS AND PROCESSING[1]

2.1 Introduction

Nanomaterials are unique because they often present safety hazards in both synthesis and health. Over the last several decades, a number of studies on biological and health hazards of nanomaterials have been published, and these studies are crucial in understanding the effects of nanomaterials on humans and the environment [28, 29]. Despite these recent advances, there is a stark absence of research assessing the process safety of nanomaterials synthesis and scale-up. The number of novel nanomaterials synthesized by researchers and small-scale manufacturing companies is increasing; thus, an intimate understanding of the process safety implications during laboratory synthesis and its scale-up is vital for faster, safer implementation of nanomaterials. A number of process safety incidents have occurred during scale-up, including several incidents in laboratories due to a lack of proper hazard identification [30]. For example, in 2010, a graduate student was injured when trying to scale-up a conventional process involving hydrazine perchlorate derivatives synthesis from 300 mg to 10 g [31].

One of the primary causes of safety incidents in laboratories is a lack of knowledge of safety issues arising during synthesis route; this is especially true in cases of new materials synthesis and novel processes where the hazards of the reactions are yet to be discovered. While most universities and research laboratories rightfully require researchers to conduct a safety analysis to identify and address potential hazards, these analyses cannot be thorough if the crucial information such as heat and gas generation rate by reaction, by-product formation, thermal stability, *etc.* are lacking. These crucial information are not immediately known for new and novel processes development in laboratory. In addition, the guidance for completing a thorough hazard assessment is often

[1]Text, figures, and tables in this chapter are reprinted with permission from "Process Safety Analysis for Ti3C2Tx MXene Synthesis and Processing" by Lakhe, P., Prehn, E. M., Habib, T., Lutkenhaus, J. L., Radovic, M., Mannan, M. S., & Green, M. J. (2019). Industrial & Engineering Chemistry Research, 58(4), 1570-1579, Copyright 2019 American Chemical Society

unavailable as the scientific community only recently adopted the concepts of process safety by the means of loss prevention. Due to these reasons, scaling-up novel processes for nanomaterials synthesis can result in catastrophic incidents as hazards can compound if not done correctly. This work is intended to highlight the importance of preventive measures in order to reduce the number and severity of incidents associated with the synthesis and scale-up.

MXenes are a growing family of atomically layered two-dimensional metal carbides and nitrides with the chemical formula $M_{n+1}X_nT_x$, where M is an early transitional metal in the periodic table, X is carbon or nitrogen, and T is a combination of several terminal groups (*i.e.* -F, -OH, -O, -Cl, *etc.*). These materials are most frequently etched from $M_{n+1}AX_n$ (MAX) phase powders, which contain post-transition groups 13-15 metal layer that are located between M and X layers in their crystal structure. Two-dimensional carbides can have tremendous applications as MXenes have impressive thermal and electrical conductivities. MXenes are currently being evaluated for use in lithium and non-lithium ion energy storage, fuel cell additives, supercapacitors, humidity and pH sensors, and lubricating additives [11, 32]. To-date, over 60 MAX phases have been synthesized, plus over 80 MAX phase solid solutions (where the M and/or X layers contain multiple constituents). These 'parent materials' can be used to synthesize MXenes via etching, but this etching step typically requires a harsh environment. One frequently used method uses a highly concentrated hydrofluoric acid to dissolve the M-A bonds, releasing heat and hydrogen gas as by-product. Although it is a relatively recent field, MXenes are a rapidly growing family of materials, and new compositions must often be accompanied by new etching techniques [33]. The etching step is a unique requirement of MXene synthesis compared to that of many other nanomaterials, and each type of MXene may require a slightly different etching procedure. **Figure 2.1** shows the graphical representation of the hazards in MXene synthesis.

$Ti_3C_2T_x$ is the best characterized and most studied MXene species due to its relative ease of intercalation and delamination, relatively low financial cost, and excellent conductive properties [10, 11]. There is a growing interest in scaling-up $Ti_3C_2T_x$ production; in fact, at present $Ti_3C_2T_x$ is being produced in quantities of 100 g per batch scale [34]. Several publications, including a

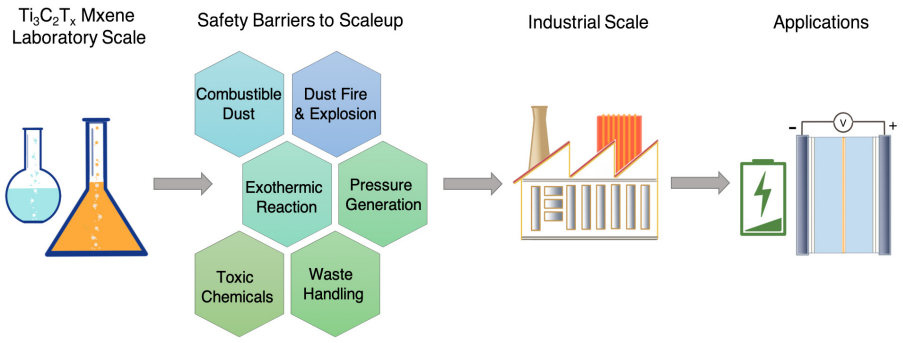

Figure 2.1: Graphical representation of the hazards in scaling up MXene synthesis [1]

recent review paper, have neatly outlined various $Ti_3C_2T_x$ synthesis routes and their advantages and disadvantages in terms of product quality [35, 33]. However, the process safety analyses associated with different synthesis routes are nowhere to be seen, despite of the serious hazards present in MXene production. $Ti_3C_2T_x$ synthesis is a multi-step process that includes handling of combustible powders like aluminum and titanium carbide or graphite to synthesize Ti_3AlC_2 MAX phase, followed by highly exothermic chemical etching of the Ti_3AlC_2 phase into the desired $Ti_3C_2T_x$ using a strong oxidizing agent. The general, step-by-step synthesis of Ti_3AlC_2 and $Ti_3C_2T_x$ materials from raw materials is depicted schematically in **Figure 2.2** along with the major hazard associated with each step.

In this paper, we identify and discuss hazards in each of these steps for $Ti_3C_2T_x$ synthesis, labeled 1 through 4 in **Figure 2.2**. The focus of this paper is to address hazards in small-scale synthesis (grams of $Ti_3C_2T_x$) and consider the implications for scale-up to kilogram quantities. As the scale of $Ti_3C_2T_x$ synthesis increases, a rigorous evaluation is necessary, and we anticipate this paper will provide a guide on conducting such hazard identification studies for the future. This work aims to facilitate safer MXene (particularly $Ti_3C_2T_x$) synthesis across all levels of scale-up, from large laboratory batches to commercial production. A similar approach can be taken to assess the hazards of other nanomaterials in the MXene family. This paper focuses on the hazards encountered with $Ti_3C_2T_x$, including handling of constituent MAX phase powders, MAX

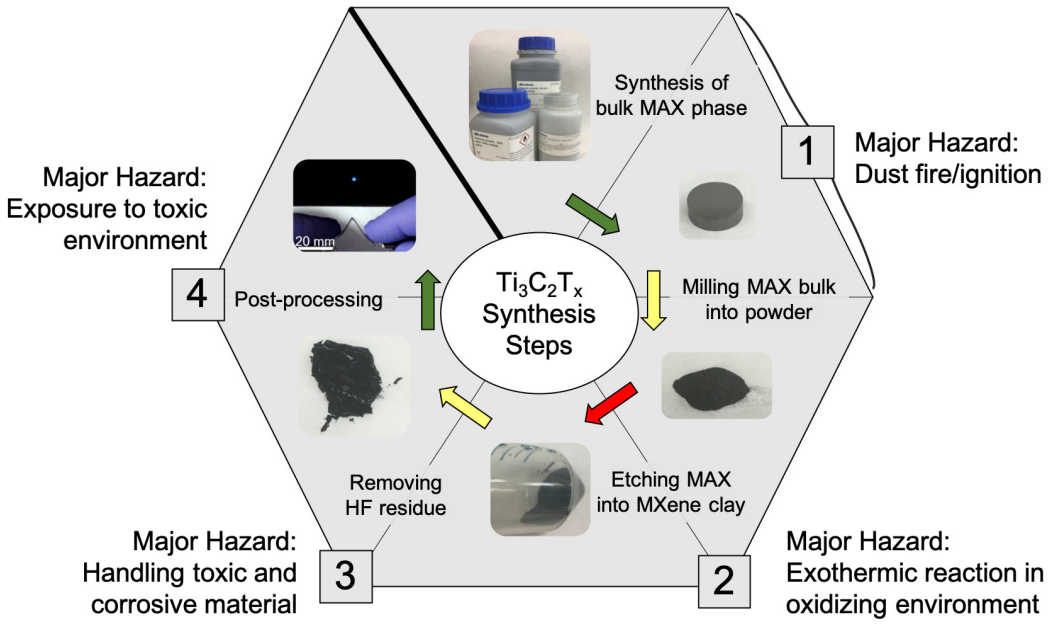

Figure 2.2: Schematic of $Ti_3C_2T_x$ synthesis from raw materials. Step 1 represents the synthesis and the milling processes of Ti_3AlC_2 phase, Step 2 is the etching of Al from Ti_3AlC_2 phase using a strong oxidizing agent such as HF, step 3 is the oxidizing agent (HF) washing, and step 4 is the drying and post-processing [1].

phase synthesis, various etching methods for synthesizing MXenes, and post-processing methods of exfoliation and optional delamination.

2.2 Methodology: The Safety Triad: Prevention, Mitigation, Response

A strong safety program in a laboratory or industry should contain all elements of a robust 'safety triad': Prevention, Mitigation, and Response [36]. In addressing safety events, the first priority is to prevent the undesirable events such as spill, fire, explosion *etc*. In order to implement preventive measures to avoid such safety incidents, hazards in a process have to be identified throughout the process, for example, identifying synthesis steps with presence of combustible dust, potential for runaway reaction, toxic gas formation, and others. Only after identification can prevention measures be implemented. If the preventive measures fail and an undesirable event (spill, fire, explosion) occurs, mitigating systems should be employed to minimize the outcome of the undesirable event. Finally, effective response mechanisms need to be planned to minimize

the consequence of an undesirable incident [37, 38]. The above sequence of considerations is very important to implement in early stages of process development to avoid safety incidents as an incident can have catastrophic effects. The importance of process safety is often undervalued as it has traditionally been seen as an 'add on' component after completion of the process design. However, the inclusion of process safety in the design stage is proven to result in an inherently safer, simpler, and more economical method [39, 40]. This paper will discuss the safety triad in safer synthesis of $Ti_3C_2T_x$ as and when applicable.

2.2.1 Preventive Measures

Identification of hazards is the first step in applying preventive measures, typically begun by reviewing the safety data sheets (SDS) of each chemical involved in the process; this identifies key hazardous chemicals and dangerous situations to avoid. However, the SDS information may not be sufficient because it may not contain all the hazard information, particularly for novel materials such as MXene nanosheets. Instead, the chemical structure, previous incidents with analogous materials, and methodical hazard identification tests should be considered in addition to consulting an SDS. In the next step, the process conditions need to be evaluated, such as heat of reaction, pressure generation rates, temperature range, toxic or stable by-product formation, and thermal stability of materials involved. Once known, these parameters can be managed through several prevention methods [37].

There are four unique types of hazards preventive measures that can be employed to manage the hazards discussed above: (i) inherently safer designs, (ii) engineering controls, (iii) administrative controls, and (iv) personal protective equipment. These preventive measures are listed in order of decreasing effectiveness. The most effective is the inherently safer design (ISD) and the elements of ISD are to minimize hazards, substitute hazardous materials with a less hazardous material, moderate the amount of hazardous material, and simplify the process. These ISD elements should be utilized whenever possible but they are more effective when it is employed in the design stage of process development [41]. As such, for the engineering profession to value past experiences and advance with enhanced inherently safer process design methods.

In processes requiring use of hazardous materials and operation, engineering controls such as physical protection, detection system, controllers, and safety interlocks should be implemented. In a laboratory setting, implementing ISD or engineering controls can be quite challenging; therefore, administrative controls such as supervision, proper training, best available work practices, manuals, and procedures should be prioritized. Finally, the use of proper personal protective equipment is the last line of defense should a safety incident occur.

2.2.2 Mitigation Measures, Emergency Planning, and Response

The main goal of implementing mitigating measures is to reduce the impact of undesirable events that cannot be prevented. Some of the mitigating measures that can be implemented in laboratories are training, familiarization with the surroundings, placement of hood, sensors and alarm systems, and evacuation plans. Automation of the most hazardous steps or maintaining supervision of the operators is key in avoiding fatal accidents from occurring.

Finally, emergency response plans are paramount when any significant hazards are present, and these plans must be established before the experiments are carried out. Planning is especially important in scaling-up $Ti_3C_2T_x$ synthesis, as hazards such as metal fires and toxic gas release can escalate quickly. The emergency plans should include communicating the hazards and risks present in every step of the process with individuals working directly or indirectly in the facility, access to emergency response personnel, and repair and recovery plans.

2.3 Hazards Analysis of $Ti_3C_2T_x$ MXene Synthesis

In this section, each step outlined in **Figure 2.2** is discussed and as a basis for the study, a laboratory production of $Ti_3C_2T_x$ MXene is investigated. **Figure 2.3** shows relative quantities of material by mass of reactant materials used in the most common $Ti_3C_2T_x$ synthesis route. As seen in **Figure 2.3**, a significant quantities of raw materials are required to get the final product. The yields below each step are generous estimates, and so significantly less MXene clay may be produced depending on the available equipment. An optimization of each step to increase yield will decrease amount of hazardous materials required on site for handling. The analysis for each

synthesis step is shown in following subsections.

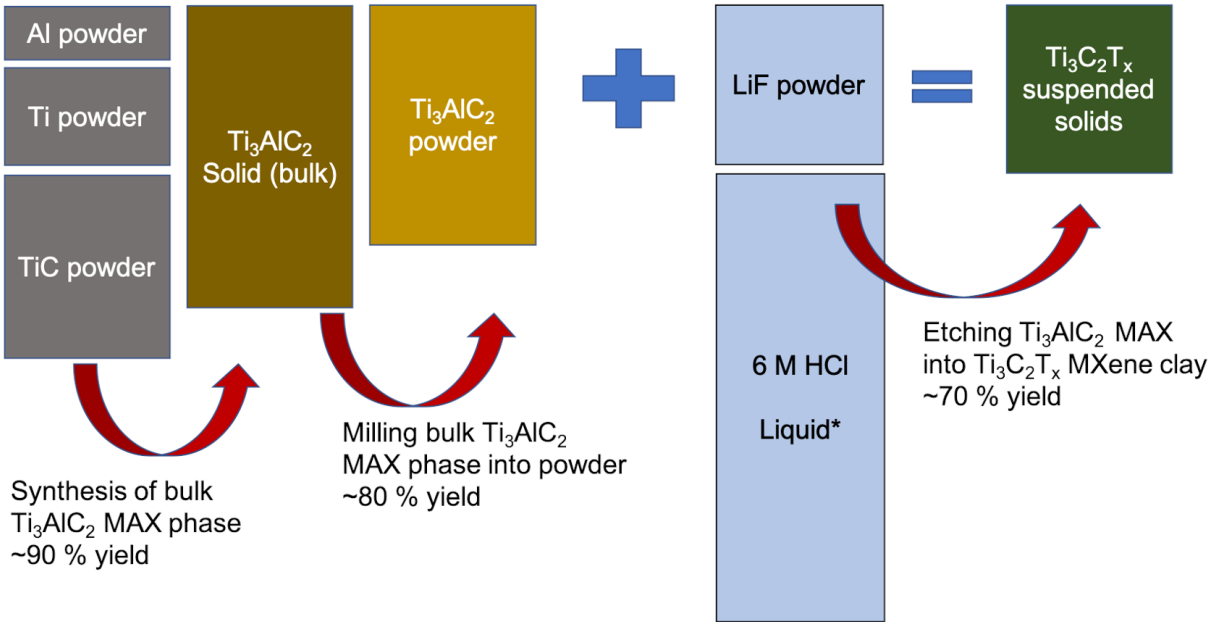

Figure 2.3: Relative quantities (by mass) of reactant materials required to produce $Ti_3C_2T_x$ MXene. *The quantity of 6 M HCl required is six times the amount shown in the figure [1].

2.3.1 Hazards Analysis for Ti_3AlC_2 MAX Synthesis

To-date, parent MAX phases have been synthesized by nearly a dozen routes, including most notably hot isostatic pressing (HIP), self-propagating high-temperature synthesis (SHS), pulsed electric current sintering (PECS, commonly known as spark plasma sintering SPS), and pressure-less sintering [42]. Oxidation of the sample is the primary concern for high-temperature methods such as pressure-less sintering, so synthesis should be performed in an inert atmosphere. Pressure-less sintering is the most promising technique for commercial scale-up because the process is relatively rapid when compared to other synthesis techniques. However, pressure-less sintering is a batch process and batch processes are inherently not safer because increasing the batch size increases the inventory of hazardous raw materials on-site [43]. An alternative to the current batch process should be studied for safer scale-up. Regardless of the synthesis method selected, powder-

handling hazards are the first concerns to address.

For most Ti_3AlC_2 MAX phase synthesis methods, powders of titanium (Ti), aluminum (Al), and titanium carbide (TiC) or graphite (C) are thoroughly mixed. These constituent powders present ignition and /or explosion hazards, and appropriate mixing methods should be implemented. Fine powders have higher dispersibility and chemical activities, thus increasing the dust explosion risk [44]. The Chemical Safety Board (CSB) recorded 281 dust and explosions incidents in the United States between 1980 and 2005, of which approximately 20% are due to combustible metals dust [45, 46]. Specifically, one of the most highly combustible metals is aluminum powder, followed by titanium powder. The inherently safer methods of powder and dust handling are well known. However, the respective hazard is often not considered and the appropriate measures are not taken.

The Minimum Ignition Energy (MIE, a measure of the ease of ignition of a suspended dust cloud) for Ti powder of average particle size of 45 μm is 21.91 mJ, but the MIE decreases as the particle size of the powder decreases. Thus nanoscale Ti powder are more prone to ignition by friction or collision [47]. Finer particle size, though more dangerous, facilitates a higher degree of mixing and generally results in a more phase-pure bulk sample. Thus, a compromise must be made between inherently safer, larger particle size and purity of parent Ti_3AlC_2 phase. Significant dust explosion hazards may be present with TiC and C as well, but these systems are not well-studied, and so their dust explosion parameters (like MIE) have not been reported to-date. Consequently, given the numerous potential applicants for MXene, research on these compounds is imperative before scaling up.

In pressure-less sintering routes, the mixed reactant powders are placed in a furnace to prepare a porous bulk MAX phase, as shown in **Figure 2.4**. Furnace work contains hazards such as potential exposure to high-temperature elements, dust ignition, and if hoses and fittings are not properly maintained, pressure build-up. To prevent oxidation, the furnace chamber should be an inert atmosphere such as argon. Depending on the synthesis temperature and constituents, some more volatile elements (including aluminum) may evaporate, clogging the inert gas exhaust tube.

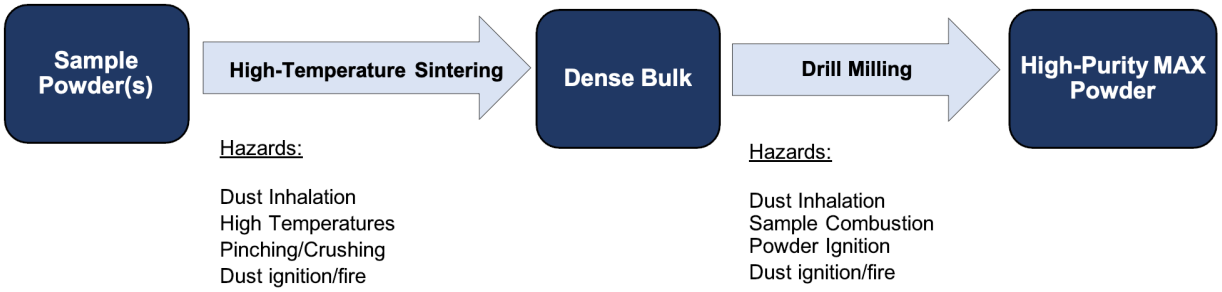

Figure 2.4: Schematic of MAX, Ti_3AlC_2 phase synthesis and hazards associated with the steps [1].

Furnaces (and inlet/outlet tubing) should be regularly cleaned to maintain an open pathway. Some synthesis methods may contain high-temperature hazards, as in the cases of self-propagating high-temperature synthesis (SHS), pulsed electric current sintering (PECS), hot pressing, and solid-state combustion synthesis (SCS) [48, 49, 50]. In these synthesis techniques, high temperatures can lead to constituent melting and leaking, so control of the heating rate is critical. Rapid heating rates in SHS and SCS can lead runaway reactions, so emergency fire systems, including class D fire extinguishers, should be accessible at all times. Other methods may contain chemical and/or high voltage hazards, as in the cases of physical vapor deposition (PVD), chemical vapor deposition (CVD), and PECS [42, 51]. In all instances, operators should avoid static buildup and other ignition sources, properly cool and vent the reaction chamber before opening, and wear proper personal protective equipment (PPE).

After removing this porous bulk material from the furnace, the sample is usually milled into powder to increase the etching rate. There are many different methods of milling, including low- or high-energy ball milling, jet milling, drill milling, and mortar and pestle to name a few [52, 53]. Mill selection is crucial to the safety of the MAX phase process, as Ti-based compounds may heat and deform, even igniting the generated fine powders in extreme situations. It is also important to consider dust dispersion to the environment. Dust fires and explosions are usually caused by dust which has knowingly or unknowingly been dispersed to the surrounding from the process area. **Figure 2.5a** shows an example of powder ignition during drill milling of a $Ti_3(AlBi)C_2$

MAX phase in the laboratory. This combustion was facilitated by the low-purity of the MAX phase and presence of flammable intermetallic impurities. Though ignition of sample powders is a rare occurrence, it is important to note fires caused by Ti-based compounds cannot be extinguished using water or CO_2-based extinguishing agents (indeed, these may cause the fire to propagate more quickly). Instead, only a Class D fire extinguisher should be used to fight metal fires.

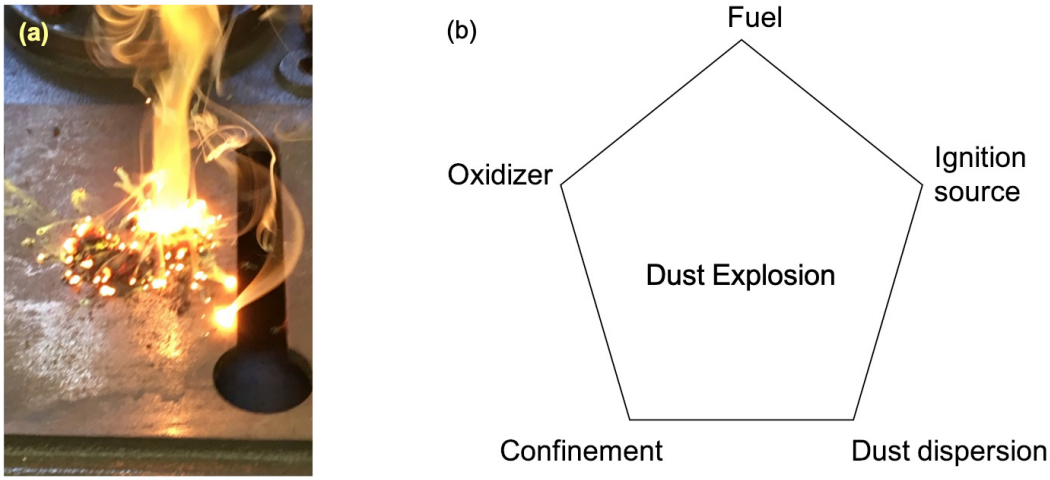

Figure 2.5: (a) Fire caused by drill-milling of $Ti_3(AlBi)C_2$ phase; (b) Schematic representing elements of dust explosion pentagon [1].

Generally speaking, for a dust explosion to occur, five elements need to be present: a fuel (combustible dust), an oxidizer (oxygen in air), an ignition source, confinement, and dust dispersion (shown in **Figure 2.5b**) [54]. The dust explosion hazard can be minimized by eliminating one or more of the elements in the pentagon, such as (a) preventing suspension of powder in the air, (b) eliminating all possible ignition sources, and (c) handling all powders in inert environments. In addition to these precautions, wearing proper PPE and equipping the user with firefighting techniques are mandatory [55]. The following preventive measures are recommended as applications of these principles to eliminate one or more elements of the dust explosion pentagon when preparing MAX phase powder for etching into MXenes.

To mitigate the risk of ignition, high-energy milling should only be performed on samples with

Table 2.1: Hazards of Ti_3AlC_2 MAX Phase Synthesis [1]

Hazard	Cause	Major Effects	Corrective/Preventive measures in a laboratory scale
Spontaneous combustion of reactants	Auto-ignition or introduction of ignition source (static)	Potential equipment damage and employee injury	Ground the container and minimize dust cloud formation
Dust particles inhalation	Handling powder reactants	Employee injury	Work in hood, limit the quantity of toxic reactant, and use proper PPE
Combustion of Ti_3AlC_2 phase during drilling	Aerosolization of powder during drilling and friction	Fire and injury	Ground the equipment, drill slowly in inert environment
Explosion of ignited sample	Extinguishing Al powder using water	Fire and injury	Use only a Class D fire extinguisher

a lubricating solvent and under an inert atmosphere. All electrical equipment should be grounded to prevent any ignition due to static discharge both during and after milling. Dust dispersion to the environment should be prevented or the accumulation dust should be thoroughly removed. Once a sufficiently fine and pure powder has been obtained, the MXene synthesis can begin. However, on an industrial scale, it is difficult to mitigate all static sources or prevent dust accumulation. The titanium industry that deals with highly flammable dust particle have incorporated alternative safer designs and this could be a starting point for design safer large-scale MAX drilling processes [56].

The hazards present in Ti_3AlC_2 synthesis and processing are summarized in **Table 2.1**along with causes, major effects, and corrective and/or preventive actions. Some causes listed in this table and subsequent tables such as leaks or loss of controls cannot be avoided all of the time in all the equipment. Therefore, during scaling-up, processes should be designed such that they do not depend heavily on equipment controls or instrumentations. Although controls and instrumentation can be a layer to prevent negative incidents, the key to safer processes is to make the processes inherently safer at the design stage.

2.3.2 Hazards Analysis for Ti_3AlC_2 MAX Phase Etching Process

MXenes are produced by etching the A layer from the powdered MAX phase, as shown in **Figure 2.6a**. In the most typical case of Ti_3AlC_2, the Al layer is removed by using aqueous solution of hydrogen fluoride (HF), which can be introduced at varying concentrations or produced *in situ* from a fluoride-based compound and an acid, such as LiF and HCl, respectively. The etching reaction is highly exothermic and produces H_2 gas and H_2O vapor. This section investigates the process safety issues with this step, especially the reaction exotherm and by-products formation.

A total of seven $Ti_3C_2T_x$ etching routes were identified, and their relative hazards were ranked. These seven methods include $Ti_3C_2T_x$ synthesis using 10 wt % HF or higher [57, 58], *in situ* mixing of LiF and HCl to form HF [59], NH_4HF_2 [60], F_3Fe/HCl [61], NaOH [62], and HCl [63]. The Dow Fire and Explosion (Dow F&EI) Index was used to rank the relative hazard level of each method [64]. Following assumptions were considered to compute the Dow F&EI.

- Moderate exotherms for etching (equivalent to that of an oxidation reaction)
- Adequate ventilation (reaction done inside hood)
- Adequate access to laboratory in case of emergency (at least two clear doorways and easy access to fire extinguisher)
- Spills are contained (doesn't spread to other experiments or equipment)
- No air sensitive material used
- H_2 released could make the environment flammable
- MAX phase particle size is < 75 micron
- No over pressure (done at atmospheric condition)
- Minor leaks
- Agitation failure could lead to bad consequences

- No flammable liquid/gas/solids in use or stored for the process
- Reaction conditions are same for all 6 methods
- In terms of toxicity, HF of concentrations >10 wt.% have same amount of toxicity

As seen in **Figure 2.6b**, the synthesis route using 10 wt % or higher HF is the most hazardous, and the routes using *in situ* production of HF using LiF and HCl, F_3Fe, and HCl are relatively less hazardous. Etching with HCl and NaOH is the least hazardous. However, it is important to note the quality and yield of $Ti_3C_2T_x$ produced varies significantly between these methods. There is no standard method to report the yield of $Ti_3C_2T_x$; nevertheless, in this paper the yield from each synthesis route is estimated using experimental masses and final concentrations reported, but the terminal group compositions and final volumes were assumed using previously reported XPS results of similar etching methods and yield images. The yields were categorized relative to each other as high (> 55%), medium (15% to 55%), or low (<15%). The synthesis routes using HF and *in situ* HF (*i.e.,* HCl/LiF, and F_3Fe/HCl) have the highest yields, methods using NaOH have medium yields, and methods using HCl and NH_4NF_3 have the lowest comparative yields.

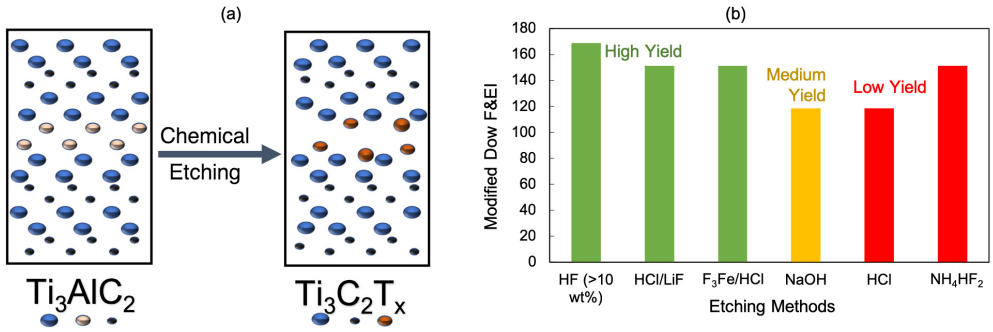

Figure 2.6: (a) Schematic of Ti_3AlC_2 MAX phase etched to $Ti_3C_2T_x$ MXene; (b) Relative hazards of various etchant used to etch Al from Ti_3AlC_2 phase to $Ti_3C_2T_x$ phase, methods using HF [57, 58], HCl/LiF [59], and F_3Fe/HCl [61] has a high yield (>55%, green bars), NaOH [62] has medium yield (15%<x<55%, orange bars), and HCl [63] and NH_4HF_2 [60] has a low yield (less than 15%, red bars) described by many authors, including Ghidiu *et al.* [59] [1].

The most common method of $Ti_3C_2T_x$ synthesis from Ti_3AlC_2 is via HCl and LiF as this method retains a high yield of MXenes and minimizes handling of HF during the etching process.However, it should be noted that HF is still present in the reaction as a by-product in this method and appropriate caution should be taken. The process is overviewed in **Figure 2.7**, where 6 M HCl solution is charged in a teflon reactor with 5 M equivalent of LiF, and powdered Ti_3AlC_2 phase is added to the solution slowly to minimize bubbling of the reaction (this procedure is described by many authors, including Ghidiu *et al.*) [59]. This reaction is exothermic, and Sharma *et al.* determined the heat of reaction (ΔH_{rxn}) from the Ti_3AlC_2 phase to $Ti_3C_2T_x$ using a calorimeter [65]. The study reported ΔH_{rxn} to be -1775 kJ/mole of Ti_3AlC_2 (equivalent to -9.12 kJ/g of Ti_3AlC_2) phase. Based on this reaction enthalpy, if all of the Ti_3AlC_2 MAX phase is added to the reaction mixture at once, the adiabatic temperature increase is estimated at 270 °C of the solution. This temperature increase was estimated using Equation 1, where *m* is the mass of a small industrial-scale reaction mixture (500 g of Ti_3AlC_2 phase) using the HCl/LiF *in situ* method. The heat capacity of solution, C_p used for calculation is same as that of 37 wt % HCl (2.46 kJ.K/kg) because in a typical synthesis around 86 wt % of the reaction mass is HCl solution, and $\Delta T_{(ad)}$ is the adiabatic temperature increase.

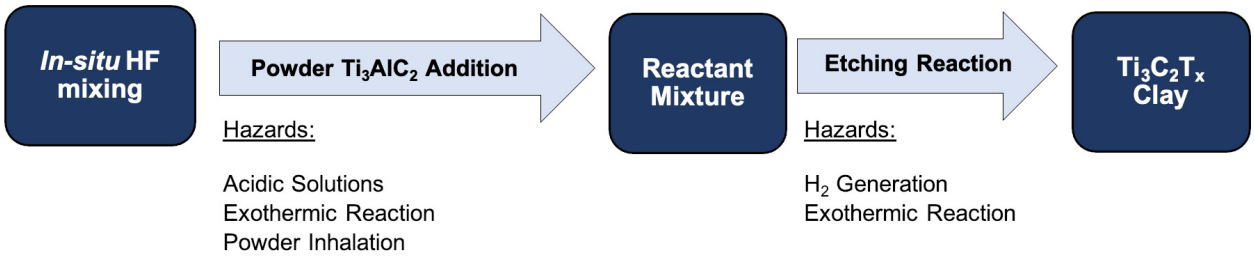

Figure 2.7: Schematic of $Ti_3C_2T_x$ MXene synthesis using LiF/HCl etchant and the hazards associated with these steps [1].

$$\Delta H = mC_p\Delta T \tag{2.1}$$

The $\Delta T_{(ad)}$ is beyond the boiling point of HF solution which is between 98 °C (for 5 wt % HF) and 110 °C (for 50 wt % HF). If the reaction is carried out at room temperature (around 23 °C), the $\Delta T_{(ad)}$ is sufficient to trigger violent boiling off of the reaction mixture, releasing HF vapor into the environment. To avoid uncontrollable temperature increases during the etching step, the feed rate of Ti_3AlC_2 MAX phase into the reaction mixture and the cooling capacity will be critical. This is especially true when scaling up this reaction as increasing the scale of reaction will likely decrease the reactor surface-area-to-volume ratio, thereby reducing the heat of reaction dissipation. In the case of uncontrollable temperature increase, the use of overhead condenser to cool vapor can also help mitigate release of hazardous vapor into the environment. The condenser should be appropriately sized and designed based on the scale of the reactor mass and volume. An additional hazards analysis, including a detailed kinetics analysis to understand the reaction pathways, is necessary if the presented $Ti_3C_2T_x$ synthesis method is to be scaled up.

Additionally, the etching reaction produces H_2 gas and water vapor as the byproduct. The etching reaction can be described by the following reaction pathway [66]:

$$Ti_3AlC_2 + 3HF \rightarrow AlF_3 + Ti_3C_2 + 3/2H_2$$
$$Ti_3C_2 + 2H_2O \rightarrow Ti_3C_2(OH)_2 + H_2$$
$$Ti_3C_2 + 2HF \rightarrow Ti_3C_2F_2 + H_2$$

The etching reaction produces three and a half moles of H_2 for every mole of Ti_3AlC_2. The calculation is done at isothermal condition at room temperature (25 °C, 298 K). Following recipe is used for the gas volume calculations [66]: 30 mL of 6M HCl, to 2 gm of LiF, 3 gm of Ti_3AlC_2.

The pressure generation accounts only in vapor space of the reactor. Therefore, the volume of the reactor mass is subtracted from the total vapor space available for gas accumulation. To accommodate the generated pressure, the reaction is performed in vented containers. **Figure 2.8** shows the estimated pressure generated by the reaction for a known container volume in an isother-

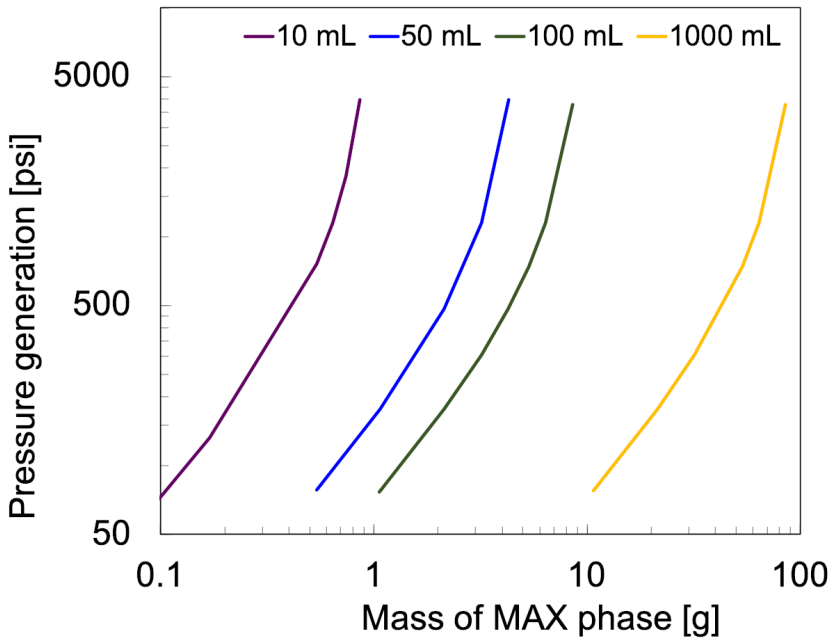

Figure 2.8: Estimated pressure generation during etching process for various container size assuming isothermal conditions. The etching reaction should be carried out in a vented container to relieve pressure buildup and to contain the reaction products [1].

mal condition. It should be noted that the gas generated (H_2) is highly flammable at 4 vol % to 75 vol %, and a static spark is enough to ignite the gas in these conditions [67]. Moreover, hydrogen gas is the one of lightest gas making it easy to escape into the surrounding environment unknowingly. Hydrogen gas burns with invisible flame and an incident involving hydrogen gas can propagate quickly. Therefore, special care should be taken to vent the H_2 gas produced. The rate of H_2 production during the etching process has not been measured at the lab scale, but this will be critical during any sort of scale-up, both for safety and for emissions purposes. **Table 2.2** shows the hazards in the etching step along with recommended corrective and preventive measures in a laboratory scale. As mentioned in the introduction of the paper, there are a number of ways MXenes can be synthesized. This paper focuses on the hazard analysis technique for one synthesis methods in detail. A similar approach can be taken to conduct hazard analysis for other synthesis routes to design safer MXene operating procedures.

Table 2.2: Hazards of Etching Process [1]

Hazard	Cause	Major Effects	Corrective/Preventive measures in a laboratory scale
Exothermic reaction	Rapid Addition of Ti_3AlC_2 to HF Solution	HF gas, H_2 gas, equipment damage	Slow addition of Ti_3AlC_2 to limit the temperature increase, adequate cooling capacity
Toxic gas release (H_2)	Loss of etching reaction controls	Flammable environment	The reaction should be conducted in a negative pressure hood with good ventilation
HF exposure	Outlined in next section		

2.3.3 Hazards Analysis for Post-Processing $Ti_3C_2T_x$ MXenes

The $Ti_3C_2T_x$ product slurry obtained after etching is washed with DI water in a filtration unit (or in centrifugation unit) to remove unreacted HF and water-soluble salts. The washing with DI water is repeated until the pH of the solution is at least 6 to mitigate risk during handling. This bulk product is labelled as $Ti_3C_2T_x$ clay, and there are several post-processing techniques for $Ti_3C_2T_x$ clay discussed in prior literature [35]. The post processing includes delamination to yield MXene nanosheets and further processing for an application. The selection of post-processing techniques depends on the applications of $Ti_3C_2T_x$. Some methods can involve direct handling of the un-delaminated $Ti_3C_2T_x$ clay, such as paint coating [59]. $Ti_3C_2T_x$ can be freeze-dried for long-term oxidation-free storage [68], spray-dried to 'crumple' the morphology thereby increasing the surface area [69], or vacuum-dried to create free-standing $Ti_3C_2T_x$ films. **Figure 2.9** shows different forms of $Ti_3C_2T_x$ used in various applications.

Delamination of the accordion-like clay yields MXene nanosheets, which are currently the most used form of MXenes. Specifically, $Ti_3C_2T_x$ can be delaminated into a thick colloidal suspension of nanosheets then assembled layer-by-layer into flexible biometric sensors [11, 32]. This thick colloidal suspension can also be diluted and mixed with additives (such as platinum nanoparticles) and used in dip- and evaporative coatings [76]. The most popular method of delam-

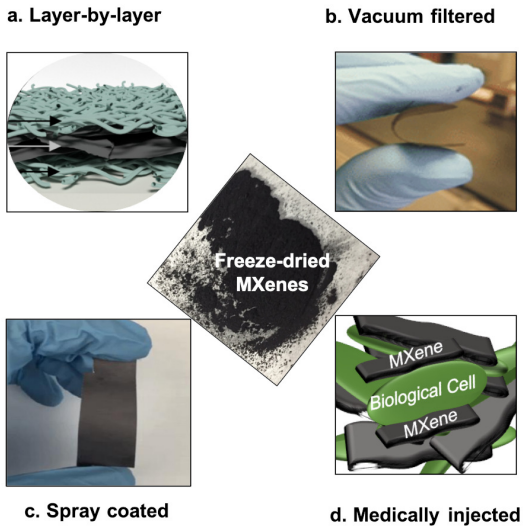

Figure 2.9: Reproduction of images showing $Ti_3C_2T_x$ processed for current applications; (a) Layer-by-layer (for wearable electronics) [32] Reproduced with permission from reference #6. Copyright 2018, AAAS (b) Vacuum filtered (for free-standing films and polymer composites) [35, 70, 71] Reproduced with permission from reference #46. (c) Painted or spray coated (for thin film coatings)[35, 72] Reproduced with permission from reference #47. Copyright 2018, AAAS (d) Medically injected (as antibiotics, drug delivery, and cancer therapy) [73, 74, 75] Reproduced with permission from reference #48. Copyright 2016, ACS, and [1].

ination is intercalation with dimethyl sulphoxide (DMSO) followed by sonication after exfoliation, as this method is relatively quick and can be varied to produce nanosheets of different sizes [59, 77, 78, 79]. Other wet chemical etchants include urea [77], tetrabutylammonium hydroxide (TBAOH), choline hydroxide, and *n*-butylamine [80] for MXene delamination.

The solvents used for both exfoliation and delamination are vital in selecting the composition of terminal groups of the MXenes [81], but of more direct pertinence to this paper are the safety concerns associated with each solvent. DMSO and urea are the safest chemical solvents to implement, with the primary hazard associated with both being irritation from inhalation, ingestion, or eye contact. Possible absorption through skin is a special safety concern, particularly for DMSO, as all of these solvents may bring nanoparticles or other chemical constituents with them. MXenes have not had a long-term biological impact study performed, so operators should avoid contact

with skin. Harsher solvents like TBAOH, choline hydroxide, and *n*-butylamine, cause severe burns when exposed to skin or eyes. Further, all of these harsher solvents, especially *n*-butylamine, can prove fatal if inhaled. All chemical solvents listed range from slightly to highly flammable, and so exposure to electrical sparks or other ignition sources should be carefully avoided. Moreover, disposal hazards should also be considered.

Inadequate washing of $Ti_3C_2T_x$ solution can expose researchers and lab equipment to HF during the post-processing steps. Furthermore, F^- ions can propagate in the final product such as paints, powder, films. Precautions should be taken when handling any nanomaterials, especially in powder form as fine powder can disperse in the environment without detection. Several *in vivo* and ecotoxicological studies have shown non-cytotoxic behavior of several MXenes, including $Ti_3C_2T_x$, but a long-term systematic analysis is still needed. MXenes are a promising chemo-synergistic and photo-thermal conversion material for cancer treatment, but control of the terminal groups and complete removal of -F ions is paramount. Despite these promising findings, biological interactions of MXenes are still not yet fully known [82, 83, 84, 85].

2.3.4 Hazards Analysis for HF Handling and Removal

The medium and high yield MXene methods are obtained by etching via HF, either from stock solution or produced *in situ*. Due to the relatively common usage of HF, it is important to look at its hazards individually. HF is an extremely corrosive chemical, able to penetrate through skin, muscle tissue, and bones. In the presence of naturally-occurring cations in the human body (such as calcium and magnesium), HF dissociates into hydrogen ion and fluoride ion. These ions can cause harm in two ways: (1) corrosive burns due to hydrogen ions and (2) chemical burns in skin and bone due to fluoride ions [86]. More importantly, these ions can affect the biological distribution of electrolytes causing death [87]. For example, in 1994, a lab technician died due to fluoride poisoning when he spilled 100 mL of 70 wt % HF [88]. The spill covered about 10 % of his body. At least 20 incidents of HF exposure have occurred since 1998 [89].

HF must be securely contained, which can pose a major challenge due to its corrosive nature [90]. HF corrodes common material of construction for laboratory equipment such as stainless

Table 2.3: Hazards with HF Handling and Removal [1]

Hazard	Cause	Major Effects	Corrective/Preventive measures in a laboratory scale
HF exposure (in solution or fume)	Improper handling of HF solution during transfer	Exposure to HF can lead to serious injury or death	Proper PPE (HF rated gloves, facemask, full sleeve clothing)
	Improper handling of HF waste		Easy access to calcium gluconate ointment near work area in case of HF exposure
	Failure of reaction or storage container	Exposure to human	Use HF compatible containers and sealant. Use secondary container

steel and glass. Few materials are compatible with HF: for laboratory purposes PTFE (or teflon) is known to be the most resistant to HF, followed by HDPE (high-density polyethylene).

The primary sources of HF exposure during $Ti_3C_2T_x$ synthesis are during the etching reaction itself and the transferring of the HF solution during washing. According to ISD principles, there is a present need to find a high-yield etching method without using HF. However, to mitigate exposure to HF using current methods, time spent adding and removing HF solution should be minimized or automated. During direct handling, proper personal protection equipment (PPE) is vital. The recommended PPE to handle HF solutions is neoprene gloves, acid resistant face shield, full-body acid resistant suit, and leather boots. In case of HF exposure, it is important to neutralize the fluoride ions with calcium or magnesium ions: application of a 10 wt % calcium gluconate solution is recommended in the exposed area. Best laboratory practices should also be followed to avoid and minimize HF exposure. **Table 2.3** summarizes the hazards with HF, including the recommended corrective and preventive measures.

Inhalation of HF vapor can also cause harm to human health. HF inhalation could be due to exposure to HF solution (>50 wt %), exposure in a confined space, or exposure through contaminated

clothing. According to the EPA, the 15 min. STEL (short-term exposure limit) for HF vapors is 6.0 ppm for 15 minutes, and OSHA regulates the 8-hour TWA (time-weighted average) to 3 ppm[91]. At concentrations of 30 ppm, it is considered immediately dangerous to life and health (IDLH) [92]. To adhere to the OSHA and the EPA standards, the $Ti_3C_2T_x$ solution needs to be washed to pH 6 or higher for safer handling of the solution.

2.3.5 Waste Treatment

An important aspect of process scale-up is also considering waste disposal. The etching and washing steps in $Ti_3C_2T_x$ produce a considerable amount of waste though exact quantities of various elements in the waste stream is not known. Based on the synthesis scheme, there are three different classes of waste produced during $Ti_3C_2T_x$ synthesis, acidic waste from LiF/HCl (majority), metal waste from Ti and Al, and solid particulate such as C, under- or over-etched Ti_3AlC_2 particles. Any waste treatment facility would have to be prepared to deal with these three kinds of waste and its associated hazards. Hu *et al.* proposed that using calcium salt to neutralize acidic water and then using an electrocoagulation-flotation technique where sodium dodecyl sulfate as an anodic surfactant is best to remove fluoride-based waste [93]. Similarly, Westerhoff *et al.* suggested that Ti-based and nanoparticle waste can be trapped using a biological treatment then settling and removing using a membrane filtration [94]. A typical amount of Al and Li in the waste stream from $Ti_3C_2T_x$ etching process is not known but these metals can be recovered on a larger scale, if necessary. **Figure 2.10** shows a schematic of waste water treatment from the s in the waste stream is not known. Based on the synthesis scheme, there are three different classes of waste produced during $Ti_3C_2T_x$ MXene synthesis.

2.4 Conclusions and Future Outlook

In conclusion, this study has identified the hazards associated with $Ti_3C_2T_x$ laboratory production and discussed the preventive, mitigating, and emergency response plan. In MAX phase synthesis, most hazards are associated with dust handling, including both reactant and post-synthesis processing. Alternative milling methods could drastically increase safety, though the high hard-

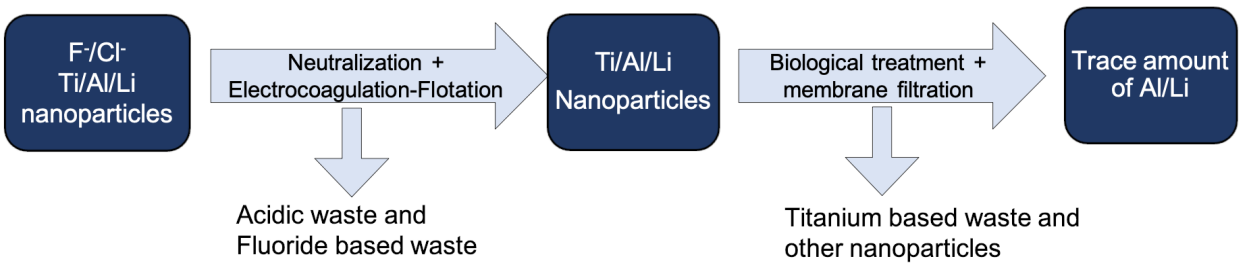

Figure 2.10: Schematic showing waste water treatment technology from $Ti_3C_2T_x$ MXene synthesis [1].

ness of the bulk sample prevents many conventional methods. Additionally, the combustible dust property of Ti_3AlC_2 MAX phase is not known. Further study is required to understand the probability of and risk associated with dust explosions of Ti_3AlC_2 MAX phase before this process can be scaled up.

Etching the aluminum layer from MAX phase to synthesize $Ti_3C_2T_x$ MXenes is highly exothermic and thus poses a significant hazard even in small batch sizes. If the Ti_3AlC_2 MAX phase is added too quickly, the increase in reaction temperature can cause the reaction to become violent and HF (or other chemical etchant) to boil, resulting in corrosive splashing and increasing the concentration of toxic fumes produced. Mechanism and kinetics are not fully understood for etching MXenes, and thus many hazards may not be fully addressed. For example, if the etching reaction produces thermally unstable by-products, the ability to mix and cool the reaction becomes paramount for scaling up to industrial batch sizes. The etching methods with the highest reported yields to-date use HF but an alternative method needs to be explored because HF is extremely toxic and unsafe. However, if HF is selected as the etchant, containment of HF is paramount but challenging as it corrodes most conventional containers, particularly in industry. A detailed worst-case scenario should be considered, and an effective emergency response plan should be in place.

Further, if the $Ti_3C_2T_x$ clay is not properly washed, HF hazards may persist through every step of the post-process. Finally, more research is required to fully understand the long-term biological impact of MXenes. As suggested by Fadeel *et al.*, an increase in the surface area of a nanostructure, especially with hazardous functional groups such as fluorine, may cause severe inflammation and

irritation in and on human tissues [29].

This study only provides general process safety considerations for the most commonly used MXene. Each application may elicit different synthesis methods, and specific processing steps may be more hazardous than those typical steps described above. Specifically, different compositions (i.e. using a different parent MAX phase) often require different etching conditions, which can increase the hazards associated with handling and washing.

3. CALORIMETRY OF EXPLOSIVE THERMAL DECOMPOSITION OF GRAPHITE OXIDE[1]

3.1 Introduction

Industrial and academic interest in graphene has grown substantially since its discovery in 2004 [95, 96, 97]. Graphene has a high thermal and electrical conductivity and therefore, it is used in applications such as conductors, energy storage devices, batteries, sensors, and others [98, 99, 100, 101]. Because of the promising development in graphene-based applications, interest in scaling-up graphene is also increasing.

Current methods to produce graphene such as exfoliation and chemical vapor decomposition are not economical [102]. However, one method to mass-produce graphene-like material economically and consistently is via the graphite oxide (GO) route. The GO route has gained prominence in recent years because it has shown potential for bulk production at high yield [103]. There are several GO synthesis routes, and the modified Hummers method is the most popular [16, 104]. This route involves the oxidation of graphite into graphite oxide and exfoliation using a sonicator to produce graphene oxide. Finally, graphene oxide is reduced thermally or chemically to decrease oxygen content. The reduced GO produces a graphene-like material referred to as "reduced graphene oxide (rGO)".

Since GO's isolation in the 1850s, the energetic nature of GO has been well documented [21, 105, 106]. Energetic materials, in general, can decompose violently if they are improperly stored or handled [107]. Two of the most recent examples of such incidents are the West Fertilizer Company explosion in West, Texas [108, 109] and the Tianjin explosion in China [110, 111], both involving ammonium nitrate. The literature in the area of GO energetics has highlighted its potential to violently decompose [112, 26, 113, 114, 98, 103]. In fact, Rodriguez *et al.* showed that when GO is heated, it decomposes in three stages: (1) the endothermic stage with evolution of water vapor at

[1]Text, figures, and tables in this chapter are reprinted with permission from "Calorimetry of explosive thermal decomposition of graphite oxide" by Lakhe, P., Kulhanek, D. L., Sun, W., Zhang, B., Green, M. J., & Mannan, M. S. (2019). Journal of hazardous materials, 366, 275-281, Copyright 2018 Elsevier

80 °C; (2) the exothermic stage where GO decomposes to CO_2, CO, and H_2O at 200 -240 °C, (this step is also known as thermal reduction of GO); (3) the internal combustion of GO in presence of air at temperatures above 530 °C [106]. Therefore, it is crucial to understand the hazards associated with bulk GO to avoid any potential safety incident during storage and handling of the material.

Kim *et al.* showed that local heating of GO can trigger rapid decomposition throughout the sample mass. Such rapid decomposition of GO resulted in large volume expansion and produced low-density rGO. Sample heating, exposure to flame, or even a camera flash can trigger this rapid decomposition of solid GO [112]. The paper by Krishnan *et al.* also reported that when GO was heated on a hotplate, it underwent explosive decomposition within a few seconds releasing H_2O and CO_2 and the initial GO produced a "puff of black plume of r-GO." [26]

Qiu *et al.* compared GO decomposition enthalpy to industrially known energetic materials to provide a perspective of GO energetic behavior. GO decomposition enthalpy is between 1400 - 1700 J/g, comparable to benzoyl peroxide at 1602 J/g and trinitrotoluene at 2305 J/g [113]. Additionally, in 2016, Qiu *et al.* concluded that the explosive thermal decomposition of GO is a function of mass because at higher masses the reaction rate is higher than the heat transfer rate to the surrounding environment[114]. The excess heat from reaction will lead to local self-heating and thermal runaway of the sample. The authors determined thermo-kinetic data such as reaction order and activation energy using Differential Scanning Calorimetry (DSC). The thermo-kinetic data were used to numerically solve for the critical temperature at which GO decomposes explosively in non-adiabatic conditions for a given mass. However, this numerical prediction needs to be validated with experimental data; which is discussed in detail below.

All the prior thermo-kinetic analysis of GO decomposition reported in the literature were performed using micro-calorimeters such as DSC which use few milligrams of material. DSC is a quick screening method to determine thermal hazard of materials early in the process. When the mass of a material increases, the thermal hazard of the material may also change. Although the intrinsic-kinetic properties remain the same, increasing size introduces uncertainty due to the heterogeneity of the material, hotspots, and decreased surface-area-to-volume ratio [115]. Therefore,

the data from DSC may not necessarily predict the behavior of GO at large scale accurately.

In this study, the pseudo-adiabatic calorimeter called Advanced Reaction System Screening Tool (ARSST) to study the thermal behavior of GO between 0.2 g to 0.5 g. Using the data from ARSST, the trend of detected "onset" temperature, T_{onset} with the mathematical model proposed by Qiu *et al.* are compared and T_{onset} of commercially available GO synthesized using the modified Hummers method is compared to the laboratory synthesized GO. Most importantly, pressure release rate during GO decomposition are quantified in this study, which has not been reported in literature to date. The effect of surface area of GO is also studied by changing the drying method to determine the critical mass necessary for GO to decompose explosively. Finally, the critical mass predicted by the Frank Kamenetskii model is compared to experimental results. The results from this study are beneficial in assessing the hazards of bulk GO during storage and handling.

3.2 Method and Experimental Setup

3.2.1 Graphite Oxide Preparation

Graphite oxide was prepared using a modified Hummers Method without pretreatment of the graphite [23]. Graphite was obtained from Bay Carbon Inc. Potassium permanganate, hydrogen peroxide, and 95-98 % sulfuric acid was obtained from Sigma Aldrich. The graphite oxide solution was washed 3 times with 10 % HCl to remove salt byproducts. 37 % HCl was obtained from Sigma Aldrich and mixed with distilled water to create the washing acid. The solution washed with distilled water until the pH was neutral at 4.5. The sample was either dried under vacuum in an oven at 40 °C for 24 hours or freeze-dried (Vitris Benchtop Freeze Dryer) for approximately 72 hours to yield a dry GO powder.

3.2.2 Thermal Decomposition Analysis

Thermal analysis of GO was conducted in the Advanced Reactive System Screening Tool (ARSST) manufactured by Fauske and Associates, Burr Ridge, IL. The ARSST is an open test cell capable of handling chemical system for temperature as high as 500 °C and pressure up to 500 psig. Therefore, ARSST is ideal to conduct experiments for up to a few grams of energetic material.

The schematic of ARSST is shown in **Figure 3.1a**. The GO sample was heated at a constant rate of approximately 6 °C/min. The sample cell is a glass test cell with a volume of 10 ml, which is placed inside a stainless-steel vessel of volume 350 ml. A thermocouple and pressure transducer tracked the dynamic temperature and pressure changes during the decomposition process. The pressure transducer was located outside the glass test cell in 350 ml vessel and for each test the thermocouple touched the sample mass.

It should be noted that the data collection rate for ARSST is every 30 s or sooner if it detects a temperature chance of 2 °C or a pressure change of 2 psi. The decomposition reaction occurs rapidly as seen in **Figure 3.1b**. Therefore, there is a possibility the data collection is not fast enough to truly capture the temperature and pressure generation rates.

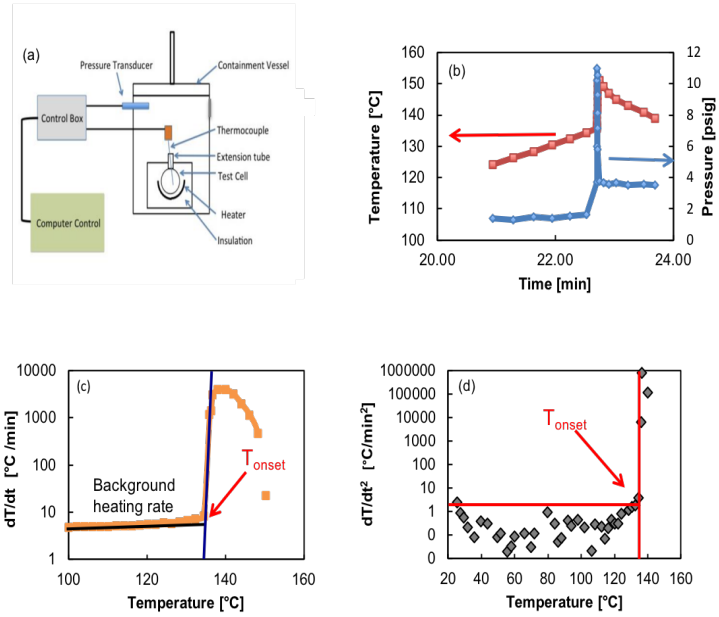

Figure 3.1: (a) shows the schematic of the Advanced Reactive System Screening Tool (ARSST). The dynamic temperature and pressure are shown in (b). The explosive decomposition is marked by sudden increase of temperature and pressure as seen around 22.5 min in (b). The graph of dT/dt vs Temperature in (c) and dT/dt vs Time in (d) is used to determine the detected T_{onset} - temperature at which GO decomposes explosively [2].

The sample is placed in an open test cell weighing around 1.34 g and a heater belt is used

to heat the sample. The sample is further insulated using aluminum foil and insulating fiber. A standard type-K thermocouple with accuracy of $\pm$ 2.2 °C is used to measure the temperature and a pressure transducer of 0.5 % accuracy is used in the experimental setup. An average heating rate of 6 °C/ min was applied to the sample until an explosive decomposition was seen or the sample temperature reached 250 °C. The T_{onset} is determined when the data points in **Figure 3.1c**.and **Figure 3.1d**. is higher than 3°C/min^2. In a perfect scenario, the dT/dt^2 should be 0 °C/min^2 up to the explosive decomposition, however due to noise in thermocouple data, the threshold value of 3 °C/min^2 was chosen to avoid false "onset" detection due to external heating. Additional information on the "T_{onset}" detection can be found in Zhu *et al.* and Golubkov *et al.*[116, 117].

3.2.3 Characterization

3.2.3.1 Thermogravimetric Analysis

The water in GO sample and mass loss due to GO decomposition were measured using a Q50 thermogravimetric analyzer (TGA) from TA Instruments, New Castle, DE. The measurements were done in a nitrogen environment. The sample was heated from room temperature to 250 °C at a constant value of 5 °C/min and held at the isothermal condition for 30 minutes at 110 °C. The final GO mass was measured after cooling to 50 °C.

3.2.3.2 Surface Area Analysis

The surface area of GO was determined using Brunauer-Emmett-Teller (BET) theory. The measurements were carried out in Micrometric ASAP2010 system. The samples were pre-treated under vacuum for 12 hours at 70 °C.

3.2.3.3 Elemental Analysis

The oxygen content and metal impurities in GO samples were determined using Fast Neutron Activation Analysis (FNAA) technique. In this technique, the atoms in the material are converted into radioactive atoms. When the radioactive atoms decay, they emit unique radiation that identifies the atom. This method can provide qualitative and quantitative analysis of elements present in a sample [118]. All the testing was done in the Elemental Analysis Lab at Texas A&M University,

College Station, TX.

3.2.3.4 Thermal Conductivity Measurement

The thermal conductivity of graphite oxide was measured using a TPS 2500S hot disc thermal constants analyzer from Thermtest Inc., Canada. A Kapton sensor of 2 mm radius was used for the analysis. A heating power of 8 mW was applied for 10 seconds to the sample at room temperature of 20.1 °C. An average thermal conductivity value after 4 tests were used for the analysis.

3.3 Results and Discussion

3.3.1 Thermal Decomposition of GO

In this study, GO was synthesized using the modified Hummers method and dried in a vacuum oven at 40 °C for 24 hours. The thermal stability experiments were conducted in an ARSST with GO mass at least two to three orders of magnitude higher than previously reported sample sizes. The explosive decomposition of GO is marked by a rapid increase in temperature and pressure of the sample. The T_{onset} is defined as the temperature at which the system (ARSST) detects a rapid increase in temperature and pressure. The T_{onset} for the ARSST system in this study is the temperature at which the second derivative of dT/ dt with time is greater than 3 °C/min^2. In a perfect scenario, the dT/dt^2 should be 0 °C/min^2 up to the explosive decomposition, however due to noise in heating rate and thermocouple data, the threshold value of 3 °C/min^2 was chosen to avoid false "onset" detection due to external heating. A detailed explanation is shown in the supplementary information (SI).

Figure 3.2a shows a negative correlation between T_{onset} with increasing GO mass. The mass was varied from 0.2 g to 0.5 g and noticed T_{onset} decreased from 144 $\pm$ 8 °C to 128 $\pm$ 6 °C respectively. The experiments were repeated four times for each data point to account for uncertainty in the measurement. The correlation between T_{onset}, ΔP and dP/dt with varying mass are statistically significant. The details on the statistical test is shown in SI. Based on the experimental result, the rate of change of T_{onset} with increasing mass was -18 °C/g. The negative correlation between T_{onset} with a mass of GO is consistent with the theory: as the mass of GO increases, the

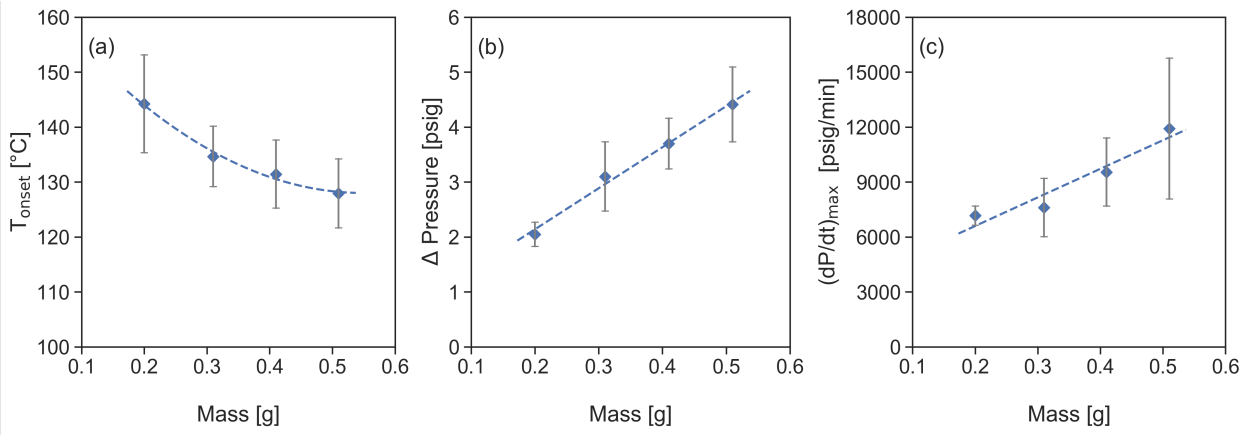

Figure 3.2: Experimental data for thermal decomposition of GO synthesized using the modified Hummers method. The GO was dried in vacuum oven. (a) Shows T_{onset} with varying GO mass. T_{onset} is defined as the temperature at which GO decomposed explosively. (b) Shows pressure generated due to non-condensable gasses generated during GO decomposition. (c) Shows the maximum pressure generation rate during GO decomposition with varying GO mass [2].

rate of reaction increases producing heat and releasing gaseous products. Due to the limited heat transfer from the material to the environment, the excess heat feeds into the reaction, thus making the reaction proceed rapidly resulting in explosive decomposition of the material.

The correlation between T_{onset} vs. mass, Δ P vs. mass, and change in pressure with time (dP/dt) vs. mass shown in **Figure 3.2** was analyzed using statistically analysis software SPSS. The trend observed in **Figure 3.2** is statistically significant as seen in one-way analysis of variance (ANOVA) calculation. The results of ANOVA uses SPSS software is shown in **Figure 3.3**. The significant value of less than 0.05 indicates that the data is statistically significant.

Qui *et al.* (2016), proposed a differential energy balance model to predict the T_{onset} of GO [114]. Equations 3.1 and 3.2 were solved simultaneously to solve for a temperature at a given mass above which the GO observed significant temperature increase. This temperature is called the critical temperature (or T_{onset}). **Figure 3.4** shows the trends of T_{onset} with varying mass which hS is known.

ANOVA

		Sum of Squares	df	Mean Square	F	Sig.
Tonset	Between Groups	589.360	3	196.453	4.206	.030
	Within Groups	560.525	12	46.710		
	Total	1149.885	15			
DelP	Between Groups	11.944	3	3.981	14.148	.000
	Within Groups	3.377	12	.281		
	Total	15.321	15			
dPdt	Between Groups	56336508.349	3	18778836.116	3.580	.047
	Within Groups	62949014.341	12	5245751.195		
	Total	119285522.690	15			

Figure 3.3: The figure is the output table obtained from SPSS software for analysis of variances. The significant calculation for T_{onset}, Δ P and dP/dt with varying mass is below 0.05, therefore indicating these data statistically significant [2].

$$\left(\frac{dx}{dt}\right) = Ae^{\left(\frac{E_a}{RT}\right)}(1-x)^n \tag{3.1}$$

$$mC_p\frac{dT}{dt} = -m\Delta H\frac{dx}{dt} - hS(T-T_o) \tag{3.2}$$

where, x is the conversion, t is time, A is exponential factor, E_a is activation energy, n is the reaction order, m is the mass of GO, C_p is heat capacity of GO, T is the temperature, T_o is temperature of surrounding, ΔH is heat of reaction, h is convective heat transfer coefficient, and S is the lateral surface area of bulk GO exposed to surrounding. The thermo-kinetic parameters were solved by the authors using DSC and Kissinger equation and the detail analysis can be found in Qiu *et al.* (2016) [119].

The rate of reaction dx/dt in Equation 3.1 was calculated using the Arrhenius equation, *m* is the mass of reactant, C_p is heat capacity, ΔH is heat of reaction, and T_o is the temperature of the surrounding. The graphical solution to Equation 3.2 reproduced from Qiu *et al.* is available in **Figure 3.4**. The slopes predicting the T_{onset} were generated by solving Equation 3.1 for a range of hS. The resulting slopes are shown in **Table 3.1** along with experimental result from the current

study.

Table 3.1: Change in T_{onset} with increasing GO mass [2]

Determination technique	hS [W/K]	slope
Model [114]	0.0013	-0.925 °C/g
	0.049	-10.85 °C/g
	0.49	-12.21 °C/g
Experiment (this study)	0.019	-18.00 °C/g

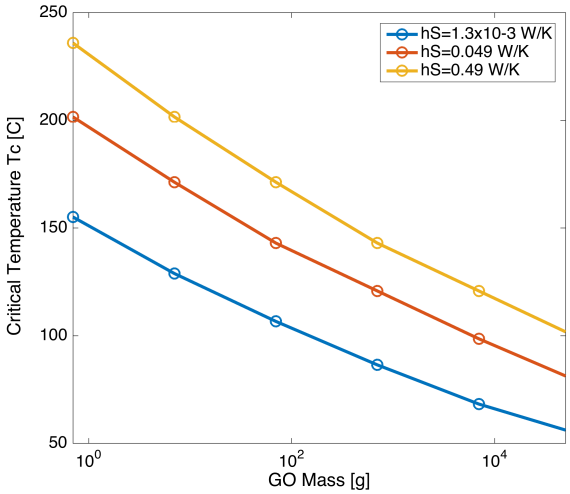

Figure 3.4: Reproduction of T_{onset} calculation from differential energy balance [114] [2].

The result indicates stronger dependency of T_{onset} with mass than previously predicted. The maximum hS for the study was 0.019 W/K. The detected T_{onset} for the ARSST system and mass dependency is stronger because the model assumes homogeneous solid with uniform temperature distribution. However, the heat transfer in bulk GO is non-uniform and the probability of hotspots in higher. In addition, the system for this study is pseudo-adiabatic and the heat transfer to the surrounding is minimum. Therefore, the self-heating of GO is accelerating the explosive thermal decomposition of GO in the system.

Furthermore, as we increase the mass increases, pressure after GO decomposition should also increase. **Figure 3.2b** shows that pressure generated due to GO decomposition increases linearly with GO mass. In fact, pressure increased at a rate of 7.44 psig/g. As we increase the mass, we expect to see an increase in pressure after GO decomposition. The amount of pressure generated at the end of GO decomposition corresponds to 40 wt% mass loss of initial GO. This result agrees with mass data from Thermogravimetric Analysis (TGA) and literature [26].

Previous literature in the area of thermal stability of GO made no attempt to quantify the pressure generation rate during rapid decomposition of GO. This study quantified the pressure release rate and **Figure 3.2c** shows the maximum pressure release rate during explosive decomposition. The maximum pressure release rate is thousands of psig per minute and this rate is for material less than a gram. Based on these data, if large quantities of GO stored in a closed container decomposes suddenly, the effect of pressure generation could be catastrophic depending on the quantity of GO and the size and container it is store in.

3.3.2 Thermal Decomposition of Commercial GO

Further, the explosive decomposition of two commercially available GO was compared with that of GO synthesized in the laboratory. All three GO were prepared using the modified Hummers method, however, the exact parameters used to synthesize commercial GO are not available, especially for the washing step. The commercial GO were bought from Graphenea, Spain and The Sixth Element Inc, China, labelled commercial GO-A and commercial GO-B respectively. The commercial GO-A was supplied in a powder form and the initial water content was 19 wt %, therefore, the GO was dried under vacuum at 40 °C for 4 hours. Similarly, the commercial GO-B was supplied as a wet powder in 55 $\pm$ 5 wt% water. The GO was dried under vacuum for 24 hours at 40 °C. The thermal decomposition data for GO synthesized in the lab is shown in **Figure 3.5a** and **Figure 3.5b**, commercial GO-A is shown in **Figure 3.5c** and **Figure 3.5d**, and the thermal decomposition data for commercial GO-B is shown in **Figure 3.5e** and **Figure 3.5f**. For a sample mass of 0.50 g, the T_{onset} for commercial GO-A was 116 $\pm$ 1 °C, for commercial GO-B was 100 $\pm$ 2 °C compared to the T_{onset} for GO synthesized in the lab at 128 $\pm$ 6 °C. The T_{onset} of commercial

GO-B is lowest as shown in **Table 3.2**. In order to understand the cause of the difference in T_{onset} of the GO, a detailed analysis of the materials was done, and the result is tabulated in **Table 3.2**.

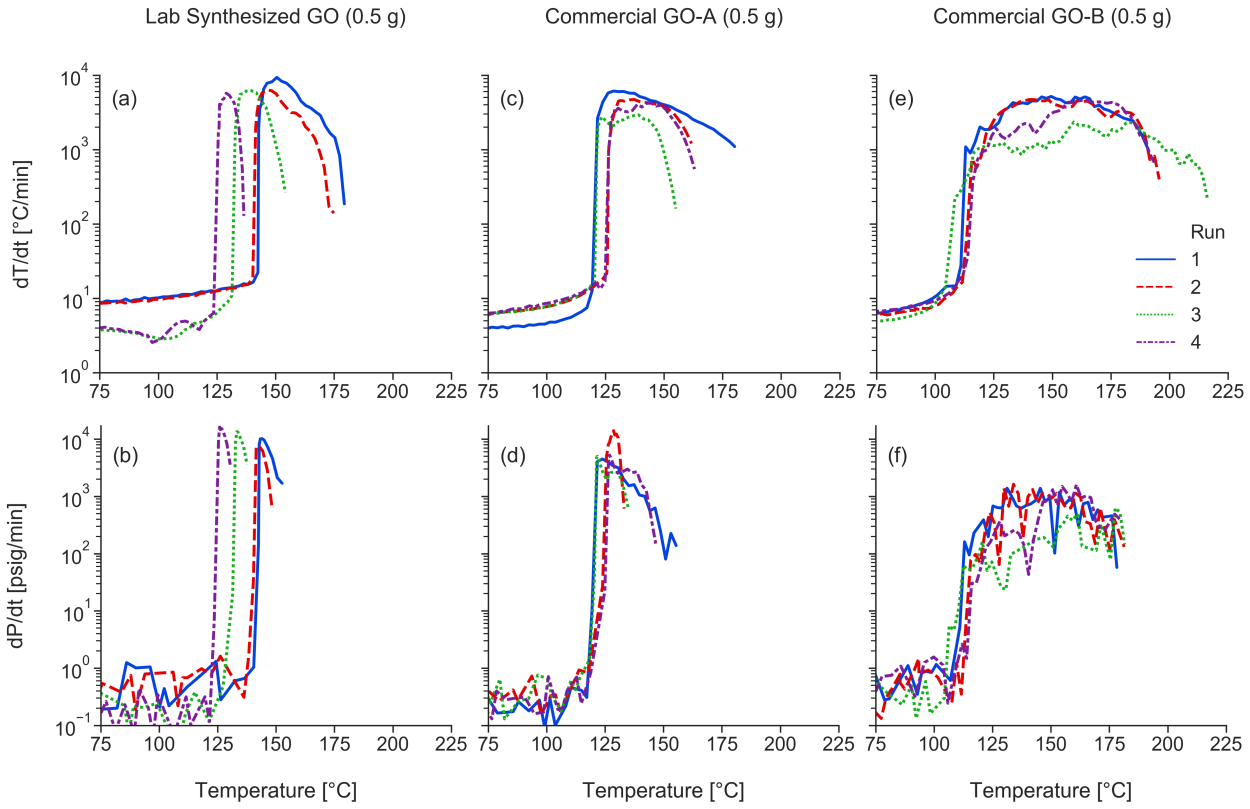

Figure 3.5: Experimental data for thermal decomposition of GO synthesized using modified Hummers method and commercial GO. The 4 runs are repeated experiments for 0.5 g each. (a) and (b) are for GO synthesized in lab and, (c) and (d) are for commercial GO-1 and (e) and (f) are for commercial GO-2. The average heating rate of 6 °C/min was applied for all the tests. Explosive decomposition was seen for all GO with temperature increase rate of 1000s °C/min (Figures a, c, and e). The pressure increase rate for GO synthesized in lab and commercial GO-A (b and d) is 10 times higher than the commercial GO-B (f) [2].

The presence of potassium salt impurity was monitored because it is the most common impurity present in GO and there are a few literature studying the effect of metal salt impurities on the decomposition of GO at temperatures between 100 °C - 200 °C. Yuan *et al.* reported potassium salt impurities in GO increase the heat release during thermal decomposition of GO but the authors

do not mention if the potassium content effects the decomposition temperature [120]. However, Qiu *et al.* reported that the presence of potassium salt impurity only effects the combustion of rGO in air at temperature over 500 °C. They further concluded that increasing hydroxyl ion (or pH) before drying decreases the thermal stability of GO, thus lowering the T_{onset} of GO and not the presence potassium salt impurities [114]. In their study, the Δ pH of 10 showed change in onset by 50 °C. The analysis of the commercial GO and GO produced in laboratory shown in **Table 3.2**. indicates that GO synthesized in laboratory has less than 110 ppm potassium salt impurity and higher pH compared to commercial GO-B. The oxygen and water content in all the samples are comparable. Based on literature, higher pH of GO synthesized in laboratory should have lower onset, but the opposite is observed in the experiment. Nonetheless, it is important to note that the difference in pH between the GO synthesized in laboratory and commercial GO-B (Δ pH = 1.5) is significantly less compared to pH difference studied in literature (Δ pH = 10), therefore, the effect of pH on the samples studied in this work is not dominant. It should be noted; the pH of commercial GO-A should not be measured because the material was supplied as solid powder.

Table 3.2: Comparison between GO synthesized in lab and commercial GO [2]

Variable Measured	GO synthesized in lab	Commercial GO-A	Commercial GO-B
T_{onset} at 0.5 g GO	128 $\pm$ 6 °C	116 $\pm$ 1 °C	100 $\pm$ 2 °C
Potassium Salt Content	< 110 ppm	583 $\pm$ 22 ppm	9 $\pm$ 1 wt%
Oxygen Content	37 $\pm$ 2 wt%	47 $\pm$ 3 wt%	39 $\pm$ 3 wt%
Water Content	12 wt%	12 wt%	10 wt%
pH	4.5	Not applicable (solid sample)	3.0
BET Surface Area	12.2 m^2/g	7.0 m^2/g	0.8 m^2/g
Oxygen Content after decomposition	< 10 wt%	23 $\pm$ 2 wt%	26 $\pm$ 10 wt %

Therefore, the surface area of bulk GO has more significant effects on T_{onset} than impurities such as potassium salt or the pH of the material. As shown by BET surface area analysis, GO

synthesized in the lab has a surface area (SA) almost twice larger than commercial GO-A and fifteen times larger than commercial GO-B. The lower surface area limits the materials capability to transfer heat to the surrounding environment. For any material to undergo runaway thermal decomposition, the rate of reaction needs to be higher than the rate of heat transfer to the surroundings. Thus, in case of commercial GO, the lower SA decreases the thermal stability of the material.

In addition, the maximum pressure increase rate for GO synthesized in the lab (**Figure 3.5b**) and commercial GO-A (**Figure 3.5d**) is 10 times higher than for commercial GO-B (**Figure 3.5f**). The difference is due to the degree of reduction of GO. The oxygen content analysis of the residual material after the decomposition - also known as reduced Graphite Oxide (rGO) - showed no detectable oxygen content for GO synthesized in lab whereas for commercial GO-B the oxygen content was 26 $\pm$ 10 wt%. Therefore, the GO synthesized in the lab and commercial GO-A released most of its oxygen as CO or CO_2 as confirmed in the pressure increase rate, and commercial GO-B released only 35 % of its original oxygen content after decomposition.

The analysis thus far was done for dry GO powder. However, GO are often commercially shipped as a wet powder. The commercial GO-B procured for this study was delivered as a wet powder in 55 wt% water. It is noteworthy that in 3 of the 4 tests of the wet GO also underwent explosive decomposition. The rate of temperature and pressure increase for wet GO was in 100s of °C and psig per min, respectively. These rates are significantly lower compared to its dry counterparts. However, the thermal hazard of GO is present even in solution form and caution must be taken while drying GO. Detailed graphs for wet GO are available in **Figure 3.6**.

Figure 3.6 shows ARSST data for wet commercial GO (55 wt% water). Explosive decomposition is seen in three of the four experiments. After water evaporates at 100 °C, explosive decomposition of the material is seen. The maximum temperature and pressure increase rate is 600 °C/min and 600 psig/min respectively. The intensity of explosive decomposition is not as severe as noticed in dry GO.

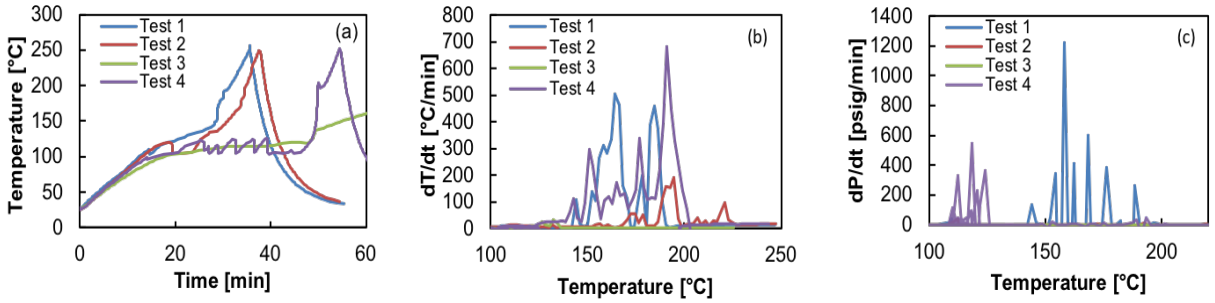

Figure 3.6: (a) is the thermal stability of wet commercial GO (in 55 wt% water). (b) and (c) shows the rate of change of temperature and pressure with temperature of the sample respectively [2].

3.3.3 Determination of Critical Mass of GO

Explosive decomposition of a sample occurs when the rate of heat generated by the decomposition reaction is higher than the rate of heat dissipated into the surrounding environment. For small quantities of GO mass, heat transfer to the surrounding is faster than the heat generated by the decomposition reaction and explosive decomposition is not seen. However, above a certain critical mass, heat dissipation to the surrounding is not fast enough, and the material shows explosive decomposition behavior. Oven-dried GO is compact, with high bulk density and low specific surface area, hence the critical mass necessary for it to undergo explosive decomposition is less than 5 milligrams[113].

The freeze-drying method was used to produce a porous GO with higher surface area (19 m^2/g). The freeze-drying method produces a highly porous dry material because there is no capillary-induced aggregation in the material. Visually, the freeze-dried GO (GO-FD) appears fluffy compared to vacuum oven-dried material.

For a porous material with high surface area, the critical mass at which the material decomposes will be higher than for a material with a low surface area. The experiments were carried out in an ARSST with constant heating of 6 °C/min. For GO-FD, the critical mass was observed to be 60mg. GO-FD masses greater than 60 mg underwent explosive decomposition, which is shown by

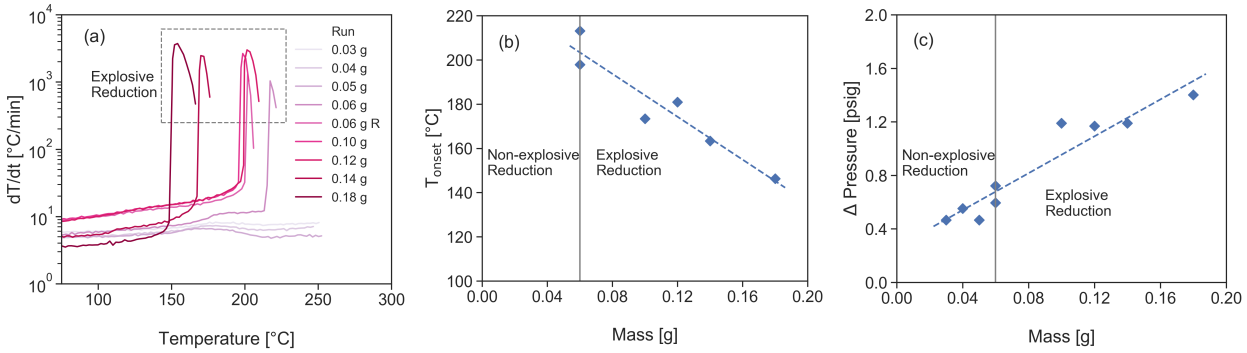

Figure 3.7: Experimental data for thermal decomposition of freeze-dried GO (GO-FD) synthesized using modified Hummers method. (a) Shows the rate of temperature increase with temperature. An abrupt increase in temperature as seen in tests 60 mg and above indicates explosive decomposition of the material. The GO-FD was heated at an average heating rate of 6 °C/min. The critical mass necessary for freeze-dried GO-FD to undergo explosive decomposition is 60 mg in a spherical vessel of 1.34 cm radius. (b) Shows the T_{onset} with varying mass of GO-FD. (c) Shows the pressure generate at the end of experiment. The T_{onset} and pressure generated for GO-FD is consistence with the previous experiments [2].

an abrupt increase in pressure and temperature in **Figure 3.7a**. **Figure 3.7b** and **Figure 3.7c** show the correlation between GO-FD mass and T_{onset} and pressure generated, respectively. The T_{onset} and pressure trends for GO-FD agree with the trends seen in **Figure 3.2** for oven-dried GO.

3.3.4 Frank Kamenetskii Model

In this section, the experimental critical mass of GO necessary for explosive decomposition is compared to the critical mass of GO predicted by thermal explosion theory and models available in the literature. A commonly used model to describe thermal decomposition for homogeneous solids is the Frank Kamenetskii (FK) model. The FK approach assumes a non-homogenous system and assumes the temperature difference between the center of the solid and its surface is the most critical factor for determining explosiveness [121]. In ideal cases, the FK parameter δ combines critical parameters such as reactant geometry, reaction kinetics, heat transfer, and temperature into a single equation to determine critical conditions necessary for explosive decomposition of the material [122, 123, 124].

$$\delta = \rho \frac{q}{\lambda} \frac{E_a}{RT_f^2} d^2 A e^{\left(\frac{-E_a}{RT_f}\right)} \tag{3.3}$$

where ρ is the density, q is the specific heat of reaction, λ is thermal conductivity, E_a is the activation energy, R is the gas constant, d is the characteristic linear dimension in meters, A is the exponential factor, and T_f is the temperature of the vessel. In the experiment, the material was constantly heated using an external heater, therefore T_{kis} (the temperature at which the reaction rate is the maximum) given by Kissinger's equation (Equation 4.4) was used instead of T_f. The heating rate is denoted by b [119]. A heating rate of 6 °C/min used in the model is consistent with the experimental procedure in Section 3.3.

$$\left(\frac{E_a}{RT_{kis}^2}\right) = \frac{A}{b} e^{\left(\frac{-E_a}{RT_{kis}}\right)} \tag{3.4}$$

The FK approximation assumes energy conservation equation in poorly conducting solids with a distributed internal temperature and no resistance to heat transfer at the surface [125]. However, the FK model neglects reactant consumption and assumes activation energy is large. Babushok *et al.* proposed a correction to the FK parameter to account for reactant consumption as shown in the equation below [126].

$$\delta(1-\varepsilon)\{1 - 2.946(1+2\varepsilon)\left(\frac{n}{\Theta_T}\right)^{\frac{2}{3}} + \frac{4}{9}(1+6\varepsilon)\frac{n}{\Theta_T}\ln(\Theta_T)\} = C \tag{3.5}$$

where

$$\varepsilon = \frac{RT_f}{E_a} \tag{3.6a}$$

$$\Theta_T = \frac{E_a}{RT_f^2}\frac{q}{C_p} \tag{3.6b}$$

Here, C is the geometry factor for the critical condition, which for a sphere is 3.32, n is the reaction order, and C_p is the heat capacity. The values used in the Frank-Kamenetskii calculations are ΔH =1600 J/g, A = 1.3×10^{13} /s, and E_a = 147 KJ/mol. This model is most accurate for finite values of activation energy but not for low activation energies [127]. Sanchez *et al.* further worked

on the model proposed by Babushok *et al.* to get an accurate numerical model for evaluation of a critical condition with a low activation energy for thermal explosion. The equation is shown below and was validated for $Ba(TFA)_2$ and $Y(TFA)_2$ systems by the authors [128].

$$\delta(1-\varepsilon)\{1-2.25(1+3.76\varepsilon)\left(\frac{n}{\Theta_T}\right)^{\frac{2}{3}}\} = C \tag{3.7}$$

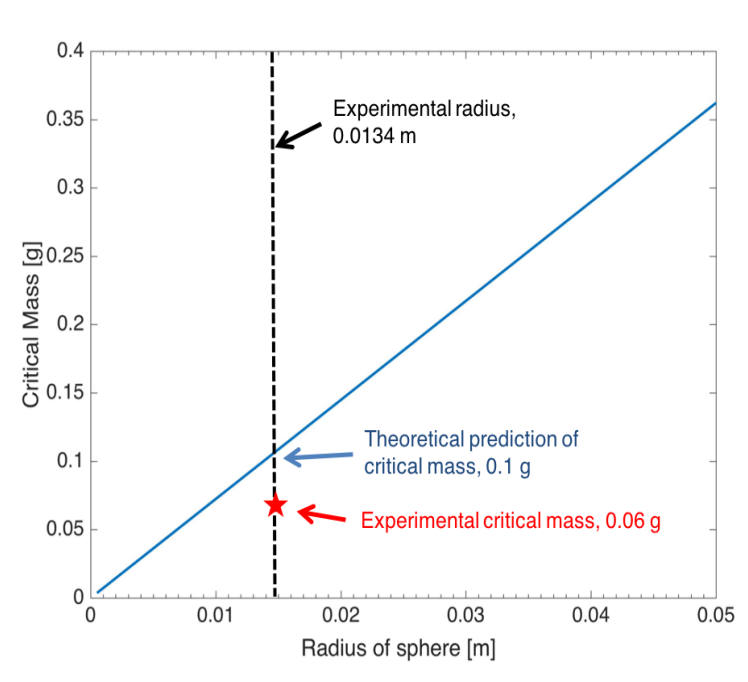

Figure 3.8: This figure shows the critical density and critical mass predicted by solving the modified Frank Kamenetskii's equation (Equation 3.7). The blue line in the graph shows the critical density necessary for GO-FD to undergo explosive decomposition. The black dotted line in the graph represents the corresponding critical mass in a spherical container. The critical density of 9.63 kg/m^3, which corresponds to critical mass of 0.097 g for 0.013 m radius is comparable to experimental critical mass of 0.060 g for same 0.013 m radius [2].

Equation 3.7 is used to calculate critical density necessary for GO to undergo thermal decomposition with increasing radius of a sphere as shown in **Figure 3.8**. Because the ARSST experiments were carried out in an open test cell, the rapid volume expansion of GO during explosive decomposition resulted in mass loss of GO from the test cell. Consequently, the experimental data could not

be used to determine the thermokinetic parameters of the reaction. Instead the kinetic parameters for decomposition in the model such as activation energy and frequency factor were used from literature [114].

The model predicted the critical density necessary for thermal decomposition of GO-FD to be 9.63 kg/m^3 for a sphere of radius 1.34 cm, which corresponds to the critical mass of 0.1 g which is the first point in the graph in **Figure 3.7b**. However, experimentally the explosive decomposition of GO-FD was seen at 0.06 g for a sphere of radius 1.34 cm. The difference in model and experimental result could be a result of the thermal conductivity value used. A thermal conductivity value of 0.44 W/mK was obtained experimentally using hot disc method for GO paste and used in the simulation. In reality, the thermal conductivity will be lower than 0.44 W/mK because the model does not account for sample porosity or void fraction of freeze-dried GO in Section 3.3.3. Increasing void fraction in the GO mass will decrease the thermal conductivity of the material. Lower thermal conductivity will decrease the sample's ability to dissipate the heat to the surrounding environment, therefore, explosive decomposition is observed at a lower mass. Thus, if lower thermal conductivity is account for in the model, the critical sample mass predicted will decrease and further align with the experimental data.

Therefore, the result from the FK model is comparable to the experimental results. The remaining data points in **Figure 3.8** show the predicted critical mass of GO necessary for GO to undergo explosive decomposition in a spherical container. The model assumes the spherical vessel is completely filled with GO. This information is valuable to GO manufacturers to determine the safe transport and storage size for bulk GO. Hence, if the GO morphology and decomposition kinetics are known, the model can predict the critical density and thus the critical mass necessary for the GO to decompose explosively.

3.4 Conclusions

As seen in this study, dry GO with a mass of 0.5 g can release 1000s of psig pressure per minute during its explosive decomposition. The experiments also suggest that bulk GO explosive decomposition can occur at temperatures close to those used in common drying processes *i.e.,*

<150 °C. Furthermore, the decomposition temperature or T_{onset} is negatively correlated with GO mass at a rate of -18 °C/g for this study.

Similarly, a comparison of decomposition of GO from different sources shows that the surface area of GO determines whether it decomposes explosively or not. If the surface area is low, upon heating the rate of reaction dominates the rate of heat dissipation to the surrounding, initiating runaway scenarios or explosive decomposition.

Moreover, high surface area GO was obtained by changing the drying method from oven drying to freeze-drying. In a spherical container of radius 1.34 cm, freeze-dried GO decomposed explosively at a critical mass of 60 mg. The experimental results were compared with the Frank Kamenetskii model, and the model predicted the critical mass to be 100 mg. The discrepancy in the result is due to the high porosity of the sample used in the experiment, which reduces the thermal conductivity of the material, and caused the experimental results to be lower than the prediction.

Finally, precautions should be taken when handling bulk GO in both industry and laboratory settings, especially if the material will be stored in a closed container. The decomposition results of this study can further be used in conducting a risk assessment of bulk GO during storage and transportation by industry interested in producing and shipping bulk quantities of GO.

4. GRAPHENE OXIDE SYNTHESIS: REACTION CALORIMETRY AND SAFETY[1]

4.1 Introduction

Since it was first isolated as a two-dimensional atomic monolayer in 2004, graphene has revealed a broad array of valuable applications ranging from electronic devices to pharmaceuticals to structural reinforcement [129, 130, 131]. Industrial interest in large-scale production of graphene has rapidly increased as these applications approach commercial feasibility [132]. While bottom-up synthesis procedures such as chemical vapor deposition result in a pristine, high-quality graphene, they have extremely low yield and are difficult to scale-up to meet the demand [133]. Alternatively, top-down procedures involving the chemical synthesis of graphite oxide (GO) from graphite are being considered for their high yield and scalability, despite resulting in sheets with more defects [134]. In the chemical synthesis approach, graphite is initially converted to graphite oxide before being exfoliated into single-layer graphene oxide. The graphene oxide may then reduced either chemically or thermally to remove oxygen functional groups and form a graphene-like material, termed reduced graphene oxide (rGO) [16].

Modified Hummers' method is one of the most commonly used chemical procedures for producing GO. The oxidation of graphite occurs in three stages: (1) Formation of graphite intercalated compound (GIC) in the presence of H_2SO_4, (2) oxidation of GIC by $KMnO_4$, and (3) termination of oxidation reaction by water addition [135]. The addition of H_2O_2 after water addition dissolves the Mn species, assisting in GO purification [24, 104]. Morimoto *et al.* examined each step of the modified Hummers' method to optimize the oxidation process and eliminate steps that do not positively affect oxidation [24]. They summarized that the optimal conditions to synthesize GO were to react $KMnO_4$ and graphite at a ratio of 3:1 in sulfuric acid at a reaction temperature of 35 °C for 2 hours, followed by water and hydrogen peroxide addition respectively. Lavin-Lopez *et al.* have optimized the modified Hummers' method to make the process scalable and economic [136]. Dimiev *et al.* concluded that the oxidation reaction is diffusion-controlled and dependent on the

[1] Part of this chapter is submitted as a research paper to a journal and is currently under review

graphite grain size [135]. Seiler *et al.* further reported that the degree of intercalation of graphite by the acid determines the degree of oxidation of graphite and that intercalation can happen in matter of minutes [135, 137, 138]. The authors further noted that the oxidation reaction does not occur at low temperatures (< 20 °C) and high temperature (> 35 °C) oxidation leads to the formation of defects in GO [24, 17]. We focus on the case of 3:1 $KMnO_4$ to graphite ratio in sulfuric acid and at a reaction temperature of 35 °C for 2 hours.

While several studies have been published to optimize the oxidation-exfoliation process [104, 24], relatively few studies have explored the effect of operating conditions on the heat of reaction and the final GO produced. Lee *et al.* reported the heat of solution between sulfuric acid and $KMnO_4$, and the oxidation reaction of graphite [139]. They reported a higher heat of solution compared to the heat of reaction and concluded that controlling the heat released during $KMnO_4$ addition step is more important than the oxidation reaction step [139]. In principle, the heat of reaction and solution should not vary with operating parameters such as reaction temperatures and stirring rate. However, if a difference is detected in these quantities due to change in operating conditions, it indicates that the operating conditions are affecting the reaction kinetics.

The heat of reaction can indicate the type of final GO produced (degree of oxidation and funcationalization) and related safety considerations for modified Hummers' method. A greater understanding of the risks associated with the production of GO, such as thermal management and chemical stability, will be increasingly important as the process is brought to an industrial scale. Prior studies have pointed out the importance of controlling the heat released by $KMnO_4$ addition and oxidation reaction [24, 139] because dissolution of $KMnO_4$ in acid produces dimanganese heptaoxide, Mn_2O_7, which is considered to be unstable at elevated temperature of 55 °C and sensitive to organic impurities [27, 140].

Here, we evaluate the oxidation reaction from a reaction engineering perspective to address potential safety issues in scaling up this process. Our focus is the heat release rate at the oxidation step. The heat release rate is quantified using a heat flow reaction calorimeter. The effects of operational conditions such as oxidation temperatures, acid treatment time, and stirring rate are

investigated and their influence in heat of reaction and the final final GO product we studied. Finally, the thermal hazards of Mn_2O_7 are studied in a pseudo-adiabatic calorimeter at the operating conditions of modified Hummers' method.

4.2 Methodology

4.2.1 Materials

Graphite powder with an average particle size of 81 μm was obtained from Bay Carbon, Inc. Potassium permanganate, hydrogen peroxide, 37 wt.% hydrogen chloride, and 95 wt.% sulfuric acid were procured from Sigma Aldrich. All the materials were used as received without further purification or treatment.

4.2.2 Reaction Calorimeter

The oxidation reaction was carried out in a Mettler Toledo Reaction Calorimeter (RC1e). The calorimeter features a 1.2 L glass reaction vessel with an anchor impeller and hastelloy thermocouple. The temperature of the reactor is maintained by a heating/cooling jacket filled with silicon oil which runs through a Jubalo recirculating chiller. Using data from vertical and horizontal heat flux sensors on the reactor wall, the temperature was actively controlled by an RTCal thermostat, and the energy released by the reaction was captured by the iControl software in real-time. The schematic of the calorimeter is shown in **Figure 4.1**.

The reaction calorimeter is a double walled reactor with temperature sensors. The vertical and horizontal band shown in the diagram records the heat flux though to calculate the heat the released by the reaction inside the reactor. The temperature sensors communicate with the heat flux sensor to keep the reactor temperatures at set conditions.

4.2.3 Experimental Procedure

Graphite oxide was prepared using modified Hummers' method without pretreatment of the graphite [23]. 3 g of graphite was added to a reactor with 250 mL of 95 wt.% sulfuric acid. The reactor was held constant at 10 °C. 9 g of potassium permanganate was added slowly to the reactor maintaining the temperature of the reactor at 10 °C. After permanganate addition; the reactor

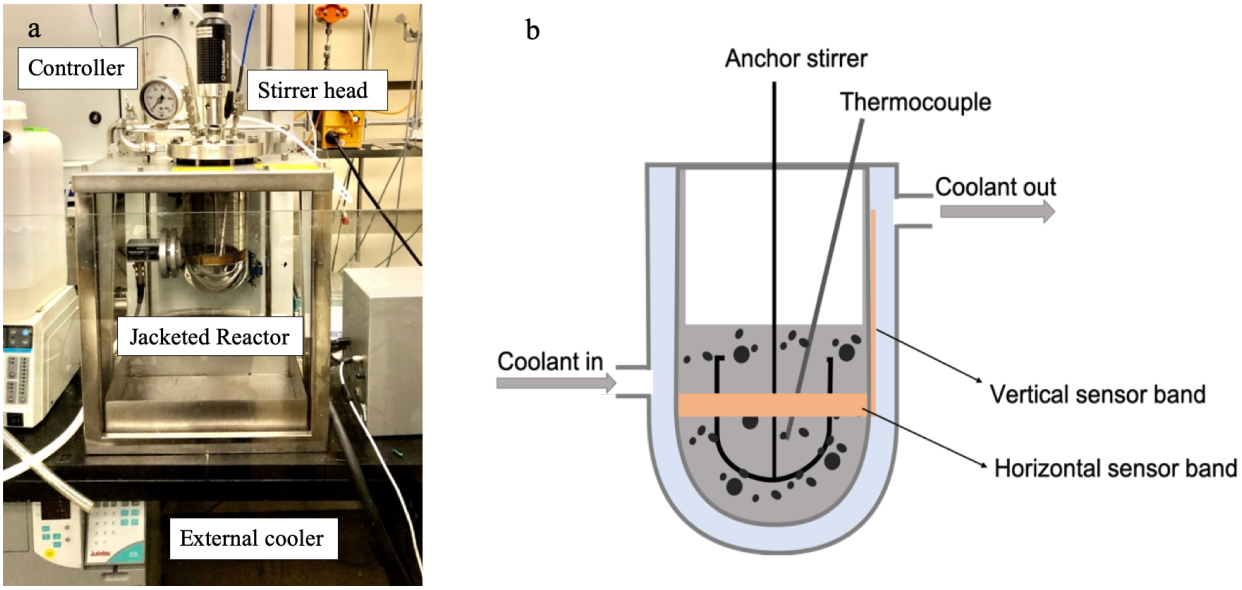

Figure 4.1: (a) Picture of the Reaction Calorimeter RC1e set up in the laboratory. (b) Schematic of the RC1e reactor.

was heated to 33 °C and held at this temperature for 2 hours. The reactor was then cooled to room temperature and the reaction mass was transferred into a flask. The oxidation reaction was terminated by adding water to the mixture, followed by hydrogen peroxide addition.

The graphite oxide solution was washed with approximately 2,100 mL of 10 wt.% HCl to remove salt byproducts. 37 wt.% HCl was mixed with distilled water to create the washing acid. The acid-washed solution was further washed with distilled water until the pH was neutral at 4.5. The sample was either dried under vacuum in an oven at 40 °C for 24 h or flash-frozen in liquid nitrogen and freeze-dried (Vitris Benchtop Freeze Dryer) for approximately 72 h to yield a dry GO powder.

4.2.4 Characterization Methods

4.2.4.1 Thermogravimetric Analysis

The mass loss due to GO decomposition were measured using a Q50 thermogravimetric analyzer (TGA) from TA Instruments, New Castle, DE. The measurements were done in a nitrogen environment. The sample was heated from room temperature, samples were heated at 1 °C/min to

30 °C. After holding isothermal for 10 minutes, the samples were heated to 750 °C at a constant rate of 4 °C/min.

4.2.4.2 XPS

X-ray photoelectrron spectroscopy (XPS) measurements were conducted using Omnicron XPS. Deconvolution of XPS C1s spectra was done using CasaXPS software using shirley type background.

4.2.4.3 Elemental Analysis

Via a third party testing service, CHN and direct oxygen analysis were conducted according to ASTM D-5291 standard using a PE 2400 CHN Analyzer fitted with an oxygen accessory kit.

4.2.5 Thermal Analysis

Thermal stability of Mn_2O_7 produced as a result of mixing sulfuric acid and $KMnO_4$ was conducted in the Advanced Reactive System Screening Tool (ARSST) manufactured by Fauske and Associates, Burr Ridge, IL. The ARSST is an open test cell capable of handling chemical system for temperatures as high as 500 °C and pressures up to 500 psig. The acid and $KMnO_4$ samples were heated at a constant rate of approximately 1.2 °C/min. The sample cell is a glass test cell with a volume of 10 ml, which is placed inside a stainless-steel vessel of volume 350 ml. A thermocouple and pressure transducer tracked the dynamic temperature and pressure changes during the decomposition process. The pressure transducer was located outside the glass test cell in 350 ml vessel and for each test, the thermocouple touched the sample mass.

4.3 Results and Discussion

4.3.1 Heat of Solution

In **Figure 4.2**, a representative plot of the reactor temperature (green), jacket temperature (orange), and heat flux from the reactor (blue) during the reactor operation in a RC1*e* is shown. The heat flux shows distinct thermal events that occur during the experimental procedure. Prior to t = 0, the reactor was held isothermally at 10 °C and contained 250 mL of 95 wt. % H_2SO_4; then, five

distinct events can be seen in the heat flux curve: (1) Just after t = 250 s, 3 g of graphite is added to the acid solution and brought from room temperature to 10 °C. (2) At 4200 s, 9 g of $KMnO_4$ was added in 1 g increments and appear as a set of nine exothermic peaks. (3) At 6000 s, the set point of the reactor was increased to the reaction temperature of 33 °C, hence an endothermic peak appears as the reaction mixture is heated up. (4) Immediately after heating, a broad exothermic peak corresponds to the heat of reaction between $KMnO_4$ and graphite. (5) Finally, an endotherm appears when the product mixture is rapidly cooled back to room temperature at 12000 s.

The total heat released or absorbed by the reactor for a given time can be computed by numerical integration of the heat flow rate over that period, *i.e.,*

$$\Delta H = \int_{t_i}^{t_f} q_r dt \tag{4.1}$$

where initial (t_i) and final (t_f) reaction times and the baseline of heat flux are manually selected. The baseline (grey line in **Figure 4.2**) shows the overall heat flux when no reaction was occurring in the reactor.

Adding an increment of $KMnO_4$ to the reactor causes the heat flux to increase rapidly and as $KMnO_4$ dissolves, the heat flux returns to baseline. $KMnO_4$ was manually added to the reactor in 1-gram aliquot. A total of 9 g of $KMnO_4$ was added which is seen in the $KMnO_4$ addition in **Figure 4.2**. The heat of solution of $KMnO_4$ in sulfuric acid is addition limited because when the first aliquot of the oxidizer is added, the heat flux curve increases and then decreases as the oxidizer dissolves. Similarly, addition of second aliquot of oxidizer increases the heat flux and then it decreases as it dissolves. The $KMnO_4$ addition in **Figure 4.2**. shows multiple peaks for multiple aliquots of oxidizer added to the reaction mixture. Therefore, the heat released during this step can be controlled by controlling the feed rate of $KMnO_4$.

Table 4.1 summarizes the heat of the solution obtained from the reaction calorimeter. When permanganate and sulfuric acid were mixed at 10 °C without graphite, the obtained heat of solution was 79.1 kJ/mol of $KMnO_4$. This is higher than previously reported value of an average 49.1 kJ/mol of $KMnO_4$ by Lee *et al.* [139]. Lee *et al.* observed values close to this average at both 10

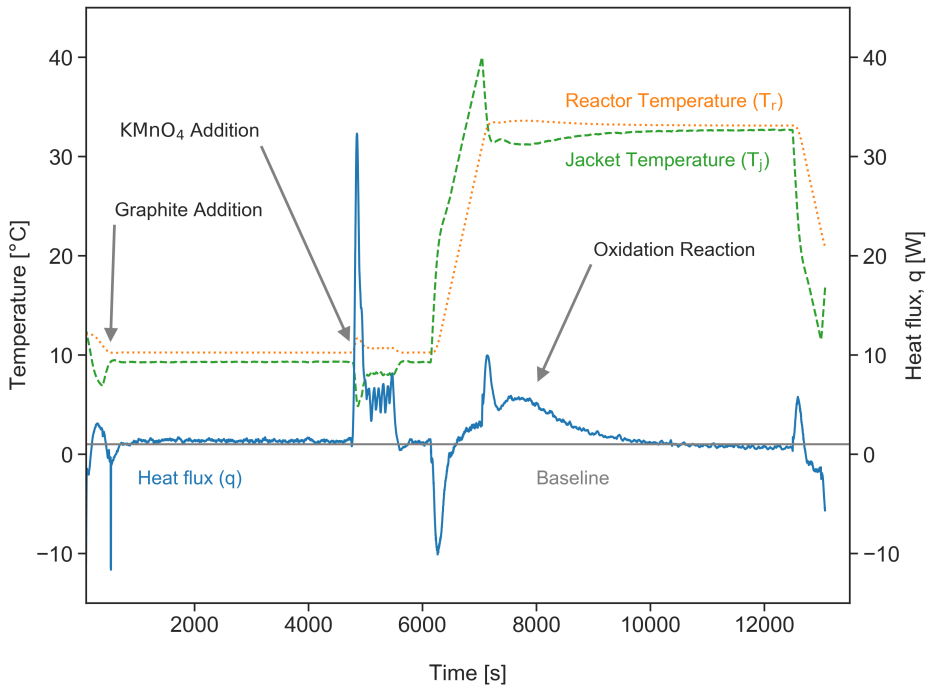

Figure 4.2: Data obtained from the RC1*e* reactor. The green line represents the reactor temperature (T_r), the orange line represents the jacket temperature (T_j), and the blue line represents the heat released by the reaction, heat flux (q). The baseline is the heat released curve when no reaction is happening in the reactor. In order to calculate the heat of dissolution or reaction, the heat flux curve (q) is integrated over time from when it gets higher than the baseline and until q recovers back to the baseline.

°C and 35 °C and with varying permanganate quantities.

Prior literature indicates that oxidation reactions do not occur at 10 °C; however, we noticed a higher heat of solution (an average of 116.3 kJ/mol of $KMnO_4$) when permanganate was added to H_2SO_4 and graphite mixture. The higher heat of solution with graphite in the reaction mixture observed here can be attributed to some degree of oxidation reaction even at 10 °C.

4.3.2 Heat of Reaction

A major consideration in scaling up an exothermic reaction is the understanding of the intensity and the consequences of exothermic behavior of the reaction. This information helps to design the reactor's cooling capacity to maintain the desired reaction temperature and avoid thermal runaway reactions. In this section, we determined the heat of the oxidation reaction. After the contents

Table 4.1: Heat of solution at 10 °C

Condition	Heat of solution [kJ/mol. of $KMnO_4$]	Notes	Source
$KMnO_4$ and sulfuric acid	79.1	460 g of sulfuric acid	This study
$KMnO_4$, sulfuric acid, and graphite	116.3	460 g of sulfuric acid	
$KMnO_4$ and sulfuric acid	49.1	840 g of sulfuric acid	[139]

of the reactor (graphite, sulfuric acid, and $KMnO_4$) were heated to 33 °C, the heat of reaction appeared in the heat flux curve as a broad, exothermic peak (starting at around 6800 s in **Figure 4.2**). At this temperature, the reaction is kinetically controlled as seen in **Figure 4.2**.

Here the term "acid-soaked" refers to experiments or GO produced where the parent graphite material was stirred in sulfuric acid for 70 minutes before $KMnO_4$ was added, whereas "non-acid soaked" refers to experiments or GO produced where the parent graphite material was stirred in sulfuric acid for less than 10 minutes. Every experiment was run with the same quantities of graphite, oxidizer, and solvent.

Figure 4.3a shows the heat of oxidation reaction for acid-soaked and non-acid soaked oxidation reaction at three different stirring speeds and at 33 °C reaction temperature. The different stirring speeds are 100, 150, and 200 RPM. Each experiment was repeated at least twice and the straight line is the average values of the two runs for each RPM experiment. The temperature of the reaction mass was held at 33 °C for 2 hours before it was cooled and quenched.

Figure 4.3b is the C/O molar ratio of the GO determined by the elemental analysis (EA). The blue line represents the molar ratio of GO produced acid soaking the parent graphite in acid and the green line is the molar ratio of GO produced by non-acid soaking the parent material. Lee *et al.* had previously reported the heat of oxidation reaction for Hummers' method as 126.9 kJ/mol of $KMnO_4$ at 1:3 mass ratio of graphite to $KMnO_4$ and reaction temperature of 35 °C. Our data indicated similar heat of reaction for non-acid soaked experiments. Non-acid soaked graphite

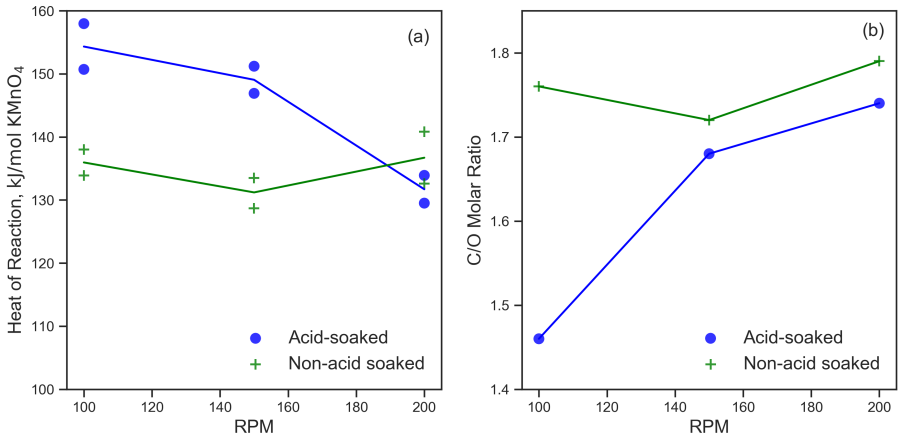

Figure 4.3: (a) Reported values of heat of oxidation reaction (b) and C/O ratio obtained from elemental analysis with varying agitation (rotation per minute). The blue marker represents the acid soaked runs whereas the green markers represent the non-acid soaked runs. The lines represent the average value of the data points.

Table 4.2: Elemental Analysis Data for GO synthesized in the RC1

Sample Name	C [%]	H [%]	O [%]	C/O molar ratio
100 - acid-soaked	42.11	2.36	38.40	1.46
150 - acid-soaked	52.54	1.73	41.62	1.68
200 - acid-soaked	51.02	1.82	39.20	1.74
100 - non-acid soaked	53.03	1.66	40.12	1.76
150 - non-acid soaked	47.05	2.12	36.44	1.72
200 - non-acid soaked	52.34	1.77	38.91	1.79

shows a consistent heat of reaction regardless of RPM with an average of 133 kJ/mol $KMnO_4$ (**Figure 4.3b**). This is within the error bar of the data for each RPM tested. EA of the product GO shows a consistent C/O molar ratio of 1.32 (between 1.29 to 1.35) for non-acid soaked GO.

The varying heat of reaction correlates to the C/O molar ratio for the acid-soaked runs in **Figure 4.3a**, *i.e.,* a decreasing heat of reaction corresponds to increasing C/O molar ratio, **Figure 4.3b**. Lower C/O ratio indicates a higher degree of oxidation and vice versa. Graphite that had 70 minutes of acid soaking showed a higher average heat of reaction and a higher degree of oxidation as indicated by elemental analysis of the final GO product.

Based on the trends seen in **Figure 4.3**, two key observations stood out. (1) Acid soaking for an extended time is affecting the degree of oxidation reaction, and (2) for the acid-soaked runs, the RPM affects the degree of oxidation.

To understand these observations, we first examined the TGA data of the final GO produced by acid soaking and non-acid soaking the parent graphite. The TGA analysis for acid-soaked runs in **Figure 4.4a** shows different decomposition trend than non-acid soaked runs in **Figure 4.4b**. TGA data of the acid-soaked GO indicated a decreased mass loss for increasing RPM. The decreased mass loss indicates that the sample has less oxygen groups in the GO **Figure 4.4a**. Therefore, 100 RPM acid-soaked GO has the most oxygen group compared to all other GO synthesis condition. This TGA trend further aligned with the heat of reaction and EA results. As the EA showed in **Figure 4.3b**, the 100 RPM acid-soaked sample has the most oxygen compared to 150 and 200 RPM samples. In contrast, **Figure 4.4b** shows a consistent decomposition trend for all non-acid soaked samples with different RPM. Therefore, for non-acid soaked GO, the degree of oxidation does not change with varying RPM.

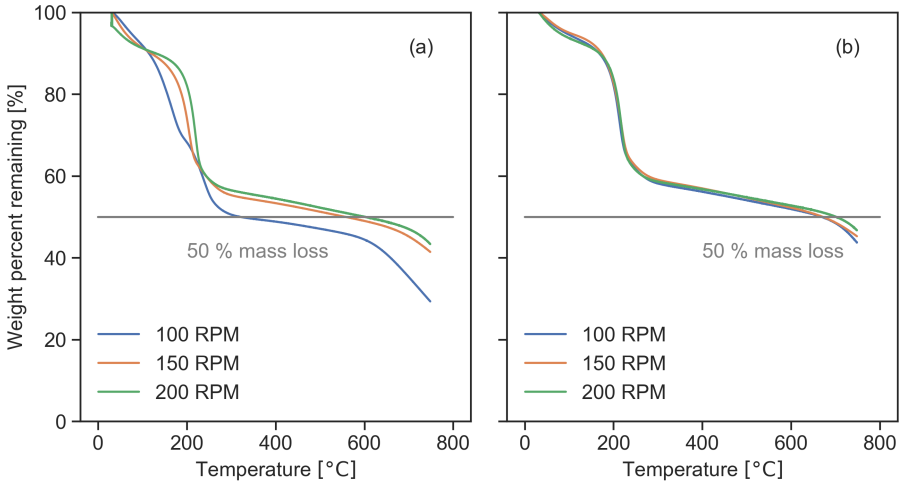

Figure 4.4: TGA of the samples. (a) Decomposition data for the acid-soaked samples. 100 RPM acid soaked sample decomposes rapid compared to the 150 RPM and 200 RPM samples. (b) Decomposition data for the non-acid soaked samples.

In order to understand the first observation, we hypothesize that the extended acid soaking is influencing the degree and type of oxidation occurring in graphite. It is known that intercalation helps with the oxidation of graphite but prior literature noted that a GIC (graphite intercalated compound) would form in a matter of minutes [135, 138]. To our knowledge, there are no studies in the literature investigating the oxygen functionalization of final GO product synthesized by extended soaking of graphite in acid before the addition of $KMnO_4$. However, our results indicate that longer soaking time of parent graphite in acid increases the degree and type of oxidation of graphite.

To investigate the hypothesis that the type of oxidation of graphite is influenced by acid soaking, an XPS analysis was run on the final GO samples. **Figure 4.5** shows the C 1s spectra of GO synthesized by acid-soaked and non-acid soaked graphite in sulfuric acid. The acid-soaked GO has two distinct peaks (**Figure 4.5a**) compared to non-acid soaked GO (**Figure 4.5b**). Deconvolution of C 1s spectra for acid-soaked GO shows three peaks for sp^2 carbon (284.6 eV), the epoxide (286.6 eV), and the carboxyl (287.5 eV) functional groups, whereas the non-acid soaked GO have dominantly sp^2 carbon, the carboxylic acid (288.5 eV), and the carboxyl functional groups. Between these samples, the presence of the C-O-C functional group in acid-soaked GO indicates surface functionalization and the presence of O-C=O in non-acid soaked GO indicates edge functionalization. Seiler *et al.* noted the intercalation of graphite increases the layer distance between the graphite sheets and assists in basal or surface oxidation [138]. Therefore, we can conclude, the acid soaking in increasing the basal (or surface) oxidation.

The corresponding area percent of XPS data is shown in **Table 4.3**

Table 4.3: XPS data for GO

Sample Name	Acid-soaked GO	Non-acid soaked GO
Sp^2	64.9 %	84.4 %
C-O-C	23.9 %	0.0 %
O-C=O	0.0 %	10.4 %
C=O	11.2 %	5.2 %

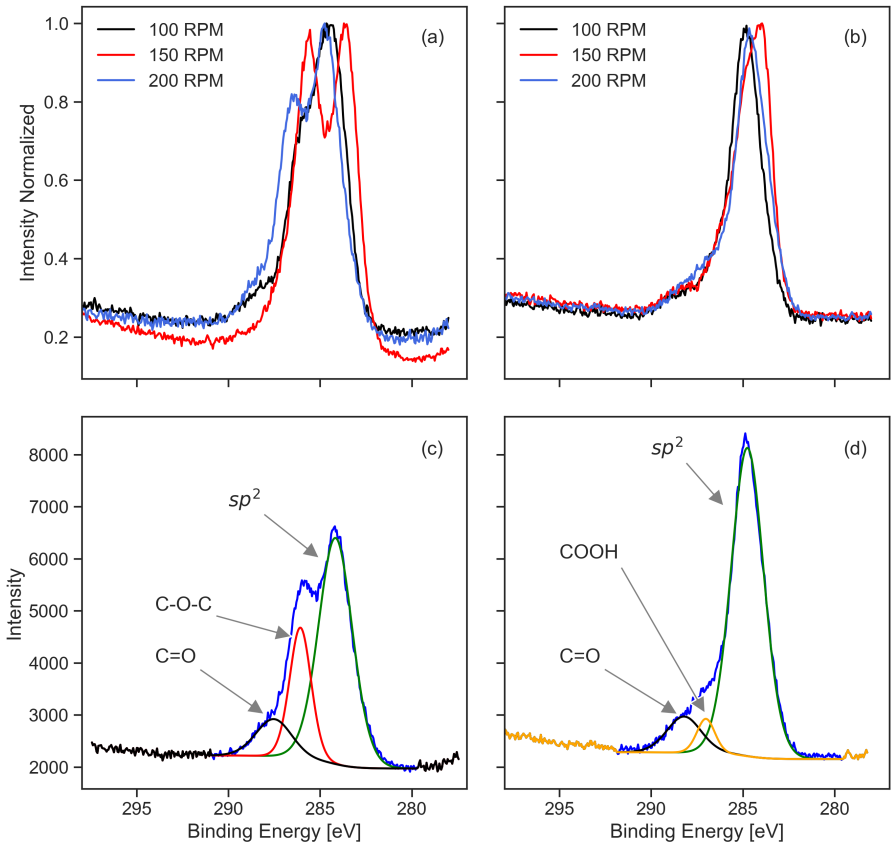

Figure 4.5: XPS data for the GO. (a) shows the XPS for acid soaked GO. (b) is the XPS of non-acid soaked samples. The intercalation increases the amount of functional oxygen group in the sample. (c) and (d) are the individual peaks for the oxygen functional group for acid soaked (c) and non-acid soaked (d) samples at 200 RPM.

The second observation is that for the sulfuric acid-soaked graphite, mixing influences the degree of oxidation of the graphite. The heat of oxidation reaction in this paper was calculated by dividing energy released by the reaction by the total moles of $KMnO_4$ added into the system, not the moles of $KMnO_4$ reacted. Therefore, the variation in the heat of reaction could suggest that not all of the $KMnO_4$ added was consumed.

However, the decreasing oxidation (or reaction of $KMnO_4$) with increasing stirring rate is counterintuitive because the increased Reynolds number associated with the stirrer RPM should result in a higher external diffusion rate of $KMnO_4$ to reaction sites between graphite sheets. The calculations for Reynolds number (Re) for the three RPMs is shown below:

$$Re = \frac{nsD^2 s.g.}{\mu} \tag{4.2}$$

Where, ns is the stirring rotational speed [rad/sec], D is the diameter of the anchor stirrer [D = 75 mm] and s.g. is specific gravity [s.g. = 1.83 gm/cc], and μ is the viscosity [μ= 15.5 cP]. The s.g., and μ used are for 95 wt. % sulfuric acid at 33 °C [141]. The Reynolds number are 6955, 10,432, and 13,909 respectively for 100, 150, and 200 RPM. These Reynolds numbers are in the turbulent range *i.e.*, above 4,000 [142].

At high Re, the convective mass transfer coefficient scales with $Re^{0.5}$ as shown in equation 2 [142].

$$Sh = 2 + 0.6Re^{1/2}Sc^{1/2} \tag{4.3}$$

where

$$Sh = \frac{k_c d_p}{D_{AB}} \tag{4.4}$$

$$Re = \frac{\rho d_p v}{\mu} \tag{4.5}$$

$$Sc = \frac{\nu}{D_{AB}} \tag{4.6}$$

where Sh is the Sherwood number, Sc is the Schmidt number, k_c is mass transfer coefficient, d_p is the diameter, D_{AB} diffusivity of A in B, ρ is the density, v is the velocity, μ is viscosity and ν is the kinematic viscosity. If the reaction is limited by external mass transfer, the rate of reaction (r) is given by equation 6.

$$r = k_c(C_{bulk} - C_{surface}) \tag{4.7}$$

where the C_{bulk} and $C_{surface}$ are the concentration of the oxidation agent in bulk material and surface of the graphite, respectively. Therefore, the higher Re gives a higher heat transfer coefficient, k_c, which should improve the diffusion-controlled reaction, given that everything else in the equation is constant. This implies that external mass transfer is not the limiting step in the

reaction. Similarly, higher Re might be associated with a decrease in particle size due to shear-induced deagglomeration, which would also lead to less diffusion limitations and higher degrees of oxidation, but this is not what is observed.

Other possible physical explanations for this trend include the possibility that increased RPM is promoting a secondary reaction and not the oxidation reaction. Note that running the reactor at very low RPM is inherently unsafe because it slows down the effectiveness of the cooling jacket and allows for local hot spots. Therefore, it is interesting why the oxidation decreases with an increasing stirring rate for acid-soaked samples; this warrants further investigation.

The SEM images of GO produced from acid-soaking and non-acid soaking at various RPM is shown in **Figure 4.6**

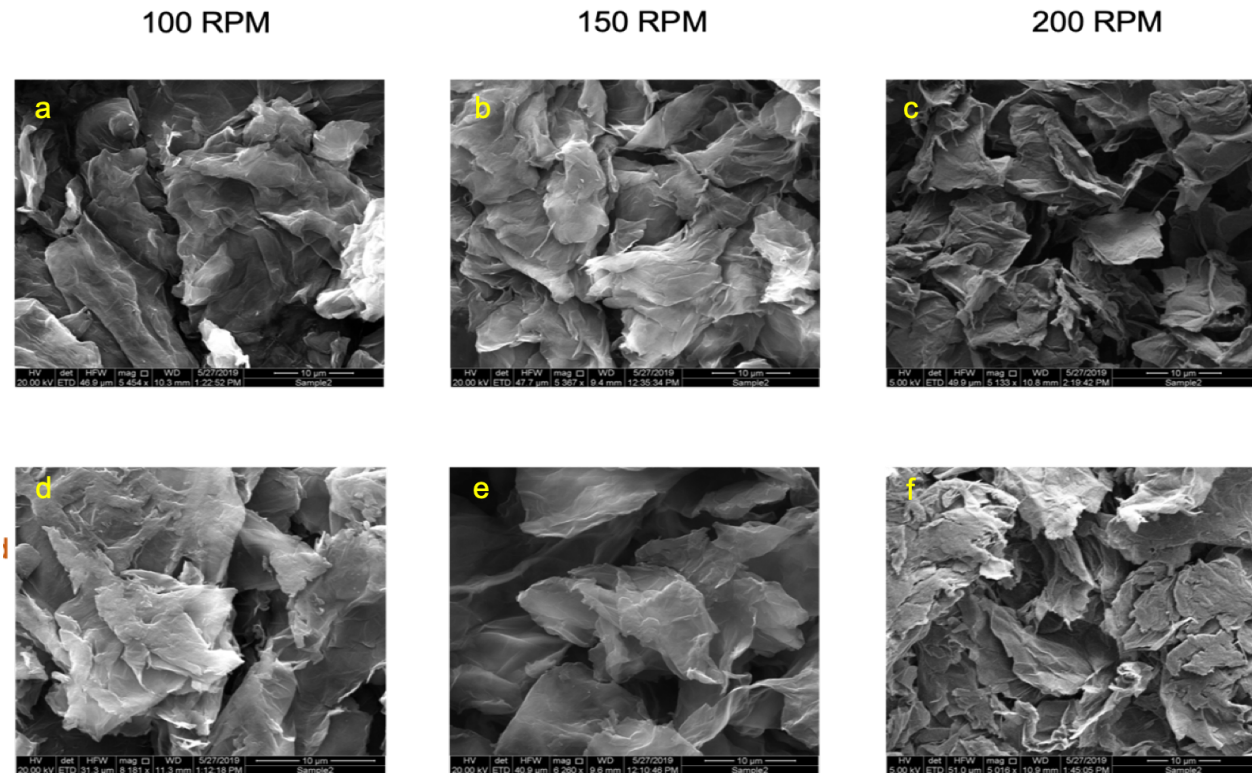

Figure 4.6: (a), (b), and (c) represents SEM of GO synthesized by acid-soaked the parent materials at three different RPMs respectively. (d), (e), and (f) represents SEM of GO synthesized by non-acid soaked the parent materials at three different RPMs respectively

4.3.3 Reaction Temperature

In this section, the effect of the oxidation reaction temperature on the final GO produced was investigated. Morimoto *et al.* in their prior work highlighted the need to maintain the temperature of the oxidation reaction at an optimal temperature of 30 - 35 °C. Their study mentioned the oxidation reaction at high temperature (*i.e.*, >35 °C) creates defective GO [24]. Therefore, the experiments were conducted for reaction temperatures 33 °C, 22 °C, and 10 °C.

As we decreased the reaction temperature, the heat of reaction decreased as shown in **Table 4.4**. The C/O ratio increased with decreasing temperature which indicates that less oxygen is present in the final GO. All three experiments were done at 150 RPM and without acid soaking. **Figure 4.7a** shows the heat flux data for reaction temperatures 10 °C and 33 °C from the RC1*e*. The heat flux data indicates that at lower temperatures, all of $KMnO_4$ in the mixture does not oxidize the graphite. **Figure 4.7b** is the XPS data of C 1s for GO made at reaction temperatures 22 °C and 33 °C. The XPS spectra resemble the non-acid soaked spectra seen for non-acid soaked GO in the previous section as shown in **Figure 4.5d**.

The adiabatic temperature calculation shown in **Table4.4** is shown below:

$$\Delta T_{ad} = \frac{\Delta H}{C_p M_R} \tag{4.8}$$

Where ΔT_{ad} is the adiabatic temperature increase in K and ΔH is the heat of reaction with units KJ/mol, C_p is the heat capacity of the reactor mixture and M_R is the is mass of the reactor. The C_p ranged from 1.92 to 2.59 kJ/ kg K. For the conservative estimate, we used 1.92 kJ/kg K to calculate the temperature increase.

At 10 °C reaction temperature:

$$\Delta T_{ad} = \frac{\Delta H}{C_p M_R} = \frac{125[\frac{kJ}{mol.KMnO_4}]}{1.92[\frac{J}{kgK}] * 473[g]} = \frac{7310}{908.16} = 8K \tag{4.9}$$

Similarly, At 22 °C, the ΔT_{ad} = 15 K and at 33 °C, the ΔT_{ad} = 16 K

Table 4.4: Heat of solution and reaction

Reaction temperature	Heat of solution [kJ/mol. of $KMnO_4$]	Heat of reaction [kJ/mol. of $KMnO_4$]	Total heat [kJ/mol. of $KMnO_4$]	Adiabatic temperature rise [K]	C/O ratio
10 °C	116	9	125	7	N/A
22 °C	113	99	212	15	1.46
33 °C	117	129	246	16	1.29

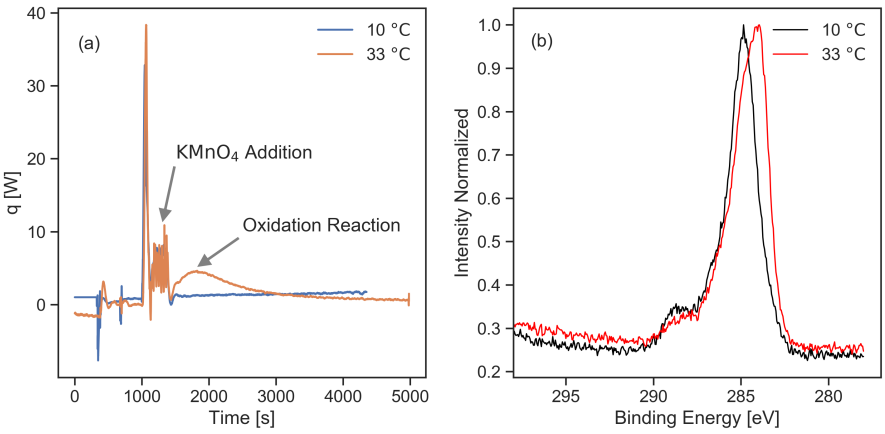

Figure 4.7: (a) Heat flux data from RC1*e* for reaction temperatures of 33°C and 10 °C. (b) XPS C 1s spectra for GO oxidized at temperatures 33°C and 22 °C

The results from **Table 4.4** indicate that a decrease in oxidation temperature decreases the degree of oxidation, but as seen in the XPS spectra in **Figure 4.5b** the oxidation temperature does not affect the type of functional groups formed in GO. However, the acid soaking time before the addition of $KMnO_4$ is affects the degree of oxidation and type of functional groups formed in the final GO product.

4.3.4 Mn_2O_7 hazards in GO synthesis

In this section, the hazards associated Mn_2O_7 are investigated. The dissolution of $KMnO_4$ in sulfuric acid is described [143, 144]:

$$2KMnO_4 + 2H_2SO_4 \rightarrow Mn_2O_7 + 2KHSO_4 \tag{4.10}$$

$$Mn_2O_7 + 2H_2SO_4 \rightarrow 2[MnO_3]^+[HSO_4]^- + H_2O \quad (4.11)$$

The dimanganese heptaoxide, Mn_2O_7 produced by the dissolution of permanganate in sulfuric acid is reported to be unstable [27, 140]. Prior literature has noted that the temperatures above 55 °C can trigger violent explosion and/or fire. In addition, Mn_2O_7 is also sensitive to the organic impurities such as acetone, methanol, cotton, *etc*. The decomposition of Mn_2O_7 is shown in equation 9 [145]:

$$4Mn_2O_7 \rightarrow 8MnO_2 + 2nO_3 + (6 - 3n)O_2 \quad (4.12)$$

where 0 <n <2. Based on the heat of solution and reaction obtained from the reaction calorimeter in the prior section, the adiabatic temperature increase for the dissolution and oxidation reaction can be up to 16 °C for about 500 g of reaction mass. If the oxidation reaction is performed at 33 °C, the adiabatic temperature increase can be adequate to reach the explosive temperature of 55 °C.

To understand the hazards of Mn_2O_7, we mixed Mn_2O_7 in sulfuric acid at a concentration typically used in modified Hummers' method, 75 mg/mL, and heated to 95 °C in an advanced reactive system screening tool (ARSST). No decomposition of the solution was detected at this concentration as shown in **Figure 4.8a**. The blue line in **Figure 4.8** is the temperature increase with time and the red line is the pressure increase with time. Constant heating of 1.2 °C/min was applied. When the sample temperature reached 95 °C, the heating was turned off. No abrupt increases in temperature or pressure were seen, which indicates that violent decomposition did not occur at these temperature ranges. Next, we examined the concentrations of permanganate in acid solution commonly used in literature to see if any of the concentration was high enough to trigger the self decomposition of permanganate. **Table 4.5** shows the concentration of oxidizer in acid for modified Hummers' method in various literature.

A higher $KMnO_4$ concentration of 150 mg/mL was studied in the reactive screening tool. Even at this concentration, no decomposition was detected as seen in **Figure 4.8b**. The temperature and

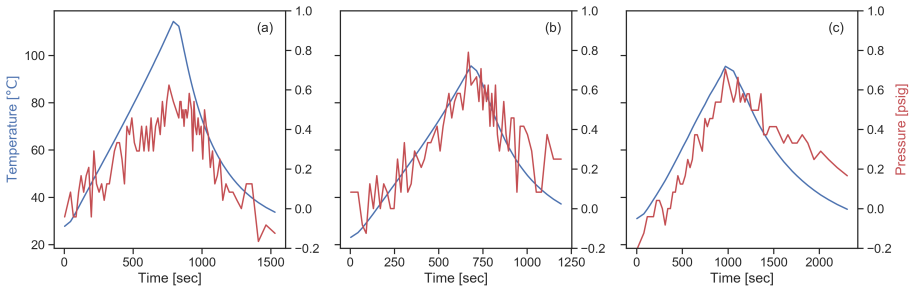

Figure 4.8: ARSST temperature (blue) and pressure (red) data. (a) 75 mg/mL of $KMnO_4$ in H_2SO_4, (b) 150 mg/mL of $KMnO_4$ in H_2SO_4, (c) Graphite in 75 mg/mL of $KMnO_4$ in H_2SO_4

pressure profile increased steadily up to 95 °C, followed by cooling to room temperature. These experiments were carried out in the air and special care was taken to free the solution of any organic impurities.

Additionally, we examined to see if the addition of graphite in the reaction mixture of sulfuric acid and $KMnO_4$ would trigger the thermal decomposition of the material. **Figure 4.8c** shows the thermal data for graphite in 75 mg/mL of $KMnO_4$ in sulfuric acid solution. The temperature and pressure profile with time shows a steady increase up to 95 °C and a steady decrease when the heating was turned off. Therefore, no thermal runaway or explosive decomposition was seen.

Table 4.5: Permanganate concentration in acid used in literature

Conc. of $KMnO_4$ [mg/mL]	Reference
36.0	This study
26.7	Dimiev *et al.* 2014 [135]
120.0	Morimoto *et al.* 2016 [146]
60.0	Morimoto *et al.* 2017 [24]
20.0 - 120.0	Li *et al.* 2018 [137]

A further literature review showed that the experiments for the decomposition of dimanganese heptaoxide reported in the literature were done for pure solid Mn_2O_7 in 1953. According to the study, the solid Mn_2O_7 can in fact self decompose when heated to temperatures above 65 °C

and the material is sensitive to shock [147]. Additionally, impurities such as alcohol, acetone, cotton, *etc*. can ignite concentrated Mn_2O_7 at room temperatures [147]. However, in the modified Hummers' method, the Mn_2O_7 is in solution and in dilute quantities. Therefore, the hazards of Mn_2O_7 may not be as critical as previously pointed out. Even so, care should be taken to free the reaction mixture of any impurities and avoid isolating or drying the Mn_2O_7 during the process.

Furthermore, a brief report in 2014 documented at least one safety incident while conducting modified Hummers' method for GO synthesis [148]. In the letter, the authors note that the alcohol (a common reagent in laboratories), reacted with reactants of Hummers' method to synthesize an explosive component. Therefore, to conduct Hummers' method safely, it is crucial no impurities are present in the reactor and associated equipment.

Another potential safety issue pointed out in prior literature is the possibility of hotspots. The hotspots could become an issue when water is added to the acidic reaction mixture to quench the reaction. The acid and water reaction is extremely exothermic and the viscosity of the mixture increases with water concentration in the mixture. When the water becomes excess in the mixture, the viscosity decreases. Therefore, it is recommended that the reaction mixture is added to the water and not the other way round.

4.4 Conclusions

This study shows the amount of heat released during the oxidation reaction in the modified Hummers' method indicates the degree of oxidation of graphite. Graphite soaked in sulfuric acid for more than an hour before oxidation reaction had more oxygen content in the final GO product and the GO consisted of surface functional oxygen groups compared to GO produced by non-acid soaking sulfuric acid in graphite. Prior literature concluded that the intercalation of sulfuric acid in graphite happens within minutes, but our results indicate that longer acid soaking time improves the degree of oxidation. However, increasing the mixing speed for acid-soaked parent materials to make the final GO decreases the degree of oxidation. This is interesting because mixing improves the diffusion-controlled oxidation reaction but that is not what we observed. We hypothesized that improved mixing for acid-soaked runs is encouraging secondary reaction instead of the oxidation

reaction.

Similarly, the GO synthesized at the oxidation temperature of 10 °C and 22 °C had comparatively lower heat of reaction compared to higher reaction temperatures. The elemental analysis showed less oxygen content in the final GO produced at lower temperatures. However, the XPS of C 1s spectra of these GO showed spectra consistent with non-acid soaked GO. Therefore, the acid soaking time of parent graphite in acid has a dominant effect on the degree and type of oxygen formed in the final GO rather than the oxidation temperatures.

Finally, the adiabatic temperature increase due to the heat of solution of acid and $KMnO_4$ and the oxidation reaction is about 16 K. The adiabatic temperature increase due to heat of solution between acid and $KMnO_4$ and the oxidation reaction is enough to get to the unstable temperatures of Mn_2O_4 at 55 °C. However, the Mn_2O_7 produced in modified Hummers' method is in solution and dilute enough that it is not likely to be explosive at 55 °C but the solution is sensitive to organic impurities and care should be taken to keep the reactants and reaction mixture free of organic impurities. Finally, in order to quench the oxidation reaction, the reaction mass is added to water. It should be noted that the acid-water reaction is highly exothermic and it could potentially cause hotspots and thermal runaway conditions in absence of adequate mixing and cooling capacity.

5. EXPLORATION OF ALTERNATE CARBON SOURCES TO MAKE GRAPHENE-LIKE PRODUCT

5.1 Introduction

Traditionally, natural graphites are used as a primary source to make graphene-like materials. Natural graphites are naturally occurring in mines. There are three different types of natural graphites (natural flakes, vein/lump graphite, and amorphous graphite). Each of these types of graphite is formed due to different geological occurrence and are generally not found in the same geographical locations [149, 150]. Only naturally occurring flake graphite has a true flake (like mica). The flake-like structure makes intercalation and exfoliation to yield very thin flakes with a high aspect ratio possible. Most of the graphene-related research so far has used natural graphite as the source graphite. Synthetic graphites are typically derived from petroleum coke or coal tar. Petroleum coke is a by-product of the petroleum cracking process. The green coke straight out of the coker unit can be classified into two types, fuel grade coke and anode grade coke as shown in **Figure 5.1**. Fuel grade coke has more impurities present compared to anode grade and is primarily used as a fuel source.

Anode grade coke can be further thermally treated (or calcined) based on the need. Depending on the structure of the coke, the anode grade coke can be further classified into four types: shot, sponge, honeycomb, and needle coke. Shot coke is the most porous, disordered, and impure coke compared to others, and these are difficult to graphitize. As the aromaticity increases and the levels of hetero-atoms decrease, we get more ordered coke (*i.e.,* needle coke). Depending on the orientation and crystallinity and the nature of the milling operations, the synthetic graphite's 'flake' like morphology may vary.

Synthetic graphites are mostly used in energy storage (such as batteries, lithium-ion) and in arc furnace applications. Synthetic graphites are preferred for these applications because synthetic graphites have very little to no impurities compared to natural graphites and the absence

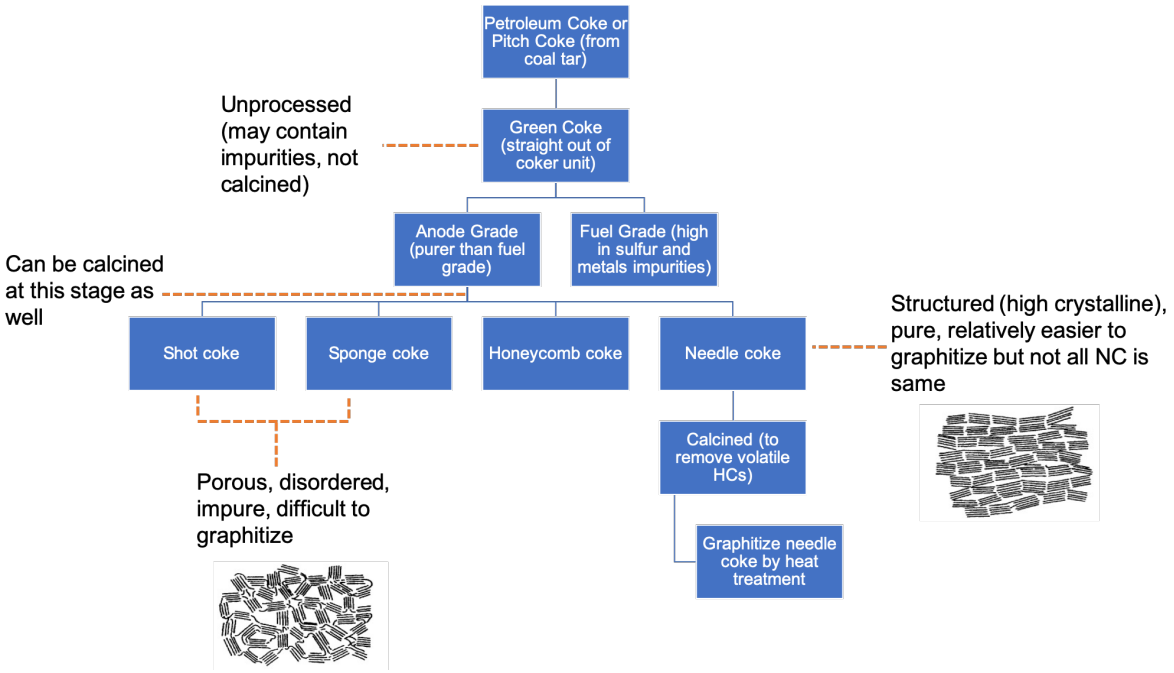

Figure 5.1: The figure shows various types of coke derived from petroleum coke.

of impurities is an important consideration in energy storage applications [150]. We are interested in investigating synthetic graphite and specifically petroleum-derived coke (pet. coke) as a source to make graphene-like materials. Pet. coke are mostly used in graphite electrode, in aluminum industries, and as fuels [150]. Graphene is a high-value product with numerous applications [101, 151, 152, 153, 154]. Therefore, if successful, the goal is to convert a very common by-product of a refinery to make a high-value product.

An earlier research in converting coke to graphene-like material was published in 2015 from Sierra *et al.* [155]. They used coke as a parent material to synthesize graphene-like material using the modified Hummers' method and the solvent exfoliation method. In the study, they used the coke (Ck) and thermally treated the coke to 2800 °C to get synthetic graphite (process called graphitization). They compared the final graphene oxide synthesized from coke (GO-C) and synthetic graphite (GO-GC). Using Hummer's method, the study reported that they needed higher amount of reactants (*i.e.,* $NaNO_3$:$KMnO_4$ of 1:7.2 compared to 1.7) to get GO-C product with

similar oxidation (2.5) as GO-GC. They also reported GO-C had more acid groups at the edges compared to basal oxidation of GO-GC. The study concluded coke is less reactive to oxidation than the synthetic graphite and GO-C oxidized in harsher condition exfoliated better after thermal treatment. The average height of monolayers of GO-C was between 1.2-1.5 nm. As for the solvent exfoliation method, they used N-methyl-pyrrolidinone (NMP) as the solvent. The study reported an average lateral size of 1 μm for EG-GC and 400 nm for EG-C.

The same research group in 2016 published another paper where they used different types of coke as parent material to synthesize graphene oxide using modified Hummers' method [156]. They investigated a premium petrochemical coke, a commercial carbo-chemical coke, and a coke obtained from coal tar. The graphite they used for baseline comparison was graphitized commercial coke at 2800 °C. The GO from cokes had a C/O ratio from 3.2 to 3.7 compared to that from the graphite whose C/O ratio was 2.2. The crystallinity of the cokes were in decreasing order from premium coke, commercial coke, and coal tar. The yield decreased with decreasing crystallinity of the parent material. They concluded that the crystalline structure with large domains facilitates the exfoliation of oxidized coke and reported that the larger crystals of the parent coke yielded larger lateral sized GO. Their conclusion is in alignment with Botas *et al.*'s study in 2012, where the researchers studied the effect of the parent graphite on the structure of GO and noted that the GO obtained from more crystalline graphite had a higher area compared to less crystalline graphite [157].

Xing *et al.* in 2018 published a paper where they synthesized graphene oxide from needle coke (NC) using modified Hummers' method. The researchers reported the layer spacing of NC as 0.344 nm, GO-NC as 0.736 nm, GO from graphite as 0.876 nm, and that of RGO-NC as 0.355 nm. Even though the NC and RGO-NC have similar layer spacing, the RGO-NC had an XRD peak that was wider and weaker, indicating several layers of graphene. They further reported the number of layers and lateral size of RGO-NC to be concentrated around 4-6 layers and 3-8 μm. The study also reported the C/O ratio of GO-NC to be 2.25 and presented optical analysis of the GO-NC.

In addition, He *et al.* published a research paper synthesizing graphene quantum dots (GQD)

from coke via the electro-chemical exfoliation (ECE) methods [158]. Achee *et al.* has shown the potential to make high-yield and scalable graphene-like nanosheets using ECE method [159]. Therefore, in this work, different types of pet. coke were explored an as alternate parent material to make high aspect ratio graphene-like material using ECE process.

5.2 Methodology

5.2.1 ECE process

3 g to 6 g of petroleum derived coke is compacted in a dialysis tube that is clipped on both the ends. A platinum wire is inserted in the tube as working electrode and copper foil is wrapped around the dialysis tube as counter electrode. A known amount of weight is added on top of the dialysis tube wrapped in copper foil and submerged in 2 L of 0.1 M solution of ammonium sulfate $(NH_4)_2SO_4$ solution. 8 volts are applied to the platinum electrode and copper foil to start the electrochemical exfoliation of pet. coke. A minimum compliance current of 0.5 A is maintained throughout the reaction time of 10 hours. The products are then shear-mixed at 8000 rpm for 4 hours and freeze dried for characterization.

5.2.2 XRD

X-ray diffraction (XRD) patterns were collected on Bruker D8 Discover diffractometer fitted with LynxEye detector in a Bragg Brentao geometry at 40 kV, 40 mA with Cukα (λ: 0.15 nm) radiation.

5.2.3 SEM and Optical

A JEOL JSM-7500F field emission scanning electron microscope (FE-SEM) with ultra high resolution is used for SEM images.

5.3 Results and Discussion

Figure 5.2 summarizes various techniques available to synthesize graphene-like materials and their pros and cons. The most common method is modified Hummers' method, however, this method produces oxidized and defective graphene oxide. The solvent exfoliation method uses

solvents such as polyvinylpyrrodine (PVP) to separate layers of graphene, but this method is not scalable. The microwave or thermal treatment method to get layers of graphene can be scalable but it has safety concerns. Finally, the electro-chemical exfoliation method is a scalable method to make graphene-like materials but in this method, separating graphite from graphene can be challenging.

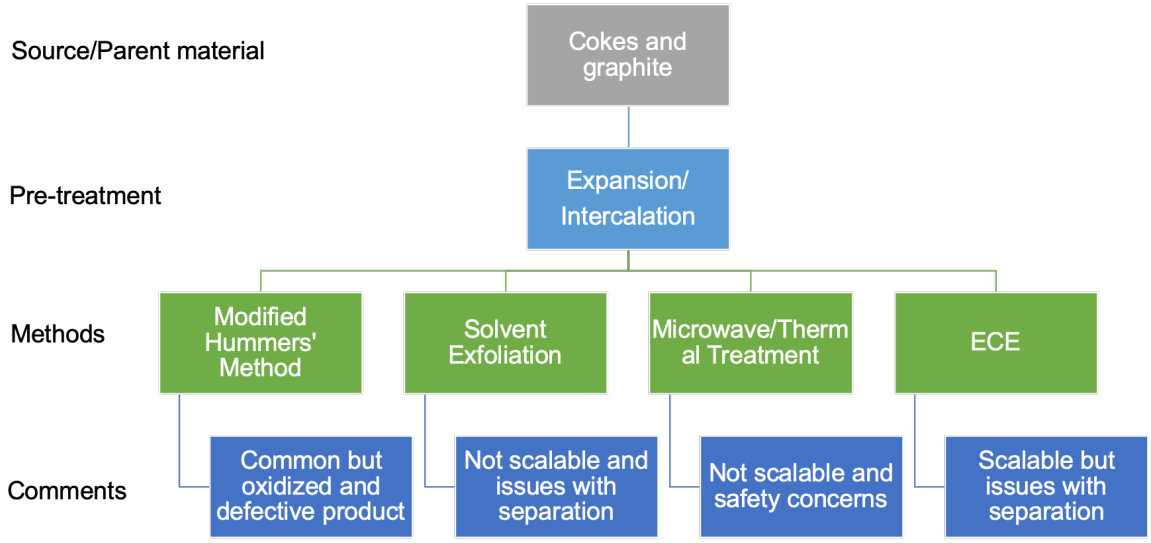

Figure 5.2: The figure represents various types of graphitic source to make graphene-like materials. The pre-treatment assists in exfoliation of graphitic source and methods are the synthesis routes to make graphene like materials

In order to explore if pet. coke can be used a parent material to make graphene-like material, modified Hummers' method and ECE process was chosen in this study. The details of ECE process is described in the methods sections. The experimental procedure is shown in **Figure 5.3**. The petroleum cokes were supplied by an industrial partner. The cokes were ground to fine powder and washed with dicholoromethane (DCM) to remove impurities. The cokes where then used as-is for the modified Hummers' method and pre-treated for the ECE process. The pre-treatment was done by mixing graphite source to 6 M nitric acid and heating the solution to 120 °C for 3 hours in a closed container. The pre-treated parent material is then washed to neutral pH. The pre-treatment of

the parent graphitic source improves the exfoliation of graphite in the electro-chemical exfoliation (ECE) method. As shown in **Figure 5.3**, the parent material were characterized after the DCM wash and the products were characterized at the end of the process.

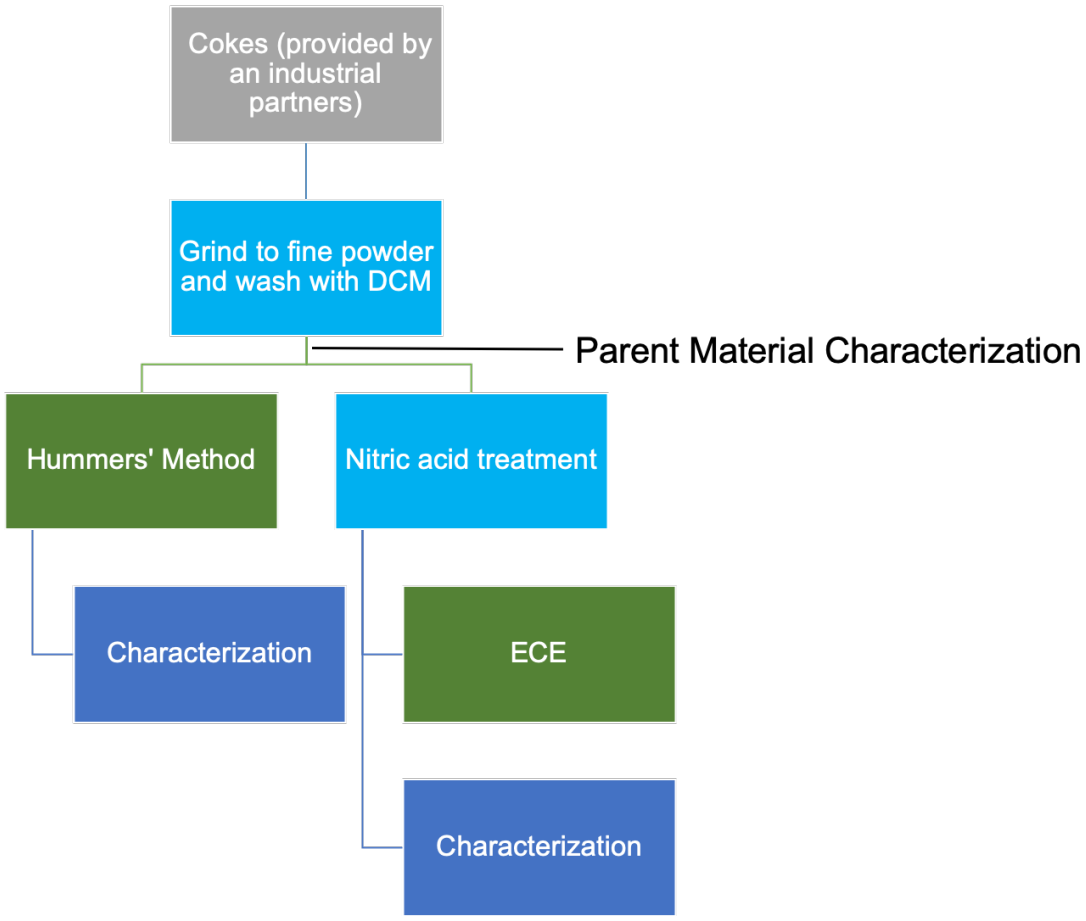

Figure 5.3: Experimental procedure for analysis of coke.

5.3.1 Parent material characterization

Figure 5.4 shows the XRD of parent material. The green line represents the XRD pattern for natural graphite and the red, blue, and black lines represents needle cokes 5, 11 and 12 respectively. **Figure 5.4b** shows the zoomed in version of **Figure 5.4a**. As we see in the figures, natural graphite has a narrow and sharp peak at around 26° and the cokes have broader and weaker peaks at 26 °.

This indicates that the cokes are not as crystalline as the natural graphite. However, within the three types of needle cokes, the difference are barely noticeable.

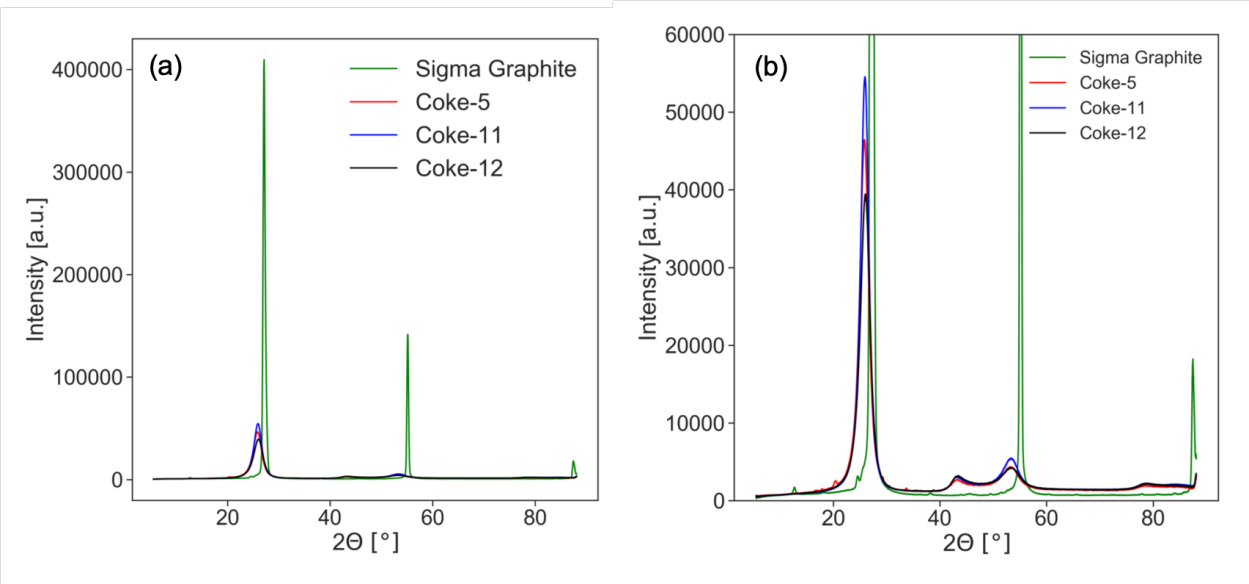

Figure 5.4: (a) shows the XRD of parent coke material (Coke-5, Coke-11, and Coke-12) in comparison to natural graphite (Sigma). (b) is the zoomed in version of (a).

Similarly, **Figure 5.5** shows the SEM images of the needle cokes 5 (a), 11 (b), and 12 (c) respectively. In these images, we notice sheet-like morphology of the cokes.

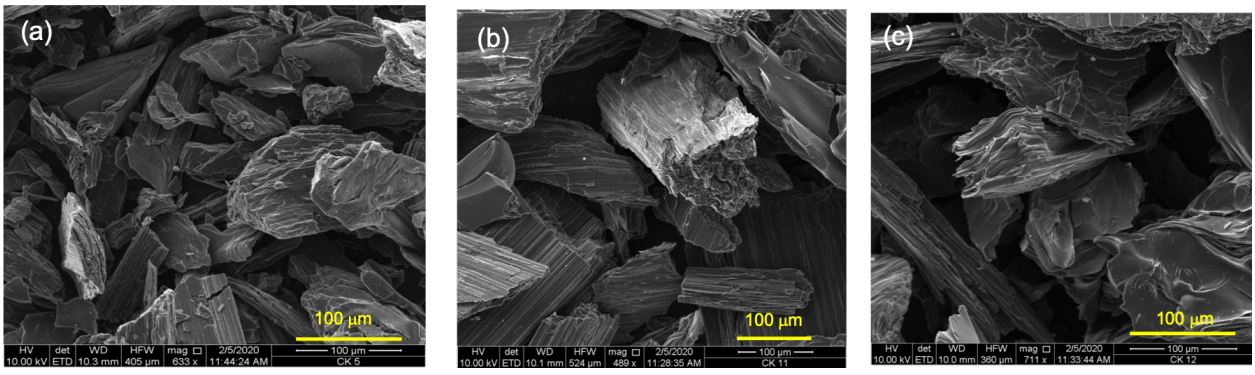

Figure 5.5: SEM images of parent coke material (a) Coke-5, (b) Coke-11, and (c) Coke-12

5.3.2 Final product characterization

The final products from ECE method are labelled as parent coke name followed by EEG for electrochemical exfoliated graphene, for example, EEG product from coke-5 is labelled as Ck-EEG. **Figure 5.6** shows XRD spectra of parent material and the EEG product. For comparison, **Figure 5.6a** is the spectra for natural graphite and EEG from natural graphite, **Figure 5.6b-d** are for Coke 5, 11, and 12 respectively, and **Figure 5.6e** are the spectra for all the EEG products. As show in the figure, the EEG products have lower intensity compared to the starting material, and the peak is shifted left. The change in intensity and left shift of the peaks indicate that after the ECE process, the parent material has changed.

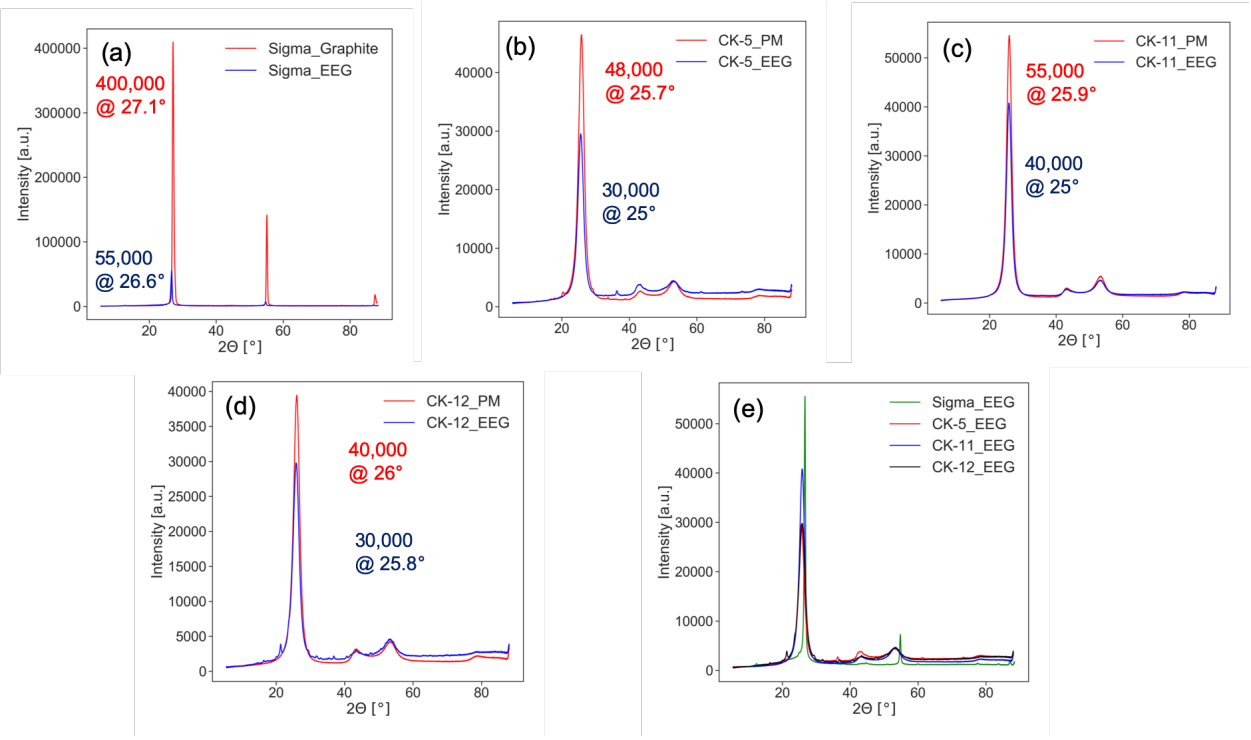

Figure 5.6: Comparison of XRD from parent material and product (a) Natural graphite, (b) Coke5, (c) Coke11, (d) Coke12, and (e) all EEG products

However, the SEM images in **Figure 5.7** show mostly sheet like structure. The sheets of EEG are not as well defined as seen in the **Figure 5.5**. Since the parent materials were not separate

from product at the end of ECE process, it is possible that these images contain a mixture of parent material and final product.

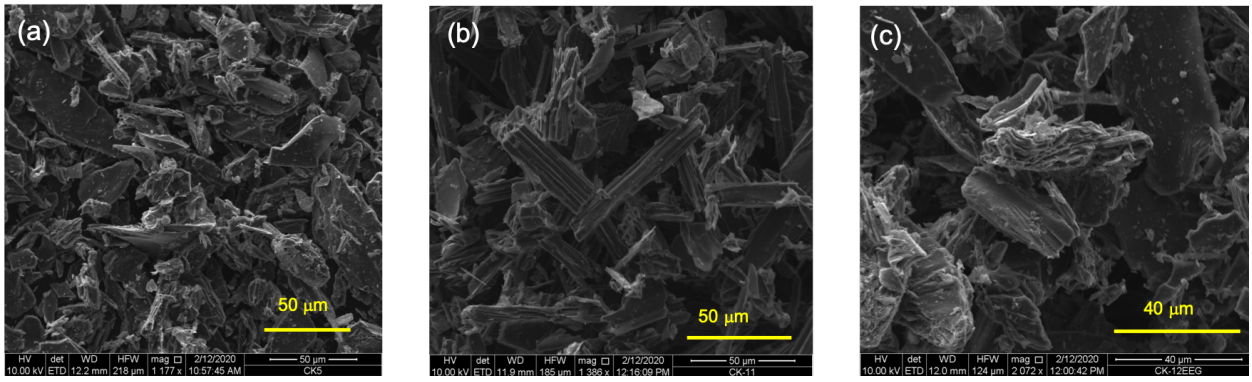

Figure 5.7: SEM images of EEG products from (a) Coke-5, (b) Coke-11, and (c) Coke-12

The optical images in **Figure 5.8** shows a possibility of few layer graphene in EEG from Coke-5 (**Figure 5.7b**). The optical images of EEG from Coke-5 and Coke-12 are inconclusive.

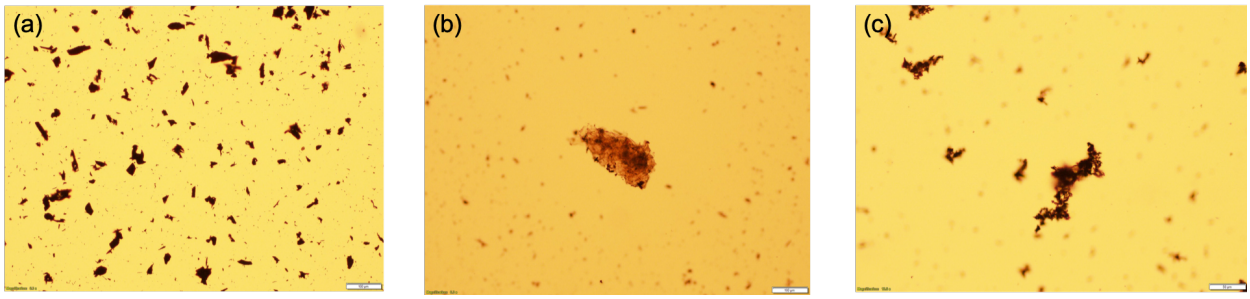

Figure 5.8: Optical images of parent coke material (a) Coke5-EEG, (b) Coke11-EEG, and (c) Coke12-EEG

5.4 Conclusion

In this work, needle cokes provided by an industrial partner were explored as an alternative source to make graphene-like material. However, based on SEM and XRD analysis of the parent

material and the products, it is inconclusive if these needle coke sources can be used to make graphene-like materials. The morphology and crystallinity of the cokes that passed through the ECE process has changes however, we failed to notice single graphene sheets on SEM. Additional characterizations are required such as AFM and Raman to make a definitive conclusion on whether cokes can be used as parent material to make high aspect ratio graphene nanosheets.

Based on literature, annealing the cokes to temperatures such at 800° C to 2800° C can make the coke sources more crystalline (process called graphitization) and potentially easier to exfoliate into individual sheets. In addition, research in developing a robust product separating method will become crucial to successfully synthesize nanosheets of graphene from pet. coke srouces.

6. CONCLUSION AND FUTURE WORK

6.1 Summary of dissertation

In this dissertation, we studied (1) the hazards associated with MXene production, (2) thermal stability of graphite oxide, (3) the synthesis condition of graphite and its implication in the product quality and safety, and (4) the alternate carbon sources to make graphene like materials. The analysis and experimental results, limitations, and future research directions for sections 2 to 5 in the dissertation can be summarized as follows.

6.1.1 Hazards analysis of MXene

In conclusion, this study has identified the hazards associated with $Ti_3C_2T_x$ laboratory production and discussed the preventive, mitigating, and emergency response plan. Five major hazards (combustible dust, exothermic reaction, pressure generation, toxic chemical release, and waste handling) were identified and discussed. Relative hazard ranking of various MXene synthesis routes is also presented in the study. A detailed experimental study of dust hazards of MXene is needed to quantify the fire and explosion probability of these new transition metal alloys. A study to synthesize MXene using an inherently safer design to avoid using hydrofluoric acid either in solution or in situ is strongly recommended.

6.1.2 Thermal Stability of GO

The study quantifies the temperature and pressure release rate of explosive thermal decomposition of dry GO. As seen the experiments, the pressure generated can be in 1000s of psig/min for a gram of material, therefore, the explosive decomposition of bulk GO can have catastrophic consequences. From the experiment, it can be concluded that the surface area and the heating rate of the dry GO are the determining factors for the GO's explosive-ness, higher surface area and lower heating rate give a more thermally stable GO compared to low surface area GO and high heating rate. Finally, using the Frank-Kamenetskii model, the critical mass necessary for the GO to undergo explosive decomposition can be determined. The detected onset temperature in the study is

observed to be close to normal drying temperatures of 100 °C. However, the detected onset temperature of GO is dependent on the equipment sensitivity. One challenge during the experiment was getting consistent heating for solid graphite oxide. The change in heating rate effects the detected onset temperature. Additionally, in this work the effect of the impurities and its effect on onset temperature was not studied and is worth investigating.

6.1.3 Synthesis of GO using modified Hummers' method

The heat released during the oxidation reaction can be correlated to the degree of oxidation of graphite in the modified Hummers' method. The study noted that the heat of reaction and the degree of oxidation increased when the parent graphite material soaked in the sulfuric acid for an extended time (*i.e.*, more than 10 min). For the GO produced by acid soaking the parent material, increasing RPM at which is the oxidation reaction was carried out increased the heat of reaction and degree of oxidation. However, for non-acid soaked runs, the RPM did not make any in the heat of reaction and the degree of oxidation. This pointed out that the chemistry of oxidation reaction is now well understood and should be investigated further. Prior literature claimed that the dimanganese helpta-oxide, Mn_2O_4 produced during modified Hummers' method were unstable at 55 °C. However, the experimental data suggests that the Mn_2O_4 produced during modified Hummers' method is dilute and in solution form and therefore is stable at 55 °C as long as the solution is free from organic impurities. Additional experiments with the $KMnO_4$ and H_2SO_4 solution are also recommended to get a better understanding of the unstable temperatures of manganese oxide by-product.

6.1.4 Alternate carbon sources

Finally, converting cokes or any other carbon source to graphene-like product is of increasing interest. However, there is a need to understand the properties of parent materials that enable some carbon sources to be converted to graphene-like materials while others can not. In this research, various types of needle cokes were explored as source parent material to make graphene-like material from modified Hummers' method and ECE process. However, the SEM and XRD results show

that the morphology of parent material has changed at the end of the ECE process, but the results were inconclusive if the products showed any graphene-like characteristics. The major areas of future research in this field are (1) determining the correct reaction conditions to make nanosheets and not GQDs, (2) separation of parent materials from products, (3) detailed characterizations, and (4) appropriate pretreatment of parent material to encourage exfoliation.

REFERENCES

[1] P. Lakhe, E. M. Prehn, T. Habib, J. L. Lutkenhaus, M. Radovic, M. S. Mannan, and M. J. Green, "Process safety analysis for ti3c2t x mxene synthesis and processing," *Industrial & Engineering Chemistry Research*, vol. 58, no. 4, pp. 1570–1579, 2019.

[2] P. Lakhe, D. L. Kulhanek, W. Sun, B. Zhang, M. J. Green, and M. S. Mannan, "Calorimetry of explosive thermal decomposition of graphite oxide," *Journal of hazardous materials*, vol. 366, pp. 275–281, 2019.

[3] K. T. Ramesh, *Nanomaterials*. Springer, 2009.

[4] C. Lee, X. Wei, J. W. Kysar, and J. Hone, "Measurement of the elastic properties and intrinsic strength of monolayer graphene," *science*, vol. 321, no. 5887, pp. 385–388, 2008.

[5] S. Bae, H. Kim, Y. Lee, X. Xu, J.-S. Park, Y. Zheng, J. Balakrishnan, T. Lei, H. R. Kim, Y. I. Song, *et al.*, "Roll-to-roll production of 30-inch graphene films for transparent electrodes," *Nature nanotechnology*, vol. 5, no. 8, p. 574, 2010.

[6] "T2 laboratories, inc. runaway reaction," September 2009.

[7] I. Rossetti and M. Compagnoni, "Chemical reaction engineering, process design and scale-up issues at the frontier of synthesis: Flow chemistry," *Chemical Engineering Journal*, vol. 296, pp. 56–70, 2016.

[8] M. S. Mannan, S. Sachdeva, H. Chen, O. Reyes-Valdes, Y. Liu, and D. M. Laboureur, "Trends and challenges in process safety," *AIChE Journal*, vol. 61, no. 11, pp. 3558–3569, 2015.

[9] I. Cameron, S. Mannan, E. Németh, S. Park, H. Pasman, W. Rogers, and B. Seligmann, "Process hazard analysis, hazard identification and scenario definition: Are the conventional tools sufficient, or should and can we do much better?," *Process Safety and Environmental Protection*, vol. 110, pp. 53–70, 2017.

[10] A. Sinha, Dhanjai, H. Zhao, Y. Huang, X. Lu, J. Chen, and R. Jain, "Mxene: An emerging material for sensing and biosensing," *TrAC Trends in Analytical Chemistry*, 2018.

[11] M. Naguib, V. N. Mochalin, M. W. Barsoum, and Y. Gogotsi, "25th anniversary article: Mxenes: a new family of two-dimensional materials," *Advanced Materials*, vol. 26, no. 7, pp. 992–1005, 2014.

[12] M. Cai, D. Thorpe, D. H. Adamson, and H. C. Schniepp, "Methods of graphite exfoliation," *Journal of Materials Chemistry*, vol. 22, no. 48, pp. 24992–25002, 2012.

[13] A. A. Balandin, S. Ghosh, W. Bao, I. Calizo, D. Teweldebrhan, F. Miao, and C. N. Lau, "Superior thermal conductivity of single-layer graphene," *Nano letters*, vol. 8, no. 3, pp. 902–907, 2008.

[14] A. Peigney, C. Laurent, E. Flahaut, R. Bacsa, and A. Rousset, "Specific surface area of carbon nanotubes and bundles of carbon nanotubes," *Carbon*, vol. 39, no. 4, pp. 507–514, 2001.

[15] H. Ahmad, M. Fan, and D. Hui, "Graphene oxide incorporated functional materials: A review," *Composites Part B: Engineering*, vol. 145, pp. 270–280, 2018.

[16] D. C. Marcano, D. V. Kosynkin, J. M. Berlin, A. Sinitskii, Z. Sun, A. Slesarev, L. B. Alemany, W. Lu, and J. M. Tour, "Improved synthesis of graphene oxide," *ACS nano*, vol. 4, no. 8, pp. 4806–4814, 2010.

[17] D. R. Dreyer, S. Park, C. W. Bielawski, and R. S. Ruoff, "The chemistry of graphene oxide," *Chemical society reviews*, vol. 39, no. 1, pp. 228–240, 2010.

[18] J. N. Coleman, "Liquid exfoliation of defect-free graphene," *Accounts of chemical research*, vol. 46, no. 1, pp. 14–22, 2012.

[19] S. Park and R. S. Ruoff, "Chemical methods for the production of graphenes," *Nature nanotechnology*, vol. 4, no. 4, p. 217, 2009.

[20] L. Shahriary and A. A. Athawale, "Graphene oxide synthesized by using modified hummers approach," *Int. J. Renew. Energy Environ. Eng*, vol. 2, no. 01, pp. 58–63, 2014.

[21] B. C. Brodie, "On the atomic weight of graphite," *Philosophical Transactions of the Royal Society of London*, vol. 149, pp. 249–259, 1859.

[22] L. Staudenmaier and B. Dtsch, "The structure of graphite oxide: Investigation of its surface chemical groups," *Chem. Ges*, vol. 31, pp. 1481–1487, 1898.

[23] W. S. Hummers Jr and R. E. Offeman, "Preparation of graphitic oxide," *Journal of the american chemical society*, vol. 80, no. 6, pp. 1339–1339, 1958.

[24] N. Morimoto, H. Suzuki, Y. Takeuchi, S. Kawaguchi, M. Kunisu, C. W. Bielawski, and Y. Nishina, "Real-time, in situ monitoring of the oxidation of graphite: Lessons learned," *Chemistry of Materials*, vol. 29, no. 5, pp. 2150–2156, 2017.

[25] R. K. Singh, R. Kumar, and D. P. Singh, "Graphene oxide: strategies for synthesis, reduction and frontier applications," *RSC Advances*, vol. 6, no. 69, pp. 64993–65011, 2016.

[26] D. Krishnan, F. Kim, J. Luo, R. Cruz-Silva, L. J. Cote, H. D. Jang, and J. Huang, "Energetic graphene oxide: challenges and opportunities," *Nano today*, vol. 7, no. 2, pp. 137–152, 2012.

[27] A. Simon, R. Dronskowski, B. Krebs, and B. Hettich, "The crystal structure of mn2o7," *Angewandte Chemie International Edition*, vol. 26, no. 2, pp. 139–140, 1987.

[28] L. M. Guiney, X. Wang, T. Xia, A. E. Nel, and M. C. Hersam, "Assessing and mitigating the hazard potential of two-dimensional materials," *ACS nano*, 2018.

[29] B. Fadeel, L. Farcal, B. Hardy, S. Vázquez-Campos, D. Hristozov, A. Marcomini, I. Lynch, E. Valsami-Jones, H. Alenius, and K. Savolainen, "Advanced tools for the safety assessment of nanomaterials," *Nature nanotechnology*, vol. 13, no. 7, p. 537, 2018.

[30] AIHA, "Lab incidents database." website, Accessed May 2018.

[31] U. CSB, "Texas tech university chemistry lab explosion." website, Accessed May 2018.

[32] H. An, T. Habib, S. Shah, H. Gao, M. Radovic, M. J. Green, and J. L. Lutkenhaus, "Surface-agnostic highly stretchable and bendable conductive mxene multilayers," *Science advances*, vol. 4, no. 3, p. eaaq0118, 2018.

[33] B. Anasori, M. R. Lukatskaya, and Y. Gogotsi, "2d metal carbides and nitrides (mxenes) for energy storage," *Nature Reviews Materials*, vol. 2, no. 2, p. 16098, 2017.

[34] "Etching reactor for mxene synthesis." website, Accessed November 2018.

[35] M. Alhabeb, K. Maleski, B. Anasori, P. Lelyukh, L. Clark, S. Sin, and Y. Gogotsi, "Guidelines for synthesis and processing of two-dimensional titanium carbide (ti3c2t x mxene)," *Chemistry of Materials*, vol. 29, no. 18, pp. 7633–7644, 2017.

[36] M. S. Mannan, "Director's corner," Accessed November 2018.

[37] H. Identification and E. T. Force, "Identifying and evaluating hazards in research laboratories," tech. rep., Americal Chemical Society, 2015.

[38] O. Safety and H. Administration, "Job hazard analysis," tech. rep., U.S. Department of Labor, 2002.

[39] D. W. Edwards and D. Lawrence, "Assessing the inherent safety of chemical process routes: is there a relation between plant costs and inherent safety?," *Process Safety and Environmental Protection*, vol. 71, no. B4, pp. 252–258, 1993.

[40] N. Ade, G. Liu, A. F. Al-Douri, M. M. El-Halwagi, and M. S. Mannan, "Investigating the effect of inherent safety principles on system reliability in process design," *Process Safety and Environmental Protection*, vol. 117, pp. 100–110, 2018.

[41] T. A. Kletz and P. Amyotte, *Process plants: A handbook for inherently safer design*. CRC Press, 2010.

[42] P. Eklund, M. Beckers, U. Jansson, H. Högberg, and L. Hultman, "The mn+ 1axn phases: Materials science and thin-film processing," *Thin Solid Films*, vol. 518, no. 8, pp. 1851–1878, 2010.

[43] T. Kletz, *Plant Design for Safety*. New York: Hemisphere Publishing Corporation, November 1990.

[44] K. L. Cashdollar, "Overview of dust explosibility characteristics," *Journal of Loss Prevention in the Process Industries*, vol. 13, no. 3-5, pp. 183–199, 2000.

[45] A. S. Blair, "Dust explosion incidents and regulations in the united states," *Journal of loss prevention in the process industries*, vol. 20, no. 4-6, pp. 523–529, 2007.

[46] OSHA, "Combustible dust." website, Accessed June 2018.

[47] H.-C. Wu, R.-C. Chang, and H.-C. Hsiao, "Research of minimum ignition energy for nano titanium powder and nano iron powder," *Journal of Loss Prevention in the Process Industries*, vol. 22, no. 1, pp. 21–24, 2009.

[48] A. Hendaoui, M. Andasmas, A. Amara, A. Benaldjia, P. Langlois, and D. Vrel, "Shs of high-purity max compounds in the ti-al-c system," *International Journal of Self-Propagating High-Temperature Synthesis*, vol. 17, no. 2, pp. 129–135, 2008.

[49] X. Wang and Y. Zhou, "Solid–liquid reaction synthesis of layered machinable ti 3 alc 2 ceramic," *Journal of Materials Chemistry*, vol. 12, no. 3, pp. 455–460, 2002.

[50] C. Yeh, C. Kuo, and Y. Chu, "Formation of ti3alc2/al2o3 and ti2alc/al2o3 composites by combustion synthesis in ti–al–c–tio2 systems," *Journal of Alloys and Compounds*, vol. 494, no. 1-2, pp. 132–136, 2010.

[51] H. Högberg, L. Hultman, J. Emmerlich, T. Joelsson, P. Eklund, J. M. Molina-Aldareguia, J.-P. Palmquist, O. Wilhelmsson, and U. Jansson, "Growth and characterization of max-phase thin films," *Surface and Coatings Technology*, vol. 193, no. 1-3, pp. 6–10, 2005.

[52] H. Fecht, E. Hellstern, Z. Fu, and W. Johnson, "Nanocrystalline metals prepared by high-energy ball milling," *Metallurgical Transactions A*, vol. 21, no. 9, p. 2333, 1990.

[53] G. Nykamp, U. Carstensen, and B. Müller, "Jet milling—a new technique for microparticle preparation," *International journal of pharmaceutics*, vol. 242, no. 1-2, pp. 79–86, 2002.

[54] P. R. Amyotte and R. K. Eckhoff, "Dust explosion causation, prevention and mitigation: An overview," *Journal of Chemical Health and Safety*, vol. 17, no. 1, pp. 15–28, 2010.

[55] J. Benson, "Safety considerations when handling metal powders," *Journal of the South African Institute of Mining and Metallurgy*, vol. 112, no. 7, p. 563, 2012.

[56] E. Poulsen, "Safety-related problems in the titanium industry in the last 50 years," *JOM*, vol. 52, no. 5, pp. 13–17, 2000.

[57] S. Lai, J. Jeon, S. K. Jang, J. Xu, Y. J. Choi, J.-H. Park, E. Hwang, and S. Lee, "Surface group modification and carrier transport properties of layered transition metal carbides (ti2ctx, t:–oh,–f and–o)," *Nanoscale*, vol. 7, no. 46, pp. 19390–19396, 2015.

[58] Y. Yoon, M. Lee, S. K. Kim, G. Bae, W. Song, S. Myung, J. Lim, S. S. Lee, T. Zyung, and K.-S. An, "A strategy for synthesis of carbon nitride induced chemically doped 2d mxene for high-performance supercapacitor electrodes," *Advanced Energy Materials*, p. 1703173, 2018.

[59] M. Ghidiu, M. R. Lukatskaya, M.-Q. Zhao, Y. Gogotsi, and M. W. Barsoum, "Conductive two-dimensional titanium carbide 'clay' with high volumetric capacitance," *Nature*, vol. 516, no. 7529, p. 78, 2014.

[60] A. Feng, Y. Yu, F. Jiang, Y. Wang, L. Mi, Y. Yu, and L. Song, "Fabrication and thermal stability of nh4hf2-etched ti3c2 mxene," *Ceramics International*, vol. 43, no. 8, pp. 6322–6328, 2017.

[61] X. Wang, C. Garnero, G. Rochard, D. Magne, S. Morisset, S. Hurand, P. Chartier, J. Rousseau, T. Cabioc'h, C. Coutanceau, V. Mauchamp, and S. Celerier, "A new etching environment (fef 3/hcl) for the synthesis of two-dimensional titanium carbide mxenes: a route towards selective reactivity vs. water," *Journal of Materials Chemistry A*, vol. 5, no. 41, pp. 22012–22023, 2017.

[62] T. Li, L. Yao, Q. Liu, J. Gu, R. Luo, J. Li, X. Yan, W. Wang, P. Liu, B. Chen, W. Zhang, W. Abbas, R. Naz, and D. Zhang, "Fluorine-free synthesis of high-purity ti3c2tx (t= oh, o)

via alkali treatment," *Angewandte Chemie International Edition*, vol. 57, no. 21, pp. 6115–6119, 2018.

[63] W. Sun, S. Shah, Y. Chen, Z. Tan, H. Gao, T. Habib, M. Radovic, and M. Green, "Electrochemical etching of ti 2 alc to ti 2 ct x (mxene) in low-concentration hydrochloric acid solution," *Journal of Materials Chemistry A*, vol. 5, no. 41, pp. 21663–21668, 2017.

[64] N. Jensen, "Modifying the dow fire & explosion index for use in assessing hazard and risk of experimental setups in research laboratories," in *12th International Symposium on Loss Prevention and Safety Promotion in the Process Industries*, 2007.

[65] G. Sharma, M. Naguib, D. Feng, Y. Gogotsi, and A. Navrotsky, "Calorimetric determination of thermodynamic stability of max and mxene phases," *The Journal of Physical Chemistry C*, vol. 120, no. 49, pp. 28131–28137, 2016.

[66] M. Naguib, O. Mashtalir, J. Carle, V. Presser, J. Lu, L. Hultman, Y. Gogotsi, and M. W. Barsoum, "Two-dimensional transition metal carbides," *ACS nano*, vol. 6, no. 2, pp. 1322–1331, 2012.

[67] K. Mazloomi and C. Gomes, "Hydrogen as an energy carrier: prospects and challenges," *Renewable and Sustainable Energy Reviews*, vol. 16, no. 5, pp. 3024–3033, 2012.

[68] T. Habib, S. Shah, Y. Chen, W. Sun, H. An, J. Lutkenhaus, M. Radovic, and M. Green, "Oxidation stability of ti3c2tx (mxene) nanosheets in solvents, films, and composites," *Submitted*, 2018.

[69] S. Shah, T. Habib, H. Gao, P. Gao, W. Sun, M. Green, and M. Radovic, "Template-free 3d titanium carbide (ti 3 c 2 t x) mxene particles crumpled by capillary forces," *Chemical Communications*, vol. 53, no. 2, pp. 400–403, 2017.

[70] H. Zhang, L. Wang, Q. Chen, P. Li, A. Zhou, X. Cao, and Q. Hu, "Preparation, mechanical and anti-friction performance of mxene/polymer composites," *Materials & Design*, vol. 92, pp. 682–689, 2016.

[71] C. Li, S. Kota, C. Hu, and M. Barsoum, "On the synthesis of low-cost, titanium-based mxenes," *J. Ceram. Sci. Technol*, vol. 7, pp. 301–306, 2016.

[72] A. Sarycheva, A. Polemi, Y. Liu, K. Dandekar, B. Anasori, and Y. Gogotsi, "2d titanium carbide (mxene) for wireless communication," *Science advances*, vol. 4, no. 9, p. eaau0920, 2018.

[73] K. Rasool, M. Helal, A. Ali, C. E. Ren, Y. Gogotsi, and K. A. Mahmoud, "Antibacterial activity of ti3c2t x mxene," *ACS nano*, vol. 10, no. 3, pp. 3674–3684, 2016.

[74] K. Huang, Z. Li, J. Lin, G. Han, and P. Huang, "Two-dimensional transition metal carbides and nitrides (mxenes) for biomedical applications," *Chemical Society Reviews*, 2018.

[75] H. Lin, X. Wang, L. Yu, Y. Chen, and J. Shi, "Two-dimensional ultrathin mxene ceramic nanosheets for photothermal conversion," *Nano letters*, vol. 17, no. 1, pp. 384–391, 2016.

[76] L. Lorencová, T. Bertok, J. Filip, M. Jerigová, D. Velic, P. Kasák, K. A. Mahmoud, and J. Tkac, "Highly stable ti3c2tx (mxene)/pt nanoparticles-modified glassy carbon electrode for h2o2 and small molecules sensing applications," *Sensors and Actuators B: Chemical*, vol. 263, pp. 360–368, 2018.

[77] O. Mashtalir, M. Naguib, V. N. Mochalin, Y. Dall'Agnese, M. Heon, M. W. Barsoum, and Y. Gogotsi, "Intercalation and delamination of layered carbides and carbonitrides," *Nature communications*, vol. 4, p. 1716, 2013.

[78] M. R. Lukatskaya, O. Mashtalir, C. E. Ren, Y. Dall'Agnese, P. Rozier, P. L. Taberna, M. Naguib, P. Simon, M. W. Barsoum, and Y. Gogotsi, "Cation intercalation and high volumetric capacitance of two-dimensional titanium carbide," *Science*, vol. 341, no. 6153, pp. 1502–1505, 2013.

[79] Z. Ling, C. E. Ren, M.-Q. Zhao, J. Yang, J. M. Giammarco, J. Qiu, M. W. Barsoum, and Y. Gogotsi, "Flexible and conductive mxene films and nanocomposites with high capacitance," *Proceedings of the National Academy of Sciences*, vol. 111, no. 47, pp. 16676–16681, 2014.

[80] M. Naguib, R. R. Unocic, B. L. Armstrong, and J. Nanda, "Large-scale delamination of multi-layers transition metal carbides and carbonitrides "mxenes"," *Dalton transactions*, vol. 44, no. 20, pp. 9353–9358, 2015.

[81] Y. Dall'Agnese, M. R. Lukatskaya, K. M. Cook, P.-L. Taberna, Y. Gogotsi, and P. Simon, "High capacitance of surface-modified 2d titanium carbide in acidic electrolyte," *Electrochemistry Communications*, vol. 48, pp. 118–122, 2014.

[82] A. Jastrzębska, A. Szuplewska, T. Wojciechowski, M. Chudy, W. Ziemkowska, L. Chlubny, A. Rozmysłowska, and A. Olszyna, "In vitro studies on cytotoxicity of delaminated ti3c2 mxene," *Journal of hazardous materials*, vol. 339, pp. 1–8, 2017.

[83] G. K. Nasrallah, M. Al-Asmakh, K. Rasool, and K. A. Mahmoud, "Ecotoxicological assessment of ti 3 c 2 t x (mxene) using a zebrafish embryo model," *Environmental Science: Nano*, vol. 5, no. 4, pp. 1002–1011, 2018.

[84] X. Yu, X. Cai, H. Cui, S.-W. Lee, X.-F. Yu, and B. Liu, "Fluorine-free preparation of titanium carbide mxene quantum dots with high near-infrared photothermal performances for cancer therapy," *Nanoscale*, vol. 9, no. 45, pp. 17859–17864, 2017.

[85] G. Liu, J. Zou, Q. Tang, X. Yang, Y. Zhang, Q. Zhang, W. Huang, P. Chen, J. Shao, and X. Dong, "Surface modified ti3c2 mxene nanosheets for tumor targeting photothermal/photodynamic/chemo synergistic therapy," *ACS applied materials & interfaces*, vol. 9, no. 46, pp. 40077–40086, 2017.

[86] M. Hatzifotis, A. Williams, M. Muller, and S. Pegg, "Hydrofluoric acid burns," *Burns*, vol. 30, no. 2, pp. 156–159, 2004.

[87] D. McKee, A. Thoma, K. Bailey, and J. Fish, "A review of hydrofluoric acid burn management," *Plastic Surgery*, vol. 22, no. 2, pp. 95–98, 2014.

[88] L. Muriale, E. Lee, J. Genovese, and S. Trend, "Fatality due to acute fluoride poisoning following dermal contact with hydrofluoric acid in a palynology laboratory," *The Annals of occupational hygiene*, vol. 40, no. 6, pp. 705–710, 1996.

[89] OSHA, "Accident database." website, Accessed May 2018.

[90] *Design of plants for handling hydrofluoric acid*, 1960.

[91] "Osha-directorate of standards and guidance." website, Accessed December 2018.

[92] OSHA, "Osha hazard information bulletins - hf." website, Accessed December 2018.

[93] C. Hu, S. Lo, W. Kuan, and Y. Lee, "Removal of fluoride from semiconductor wastewater by electrocoagulation–flotation," *Water research*, vol. 39, no. 5, pp. 895–901, 2005.

[94] P. Westerhoff, G. Song, K. Hristovski, and M. A. Kiser, "Occurrence and removal of titanium at full scale wastewater treatment plants: implications for tio 2 nanomaterials," *Journal of Environmental Monitoring*, vol. 13, no. 5, pp. 1195–1203, 2011.

[95] M. Segal, "Selling graphene by the ton," *Nature nanotechnology*, vol. 4, no. 10, p. 612, 2009.

[96] S. Ahn, J. Sung, H. Kim, and Y. Sung, "Emerging analysis on the preparation and application of graphene by bibliometry," *J Material Sci Eng*, vol. 4, no. 192, pp. 2169–0022, 2015.

[97] I. P. O. Informatics Team, "Graphene - the worldwide patent landscape in 2015," tech. rep., UK Intellectual Property Office, Cardiff Road, Newport, NP 10 8QQ United Kingdom, March 2015.

[98] D. Li and R. B. Kaner, "Graphene-based materials," *Science*, vol. 320, no. 5880, pp. 1170–1171, 2008.

[99] Y. Wang, Z. Shi, Y. Huang, Y. Ma, C. Wang, M. Chen, and Y. Chen, "Supercapacitor devices based on graphene materials," *The Journal of Physical Chemistry C*, vol. 113, no. 30, pp. 13103–13107, 2009.

[100] D. A. Brownson, D. K. Kampouris, and C. E. Banks, "An overview of graphene in energy production and storage applications," *Journal of Power Sources*, vol. 196, no. 11, pp. 4873–4885, 2011.

[101] T. Wang, D. Huang, Z. Yang, S. Xu, G. He, X. Li, N. Hu, G. Yin, D. He, and L. Zhang, "A review on graphene-based gas/vapor sensors with unique properties and potential applications," *Nano-Micro Letters*, vol. 8, no. 2, pp. 95–119, 2016.

[102] Y. Li and N. Chopra, "Progress in large-scale production of graphene. part 1: chemical methods," *Jom*, vol. 67, no. 1, pp. 34–43, 2015.

[103] S. Pei and H.-M. Cheng, "The reduction of graphene oxide," *Carbon*, vol. 50, no. 9, pp. 3210 – 3228, 2012. Festschrift dedicated to Peter A. Thrower, Editor-in-Chief, 1972 - 2012.

[104] J. Chen, B. Yao, C. Li, and G. Shi, "An improved hummers method for eco-friendly synthesis of graphene oxide," *Carbon*, vol. 64, pp. 225–229, 2013.

[105] R. Croft, "Lamellar compounds of graphite," *Quarterly Reviews, Chemical Society*, vol. 14, no. 1, pp. 1–45, 1960.

[106] A. M. Rodriguez and P. V. Jiménez, "Thermal decomposition of the graphite oxidation products," *Thermochimica acta*, vol. 78, no. 1-3, pp. 113–122, 1984.

[107] U. CSB, "Completed investigations." website, 2018.

[108] D. M. Laboureur, Z. Han, B. Z. Harding, A. Pineda, W. C. Pittman, C. Rosas, J. Jiang, and M. S. Mannan, "Case study and lessons learned from the ammonium nitrate explosion at the west fertilizer facility," *Journal of hazardous materials*, vol. 308, pp. 164–172, 2016.

[109] CBS, "West fertilizer company fire and explosion," tech. rep., U. S. Chemical Safety and Hazard Investigation Board, 2016.

[110] G. Fu, J. Wang, and M. Yan, "Anatomy of tianjin port fire and explosion: Process and causes," *Process Safety Progress*, vol. 35, no. 3, pp. 216–220, 2016.

[111] B. Zhao, "Facts and lessons related to the explosion accident in tianjin port, china," *Natural Hazards*, vol. 84, no. 1, pp. 707–713, 2016.

[112] F. Kim, J. Luo, R. Cruz-Silva, L. J. Cote, K. Sohn, and J. Huang, "Self-propagating domino-like reactions in oxidized graphite," *Advanced Functional Materials*, vol. 20, no. 17, pp. 2867–2873, 2010.

[113] Y. Qiu, F. Guo, R. Hurt, and I. Külaots, "Explosive thermal reduction of graphene oxide-based materials: Mechanism and safety implications," *Carbon*, vol. 72, pp. 215 – 223, 2014.

[114] Y. Qiu, F. Collin, R. H. Hurt, and I. Külaots, "Thermochemistry and kinetics of graphite oxide exothermic decomposition for safety in large-scale storage and processing," *Carbon*, vol. 96, pp. 20–28, 2016.

[115] G. Maschio, J. Feliu, J. Ligthart, I. Ferrara, and C. Bassani, "The use of adiabatic calorimetry for the process analysis and safety evaluation in free radical polymerization," *Journal of thermal analysis and calorimetry*, vol. 58, no. 1, pp. 201–214, 1999.

[116] W. Zhu, M. I. Papadaki, Z. Han, and C. V. Mashuga, "Effect of temperature and selected additives on the decomposition "onset" of 2-nitrotoluene using advanced reactive system screening tool," *Journal of Loss Prevention in the Process Industries*, vol. 49, pp. 630–635, 2017.

[117] A. W. Golubkov, D. Fuchs, J. Wagner, H. Wiltsche, C. Stangl, G. Fauler, G. Voitic, A. Thaler, and V. Hacker, "Thermal-runaway experiments on consumer li-ion batteries with metal-oxide and olivin-type cathodes," *RSC Advances*, vol. 4, no. 7, pp. 3633–3642, 2014.

[118] T. Chemistry, "Fnaa." website.

[119] H. E. Kissinger, "Reaction kinetics in differential thermal analysis," *Analytical chemistry*, vol. 29, no. 11, pp. 1702–1706, 1957.

[120] B. Yuan, L. Song, K. M. Liew, and Y. Hu, "Mechanism for increased thermal instability and fire risk of graphite oxide containing metal salts," *Materials Letters*, vol. 167, pp. 197–200, 2016.

[121] A. R. Shouman, "A review of one aspect of the thermal-explosion theory," *Journal of engineering mathematics*, vol. 56, no. 2, pp. 179–184, 2006.

[122] D. A. Frank-Kamenetskii, *Diffusion and heat transfer in chemical kinetics*. Plenum Press, 1969.

[123] W. Gill, A. Donaldson, and A. R. Shouman, "The frank-kamenetskii problem revisited. part i. boundary conditions of first kind," *Combustion and Flame*, vol. 36, pp. 217–232, 1979.

[124] T. Boddington, P. Gray, and D. Harvey, "Thermal theory of spontaneous ignition: criticality in bodies of arbitrary shape," *Philosophical Transactions of the Royal Society of London A: Mathematical, Physical and Engineering Sciences*, vol. 270, no. 1207, pp. 467–506, 1971.

[125] P. F. Beever and J. F. Griffiths, "Scaling rules for prediction of thermal runaway," in *International Symposium on Runaway Reactions*, pp. 1–20, AIChE, 1989.

[126] V. Babushok, V. Goldshtein, and V. Sobolev, "Critical conditions for thermal explosion with reactant consumption," *Combustion science and technology*, vol. 70, no. 1-3, pp. 81–89, 1990.

[127] D. Sánchez-Rodríguez, J. Farjas, and P. Roura, "The critical conditions for thermal explosion in a system heated at a constant rate," *Combustion and Flame*, vol. 186, pp. 211–219, 2017.

[128] D. Sánchez-Rodriguez, J. Farjas, and P. Roura, "The critical condition for thermal explosion in an isoperibolic system," *AIChE Journal*, 2017.

[129] J. Basu, J. K. Basu, and T. K. Bhattacharyya, "The evolution of graphene-based electronic devices," *International Journal of Smart and Nano Materials*, vol. 1, no. 3, pp. 201–223, 2010.

[130] Z. A. Nima, K. B. Vang, D. Nedosekin, G. Kannarpady, V. Saini, S. E. Bourdo, W. Majeed, F. Watanabe, E. Darrigues, K. M. Alghazali, *et al.*, "Quantification of cellular associated graphene and induced surface receptor responses," *Nanoscale*, vol. 11, no. 3, pp. 932–944, 2019.

[131] G. Shi, S. Araby, C. T. Gibson, Q. Meng, S. Zhu, and J. Ma, "Graphene platelets and their polymer composites: fabrication, structure, properties, and applications," *Advanced Functional Materials*, vol. 28, no. 19, p. 1706705, 2018.

[132] A. P. Kauling, A. T. Seefeldt, D. P. Pisoni, R. C. Pradeep, R. Bentini, R. V. Oliveira, K. S. Novoselov, and A. H. Castro Neto, "The worldwide graphene flake production," *Advanced Materials*, vol. 30, no. 44, p. 1803784, 2018.

[133] A. Zurutuza and C. Marinelli, "Challenges and opportunities in graphene commercialization," *Nature nanotechnology*, vol. 9, no. 10, p. 730, 2014.

[134] S. Eigler, C. Dotzer, and A. Hirsch, "Visualization of defect densities in reduced graphene oxide," *Carbon*, vol. 50, no. 10, pp. 3666–3673, 2012.

[135] A. M. Dimiev and J. M. Tour, "Mechanism of graphene oxide formation," *ACS nano*, vol. 8, no. 3, pp. 3060–3068, 2014.

[136] M. d. P. Lavin-Lopez, A. Romero, J. Garrido, L. Sanchez-Silva, and J. L. Valverde, "Influence of different improved hummers method modifications on the characteristics of graphite oxide in order to make a more easily scalable method," *Industrial & Engineering Chemistry Research*, vol. 55, no. 50, pp. 12836–12847, 2016.

[137] C. Li, Y. Shi, X. Chen, D. He, L. Shen, and N. Bao, "Controlled synthesis of graphite oxide: formation process, oxidation kinetics, and optimized conditions," *Chemical Engineering Science*, vol. 176, pp. 319–328, 2018.

[138] S. Seiler, C. E. Halbig, F. Grote, P. Rietsch, F. Börrnert, U. Kaiser, B. Meyer, and S. Eigler, "Effect of friction on oxidative graphite intercalation and high-quality graphene formation," *Nature communications*, vol. 9, no. 1, p. 836, 2018.

[139] S. Lee, S. H. Eom, J. S. Chung, and S. H. Hur, "Large-scale production of high-quality reduced graphene oxide," *Chemical engineering journal*, vol. 233, pp. 297–304, 2013.

[140] F. J. Tölle, K. Gamp, and R. Mülhaupt, "Scale-up and purification of graphite oxide as intermediate for functionalized graphene," *Carbon*, vol. 75, pp. 432–442, 2014.

[141] O. T. Fasullo, *Sulfuric acid ; use and handling. [by] Oscar T. Fasullo.* McGraw-Hill, 1965.

[142] H. S. Fogler, *Essentials of Chemical Reaction Engineering: Essenti Chemica Reactio Engi*. Pearson Education, 2010.

[143] J. H. Kang, T. Kim, J. Choi, J. Park, Y. S. Kim, M. S. Chang, H. Jung, K. T. Park, S. J. Yang, and C. R. Park, "Hidden second oxidation step of hummers method," *Chemistry of Materials*, vol. 28, no. 3, pp. 756–764, 2016.

[144] M. V. Park, E. A. Bleeker, W. Brand, F. R. Cassee, M. van Elk, I. Gosens, W. H. De Jong, J. A. Meesters, W. J. Peijnenburg, J. T. Quik, *et al.*, "Considerations for safe innovation: the case of graphene," *ACS nano*, 2017.

[145] H. Römpp, J. Falbe, and E. Amelingmeier, *Römpp kompakt Basislexikon Chemie: M-Re*, vol. 3. Thieme, 1999.

[146] N. Morimoto, T. Kubo, and Y. Nishina, "Tailoring the oxygen content of graphite and reduced graphene oxide for specific applications," *Scientific reports*, vol. 6, p. 21715, 2016.

[147] O. Glemser and H. Schröder, "Über manganoxyde. ii. zur kenntnis des mangan (vii)-oxyds," *Zeitschrift für anorganische und allgemeine Chemie*, vol. 271, no. 5-6, pp. 293–304, 1953.

[148] S. Lee, J. Oh, R. S. Ruoff, and S. Park, "Residual acetone produces explosives during the production of graphite oxide," *Carbon*, vol. 50, no. 3, pp. 1442–1444, 2012.

[149] J. F. Embury, D. L. Walker, and C. J. Zimmermann, "Screening smoke performance of commercially available powders i. infrared screening by graphite flake," tech. rep., EDGEWOOD RESEARCH DEVELOPMENT AND ENGINEERING CENTER ABERDEEN PROVING GROUNDMD, 1993.

[150] M. Wissler, "Graphite and carbon powders for electrochemical applications," *Journal of power sources*, vol. 156, no. 2, pp. 142–150, 2006.

[151] Z. Yang, J. Tian, Z. Yin, C. Cui, W. Qian, and F. Wei, "Carbon nanotube-and graphene-based nanomaterials and applications in high-voltage supercapacitor: A review," *Carbon*, vol. 141, pp. 467–480, 2019.

[152] D. Higgins, P. Zamani, A. Yu, and Z. Chen, "The application of graphene and its composites in oxygen reduction electrocatalysis: a perspective and review of recent progress," *Energy & Environmental Science*, vol. 9, no. 2, pp. 357–390, 2016.

[153] A. Carmalin Sophia, E. C. Lima, N. Allaudeen, and S. Rajan, "Application of graphene based materials for adsorption of pharmaceutical traces from water and wastewater-a review," *Desalination and Water Treatment*, vol. 57, no. 57, pp. 27573–27586, 2016.

[154] A. Nag, A. Mitra, and S. C. Mukhopadhyay, "Graphene and its sensor-based applications: A review," *Sensors and Actuators A: Physical*, vol. 270, pp. 177–194, 2018.

[155] U. Sierra, P. Álvarez, C. Blanco, M. Granda, R. Santamaría, and R. Menéndez, "New alternatives to graphite for producing graphene materials," *Carbon*, vol. 93, pp. 812–818, 2015.

[156] U. Sierra, P. Álvarez, C. Blanco, M. Granda, R. Santamaría, and R. Menéndez, "Cokes of different origin as precursors of graphene oxide," *Fuel*, vol. 166, pp. 400–403, 2016.

[157] C. Botas, P. Álvarez, C. Blanco, R. Santamaría, M. Granda, P. Ares, F. Rodríguez-Reinoso, and R. Menéndez, "The effect of the parent graphite on the structure of graphene oxide," *Carbon*, vol. 50, no. 1, pp. 275–282, 2012.

[158] M. He, X. Guo, J. Huang, H. Shen, Q. Zeng, and L. Wang, "Mass production of tunable multicolor graphene quantum dots from an energy resource of coke by a one-step electrochemical exfoliation," *Carbon*, vol. 140, pp. 508–520, 2018.

[159] T. C. Achee, W. Sun, J. T. Hope, S. G. Quitzau, C. B. Sweeney, S. A. Shah, T. Habib, and M. J. Green, "High-yield scalable graphene nanosheet production from compressed graphite using electrochemical exfoliation," *Scientific reports*, vol. 8, no. 1, pp. 1–8, 2018.